NRSP-2
98-18

The PHARUS Familiarization Programme

G.J. Rijckenberg
A.J.E. Smith
A.C. van den Broek
H. Greidanus
R.J. Dekker
J. Kogels
M.P.G. Otten
H. Landa
G.H.F.M. Hesselmans
O. Pietersen
H.W.G. Booltink
D.H. Hoekman
M.A.M. Vissers

BELEIDSCOMMISSIE REMOTE SENSING

The PHARUS Familiarization Programme

G.J. Rijckenberg
A.J.E. Smith
A.C. van den Broek
H. Greidanus
R.J. Dekker
J. Kogels
M.P.G. Otten
TNO-FEL

H. Landa
RWS-MD

G.H.F.M. Hesselmans
ARGOSS

O. Pietersen
NLR

H.W.G. Booltink
D.H. Hoekman
M.A.M. Vissers
LU Wageningen

NRSP project 5.1/TE-12
NRSP report 98-18
ISBN 90 5411 258 1

November 1998

This report describes a project, carried out in the framework of the National Remote Sensing Programme (NRSP-2), under responsibility of the Netherlands Remote Sensing Board (BCRS).

The PHARUS Familiarization program

Abstract

The Familiarization program is aimed at the acquisition of PHARUS data to demonstrate the potentials of PHARUS for a number of selected applications to potential end users. In order to demonstrate the value of the system for each application, interpretation of the data acquired has been carried out by the users involved in this project. The users have been supported by the PHARUS technical team for information about the system characteristics The selected applications are: land use classification, cartography in tidal areas, road detection, oil spill detection, ocean bottom topography, detection of ships and ship wakes, moving target detection, crop classification, forestry applications and precision farming. To demonstrate the findings to other users and invited commercial users, a closing workshop has been organized, in which all results have been presented. PHARUS data was in fact supplied for all applications, with the exception of the oil spill detection experiment, which experienced technical problems.

The following main conclusions were drawn from the study.

1. *It has been possible to demonstrate the applications in spite of the technical problems, which occurred during the data acquisition, but which could be solved.*
2. *The results from the applications tidal areas and precision farming were not satisfactory. It is expected that the results will improve if a temporal analysis is applied.*
3. *The results of the applications have been obtained with relatively little effort. It is therefore concluded that the PHARUS products are very user friendly, which facilitates the use of these data.*
4. *The PHARUS team has improved its knowledge considerably on the use of PHARUS, this has led to to an improvement plan*
5. *The logistics involved with the PHARUS flights are difficult because the platform is not always available.*
6. *There is a clear need for more images, conclusions drawn for some applications are weakened due to the low number of images use, in particular for precision farming and tidal cartography.*

With respect to the conclusions and results the main recommendations are .

1. *The user requirements which concern the calibration of the data must be clear because the calibration of PHARUS is an intensive task.*
2. *The planning of the PHARUS flights must be agreed upon, well in advance of the actual flight itself.*
3. *The current platform for PHARUS should be certified for most weather conditions, in particular ice accretion.*
4. *It is further recommended to perform an additional data acquisition program to complete the introduction of PHARUS products for the (Dutch/international) user market.*
5. *For full real time benefits, also a data link to the ground should be implemented and the processing should be faster.*

The PHARUS Familiarization program

Executive Summary

Scope

The PHARUS polarimetric SAR is an airborne synthetic aperture radar system, developed by TNO Physics and Electronics Laboratory (TNO-FEL), in co-operation with the National Aerospace Laboratory (NLR) and the Delft University of Technology (DUT). PHARUS stands for Phased Array Universal SAR..

PHARUS is the successor of the PHARS (Phased Array Rehearsal SAR) system, which was actually a testbed version of PHARUS. PHARS is a compact small weight system, compared to PHARUS it has a limited number of applications. PHARUS has an increased swath, increased resolution and increased range of incidence angles, but above all it is fully polarimetric. This last important feature will give better tools for discrimination of targets/surfaces and provides additional information on the backscattering properties of the objects in the swath.

The most important features of PHARUS are:

- *Polarimetry*
- *Phased array antenna with active Transmit/Receive modules.*

Objectives

With the arrival of the PHARUS system new polarimetric data sets have become available in the Netherlands. Consequently, the user community can obtain more experience with these type of data. It is the goal of the PHARUS Familiarization program to familiarize the SAR user community in the Netherlands with the new sensor.

Under supervision of the BCRS a group of potential users of the PHARUS has had a number of meetings in order to provide input to the PHARUS project team on user requirements. The organizations represented in this group are: BCRS, Min. of Defence, NIVR, NLR, RWS-MD, RWS-DNZ, RWS-RIKZ, WL, WAU and TNO-FEL. Within this group the use of the PHARUS system has been discussed in detail. This has led to a selection of military and civil applications for the demonstration of the capabilities of PHARUS. A technical system evaluation and data quality control is also part of the project since it has been the first opportunity to analyze the performance of PHARUS.

The Familiarization program is not aimed at scientific research in each of the application fields, but focuses on the added value of the enhancements of PHARUS with respect to PHARS (increased range, resolution and polarimetry).

Approach

In order to demonstrate the potential of the system for each application, interpretation of the data acquired has been carried out by the users involved in this project. The users have been supported by the PHARUS technical team for information about the system characteristics. Support was given at a kick-off workshop and during the program each user has communicated his requirements to the PHARUS team.

A flight plan was defined for the acquisition of the data. Five flights were originally scheduled with PHARUS mounted under a Cessna Citation. Since there were technical problems at the beginning of the project, a total of seven flights had to be performed.

Several steps were performed for the image acquisition like: the determination of user requirements; the definition of the PHARUS mode and flight trajectory; a system check;

flight operations and data acquisition; Flight data processing; Data checks; Data processing and the image distribution and support of the users in the project. This procedure was developed during the project. Furthermore, it became apparent that additional logistic actions were necessary like: operations on the ground (e.g. creation of an oil spill, radio communication, ground operations). These actions were not foreseen in the original approach but during the project it became clear that they would simplify the data acquisition significantly, because several time critical applications had to be combined in a single flight. The time dependence and the availability of the platform (e.g. ice accretion is not allowed) were also a constraint to the data acquisition.

In order to demonstrate the findings to other users and invited commercial users, a closing workshop has been organized, in which all results have been presented.

Results

Demonstration results were obtained for: Land use classification; Cartography in tidal areas; Road detection; Oil spill detection; Bottom topography; Detection of ships and ship wakes; Target detection; Crop classification; Forestry; Precision agriculture and System performance. Due to technical problems a first attempt failed to acquire data for most applications. The problems could be solved and results were finally obtained. The most important results are summarized below for each application.

Land use classification:

A PHARUS image of an area near Assen (Fochteloeërveen) has been classified into the types vegetation, urban and water. No ground data was available so foreknowledge was required like experience of signatures of land use classes.

1. *Good classification results of three test sites at Fochteloeërveen are found for six classes: water, urban, forest, grass, bare soil, and moor.*
2. *A small number of bare soil fields are grown with heather or grass so that the pixels in these fields are erroneously classified as moor or grass.*
3. *Spill over of radar reflection of a pixel to neighbouring pixels causes the lake outskirts to get an overall intensity comparable to that of moor or bare soil. As a consequence, the outskirts of lakes may be confused with these two classes.*
4. *From shadow areas behind forests no radar signal is scattered back. As a consequence, these areas are classified as water and in case of spill over from the canopy with moor or bare soil.*

Cartography in tidal areas:

For this application two images were acquired.

1. *A PHARUS image of 27 August 1996 of the 'Groote Plaat' near the island of Terschelling contains differences in contrast, and several artefacts and phenomena.*
2. *A PHARUS image of 2 June 1997 image was probably acquired during high tide. As a result only the 1996 image was investigated.*

Three classification methods have been applied to the 1996 image.

3. *As the image is divided in 10 classes, the water line can well be determined by selecting the colours assigned to the classes.*
4. *In the PHARUS images equal grey values have been given to various phenomena. Current in a channel is given the same grey value as low sandflat, as the reflection characteristics are the same. In this way a sandflat may be shown in the middle of a channel.*
5. *In every image a separate set of training pixels must be taken, as not every image has an equal histogram stretch.*
6. *It is not easy to automatically extract a precise DTM from PHARUS images because of the large numbers of characteristic elements in the individual images and differences*

between the images themselves.

7. *For a better-founded evaluation of the applied methods, new images are necessary, which should be acquired during different tidal stages.*

Road detection:
A PHARUS image of Amersfoort and a road graph file have been compared in the demonstration.

1. *There exist clear shifts between the two files. These shifts can for the greatest part be attributed to the inaccuracy of the road graph file.*
2. *Within the urban area roads in the PHARUS image are in many cases not directly recognisable, but can be deducted from the structure of the buildings surrounding the roads. This indicates that road detection from a PHARUS image corresponds to the complexity of the buildings.*
3. *Often no uniform street pattern can be derived from the building structure; main roads can mostly be clearly indicated, but street patterns in residential districts often allow for multiple interpretations.*
4. *The PHARUS image contains a lot of information about building structures and consequently also about road patterns. Direct collection of road information will be possible in areas with sparse buildings, but in areas with complex building structures this will prove to be difficult or even impossible. Here more experience on human interpretation of PHARUS images is necessary.*

Oil spill detection:
The demonstration of oil spill detection with PHARUS did not provide satisfactory results. Due to technical problems one controlled experiment failed and the participation to a second experiment had to be cancelled. It was agreed with the BCRS to postpone this application to a later stage.

Bottom topography:

1. *A PHARUS image of 27 August 1996 of the 'Groote Plaat' was geometrically corrected using suitable land marks visible in the SAR images and the most recent topographic map of the area.*
2. *An intensity change in this image was sucessfully removed by fitting a low order polynomial through the difference.*
3. *Depth maps were constructed of PHARUS and ERS images. The accuracy of the maps based on the PHARUS data has improved considerably as compared to the maps based on ERS SAR data.*
4. *The main conclusion is that high resolution SAR imagery may considerably improve the quality of calculated seabed topography. In order to increase the value of the PHARUS imagery, the following improvements are suggested:*
    - *Processing of sufficient data outside of the area visible in the imagery to avoid the edge effect.*
    - *Use of 16 bit format instead of the 8 bit format. Although use of 8 bit format reduces the file size, this advantage is only minor. On the other hand the disadvantages are considerable: loss of accuracy and truncated signals at low intensities.*
    - *The change in image intensity as a function of incidence angle, this image transformation has to be inverted in order to interpret the data quantitatively.*

Detection of ships and ship wakes:
An area of approximately 22 by 16 km was imaged in two adjacent east-west strips of approximately 22 km length near Hoek van Holland.

1. *Visual analysis of one strip yields a total count of 12 targets (assumed to be ships) within a 180 km^2 processed area. One of the ships has a wake signature. In the other strip, 22 targets and 4 wakes are found within a 140 km^2 processed area.*
2. *There are no large differences between the VV and HH channels The cross-polarized channel (HV=VH) is characterized by a still weaker signal from the sea surface. Here, most of the image background is just system noise and only at very near range, the same features as in VV and HH on the sea surface are weakly visible.*
3. *Based on visual analysis of the HH, VV, VH and HV channels (calibrated and uncalibrated), it can be concluded that ships are easily detected by PHARUS. Also ship wakes are readily imaged. The ships appear to have the highest contrast with respect to the sea clutter in the HV channel, indicating that the cross-polarized channels are best suited for this purpose.*
4. *On account of the lack of in-situ information in this experiment, it cannot be verified whether all targets detected by PHARUS were indeed ships (and not, e.g., large waves).*
5. *While this project has shown that PHARUS can be used successfully for ship detection, and that its polarimetric capability is of value, no quantitative conclusions on the performance of PHARUS could be drawn. For this, it is necessary to perform a controlled experiment with a complete set of in-situ data.*
6. *At present, PHARUS is deemed reliable enough to invest effort in such a verification experiment. Possibly, such an experiment can be combined with a future ENVISAT-ASAR experiment. An investigation into the performance of PHARUS should also take into account other modes so that conclusions may be drawn as to the operationally or economically optimal mode for the application of ship detection.*

Target detection:
This demonstration involved two applications: a) MTI (Moving Target Identification) and b) jamming (distortion) of an image.

a) MTI
A SAR image of the A12 near Zoetermeer was analyzed in this demonstration. The raw data was processed with a shifted Doppler Centroid, which is the basic MTI/SAR processing, resulting in an image with all reflections from static objects strongly suppressed, leaving only moving objects.
1. *With the velocity approximately known, the position of the targets on the A12 was calculated.*
2. *A composite image was made using the SAR image, on which the detected targets are superimposed with there respective velocities.*
3. *With these results it has been demonstrated that it is possible to detect fast moving targets with PHARUS.*
4. *The minimal detectable velocity is about 20 km/h. Detection of much slower targets requires more sophisticated MTI techniques, which in turn require modifications of the PHARUS system. On the short term, experiments are foreseen without significant hardware changes, making use of the fact that different parts of the antenna can be switched on and off, thus 'simulating' two antennas. The next step would be to modify the radar, so that it can receive of different parts of the antenna simultaneously, but through separate receiving channels. In this way, very powerful SAR/MTI modes could be realised with the PHARUS system.*

b) Jamming
A PHARUS was distorted with a simple jamming device and model calculations were performed. Secondly, it was tried whether the effects of jamming can be removed by appropriate filtering.
1. *With the jamming ground features were hidden*

2. *The image is degraded around the main beam.*
3. *There is a reasonable resemblance between prediction and test outcome.*
4. *With the aid of a filtering technique the part of the image that was initially screened by the jammer was revealed, which gave a slightly distorted image.*
5. *The results of the jamming experiment were in accordance with the model predictions; the model could be partially verified this way.*
6. *It was shown that a very simple jammer has limited effectiveness against the PHARUS system, due to the fact that*
   1) A small image region is affected
   2) Only 2 out of 4 polarimetric channels are affected
   3) The jamming signal can be detected and removed. The latter will become more difficult when the jamming power is increased, and the signal is randomised in some way, giving it a wider spectrum.

Crop classification:
A crop type classification was performed on a PHARUS image, obtained at the Zuidland test area. 194 fields were studied and selected classes were: onion, beet, cabbage, bare soil, grass, barley, potato, and wheat.

1. *All pixels inside a field were used to construct a feature vector for the crop type classification. The constructed vector comprises all relevant elements of the polarimetric covariance matrix, and gives full information on the polarimetric information of a field.*
2. *139 fieldswere correctly classified (71.7%)*
3. *An exception to the above number must be made for cabbage fields in which the plants have recently sprouted. These fields may be mistaken for bare soil fields as they have a feature vectors that are close to the class mean of bare soil. It was found that about 50% of the cabbage fields were confused with bare soil.*
4. *It was found that the distance between a feature vector and the class means plays just as an important role in the classification as the class covariance matrices. Neglecting the class covariance matrices reduces the overall result of correctly classified fields from 71.7% to 38.1%.*

Forestry:
Two PHARUS images of the Reichswald were acquired, which is a mixed deciduous and coniferous plantation forest located in Germany. A database with 150 samples (stands) was constructed covering 7 forest classes. This database was used to assess classification possibilities using a maximum likelihood procedure.

1. *For 7 selected forest types the mean backscatter values for HH-, HV- and VV-polarization do not correspond to values expected for C-band radar. This is because the radar data were not calibrated.*
2. *A classification result of 81.3% for a multi-temporal observation is found, which is not very high. This is due the the small dynamic range in backscatter of trees at C-band.*
3. *The results show that classification of forest stands in a mixed deciduous-coniferous forest plantation is well possible. A multi-temporal approach is superior to a mono-temporal approach and may be required to meet user requirements for accuracy.*
4. *Absolute calibration is still a point of concern. The backscatter values deviate strongly from expected values. Moreover, there seems to be an imbalance between the backscatter values in the different channels for the June 1997 image.*
5. *To take full advantage of the special possibilities of PHARUS, which are the high spatial resolution and the polarimetry, more study is needed.*
6. *To study polarimetry and the possibilities for geo- and bio-physical parameter retrieval with physical or semi-empirical models a good polarimetric and absolute calibration*

Precision agriculture:
A PHARUS image was taken of the van Bergeijk farm at the Zuidland test area. A detailed soil survey was carried out and the data were stored in a georeferenced relational database. The image was visually analyzed and compared to the ground data.

1. *Clear differences could be observed among different crops*
2. *Spatial variability within fields, which is the main topic in precision agricultrure, was not detected with PHARUS.*
3. *For the use in precision farming PHARUS seems not very promising. Lack of spatial resolution may be one reason. Not detecting the appropriate crop characteristics seems the most important reason.*
4. *Later in the growing season when drought effects are generally more significant PHARUS images will probably show more detail, However, precision farming is mainly dealing with the detection of differences in an early phase of the growing season to allow management adaptations.*

Data quality control and evaluation of the use of PHARUS:
The quality of the data was examined and the data were compared with system specifications.

1. *An analysis of the system performance revealed that the system characteristics are in agreement with the original specifications.*
2. *A calibration of the data was performed for the system evaluation.*
   - *Results show that steps in the overall calibration procedure like phase calibration and cross-talk removal can successfully be performed on PHARUS data.*
   - *Uncertainties in gain imbalance and absolute calibration should be be improved. This improvement is possible by means of a series of antenna measurements and a new GSP version, which accounts for the beam elevation angle.*
3. *A large amount of data has been acquired, also for PR activities, for instance on the potential Indonesian market.*
4. *An important lesson was learned on the use of the aircraft on which PHARUS is deployed. This use has two major limitations:*
   I. *Because of a shared ownership it is not always available, which has put constraints on the time critical agricultural applications.*
   II. *Another constraint on the use of the PHARUS system is the occurrence of ice accretion, in that case the aircraft is not certified and the flight must be cancelled.*

<u>Conclusions</u>
The following main conclusions were drawn from the study.

1. *Technical problems occurred during the data acquisition which could be solved so it has been possible to collect data for the applications. However, no usable data for oill spill detection were acquired. The other applications could successfully be demonstrated.*
2. *The results from the applications tidal areas and precision agriculture were not satisfactory. It is expected that the results will improve if a temporal analysis is applied.*
3. *The results of the applications have been obtained with relatively little effort. It is therefore concluded that the user friendliness of the PHARUS products is acceptable. Nevertheless, suggestions were made during the program, which further facilitate the use of these data.*
4. *The PHARUS team has improved its knowledge considerably on the use of PHARUS, this has led to to an improvement plan (PHARUS beheersplan).*
5. *The logistics involved with the PHARUS flights are difficult because the platform is not always available.*
6. *There is a clear need for more images, conclusions drawn for some applications are weakened due to the low number of images used.*

Recommendations

With respect to the conclusions and results the main recommendations are given below:

1. *The user requirements and preferences which concern the calibration of data should be made clear because the calibration of PHARUS is an intensive task.*
2. *The planning of the PHARUS flights must be agreed upon between the different users of the aircraft, well in advance of the actual flight itself. A procedure should be developed for this planning.*
3. *The current platform for PHARUS should be certified for most weather conditions, in particular ice accretion.*
4. *It is further recommended to perform an additional data acquisition program to complete the introduction of PHARUS products for the (Dutch/international) user market.*

Acknowledgements

First of all the people who are involved with the operation of the PHARUS system are acknowledged. In particular the operator who has to work in a limited space and who had to deal with strong stress situations during the first Familiarization flights.
SYNOPTICS is thanked for the collection of ground data at the Zuidland test site.
The PHARUS team should be mentioned because of their efforts in the solving of the technical problems.
Finally the BCRS is thanked for the financial contribution to this program.

Contents

1. Introduction

1.1 *Scope and objectives of the PHARUS Familiarization program*

The PHARUS polarimetric SAR is an airborne synthetic aperture radar system, developed by TNO Physics and Electronics Laboratory (TNO-FEL), in cooperation with the National Aerospace Laboratory and the Delft University of Technology (DUT). PHARUS stands for Phased Array Universal SAR.

The development of PHARUS finished in 1995. PHARUS is the successor of the PHARS (Phased Array Rehearsal SAR) system, which was actually a testbed version of PHARUS. PHARS became operational in 1990 and a number of flights has been performed since that event. PHARS is a compact small weight system, capable of generating images with a resolution of 6 meters in VV polarization. Compared to PHARUS, it has a smaller number of SAR applications, with PHARUS this number is increased significantly.

Compared to PHARS PHARUS has an increased swath, increased resolution and increased range of incidence angles, but above all it is fully polarimetric. This last important feature improves many of the applications of SAR. It will give better tools for discrimination of targets/surfaces and provides additional information on the backscattering- properties of the objects in the swath.

The most important features of PHARUS are:

- **Polarimetry**

By sending respectively horizontally and vertically polarized electromagnetic waves, and receiving simultaneously horizontally and vertically polarized electromagnetic waves, the system has become a fully polarimetric system. Four channels are recorded: HH, HV, VV and VH. The first letter indicates the received polarization and the second letter indicates the transmitted polarization. These polarizations form a linear base which permits to synthesize any other polarization. Polarimetry is an important system property for applications like crop classification, decreased jammer efficiency and many other applications.

- **Phased array antenna with active Transmit/Receive modules**

The phased array antenna allows fast beam steering capabilities for: unwanted aircraft movements, spotlight mode and Moving Target Identification (MTI) capabilities.

With the arrival of the PHARUS system new polarimetric data sets have become available in the Netherlands. Consequently the user community can obtain more experience with these type of data. It is the goal of the PHARUS Familiarization program to familiarize the SAR user community in the Netherlands with the new sensor. Of course this does not only apply to the polarimetric property of PHARUS, but also to the other enhanced features.

Under supervision of the BCRS a group of potential users of the PHARUS has had a number of meetings in order to provide input to the PHARUS project team on user requirements. The organizations represented in this group are: BCRS, Min. of Defence, NIVR, NLR, RWS-MD, RWS-DNZ, RWS-RIKZ, WL, WAU and TNO-FEL. Within this group the use of the PHARUS system has been discussed in detail. This has led to a selection of military and civil applications for the demonstration of the capabilities of PHARUS.

A technical system evaluation and data quality control was also part of the project: it has been the first opportunity to analyze the performance of PHARUS in a wide range of modes. Since the data acquisition in this project has been the first full deployment of the PHARUS system, occasional technical problems were to be expected. Therefore, the system evaluation

was necessary to be able to provide the users with data concerning the quality of delivered data.

In summary the main purpose of this project is to demonstrate the enhanced capabilities of PHARUS for a variety of applications and to provide potential users with sample data.

1.2 *Approach*

For the acquisition of the data a flight plan was defined. Five flights were originally scheduled with PHARUS mounted under a Cessna Citation. Since there were technical problem at the beginning of the project, a total of seven flights had to be performed.

Special attention was given to the supply of information concerning the data acquisition, the possibilities of PHARUS and the system characteristics. The users involved in this project have been provided with additional technical and practical information on PHARUS during a kick-off workshop, held at TNO-FEL. With the information presented at this workshop the desired modes of operation for each specific application could be determined. During the program the users have been approached individually for the determination of the necessary requirements for the data and acquisition of the data.

The selected applications are grouped as follows:

1. Cartography
   - 1.1. Land use classification
   - 1.2. Cartography in tidal areas
   - 1.3. Road detection
2. Maritime applications
   - 2.1. Oil spill detection
   - 2.2. Bottom topography
   - 2.3. Detection of ships and ship wakes
3. Target detection
   - 3.1. Detection of objects (buildings, vehicles) on land
4. Agriculture and forestry
   - 4.1. Crop classification
   - 4.2. Forestry applications
   - 4.3. Crop yield

Table 1.2-1 gives an overview of the familiarization flights. Data acquired during two flights in the framework of other projects, could also be used for two applications. Table 1.2-2 lists these two flights.

Flight number	applications	date
PV07	Precision farming, Land use, Crop classification, Target detection, Forestry	16-7-96
PV08	Ship and wake detection, Oil spill detection, Cartography in tidal areas, Technical evaluation	16-7-96
PV09	Sea-bottom topography, Cartography in tidal areas	27-8-96
PV13	PR flight over Wageningen, Crop classification, Precision agriculture, Ship and wake detection, Technical evaluation	29-5-97
PV14	Land use, Target Detection (jamming) and PR flight	29-5-97
PV15	PR flight over Freiburg area	30-5-97
PV16	Cartography in tidal areas, Technical evaluation, Target detection (MTI), Forestry, PR flight over Heerde area	2-6-97

Table 1.2-1 The seven PHARUS flights for the Familiarization program.

Flight number	applications	date
PV05	Road detetcion	25- 4-96
PV10	Forestry	12-10-96

Table 1.2-2 PHARUS flights outside the Familiarization program, during which data used for the familiarization was acquired.

Image acquisition
Several steps were performed for the image acquisition:
1. Determination of user requirements;
2. Definition of PHARUS mode (system parameters, altitude);
3. Definition of flight trajectory (test site location, planning, flight direction);
4. Pre-flight system check;
5. Flight operations (communication with Air Traffic Control and other logistics);
6. Data acquisition;
7. Data pre-processing and precision trajectory calculation;
8. Flight data processing;
9. Data pre-processing check;
10. Data format transformation, merging with flight data;
11. Data quality check;
12. SAR processing;
13. Image quality check
14. (Optional) polarimetric and/or absolute calibration;
15. Image distribution;
16. Supply of image characteristics to users, and other support.

The steps mentioned above summarize the necessary actions for the data acquisition. The steps illustrate the followed procedure, which was developed during the project.

From the user requirements it became apparent that the following additional logistic actions were necessary:
1. Creation of oil spill;
2. Operation of transponders;
3. Co-operation with a marine vessel;
4. radio communication with a marine vessel (Ship and wake detection);
5. radio communication with another aircraft (Oil spill detection);
6. radio communication with a ground crew (System performance);
7. Co-ordination of ground data acquisition;

These actions were not all foreseen in the original approach but during the project it became clear that some actions would simplify the data acquisition significantly, because several time critical applications had to be combined in a single flight. For instance the creation of an oil spill was not part of the project but it could be realized because of the co-operation of RWS-DNZ. This facilitated the data acquisition since the originally planned stand-by period of a week for the oil spill detection was difficult to schedule with the other applications.

1.3 *Presentation of the results*

Apart from the users already involved, it is an aim of the project to gain the interest of other potential commercial users. Since this is a demonstration phase of the PHARUS system, where its capabilities are demonstrated for the first time, the commercial involvement has consisted of participation in a final workshop. During this final workshop results for all applications have been presented by the involved PHARUS users to potential commercial

users. Furthermore, the data and results from this project have been used in a study, which focused on the commercial possibilities of the PHARUS system (Ritt-Fischer et al., 1997).

This report contains a detailed description of the results for the applications, obtained with the PHARUS data. In chapter two the cartographic applications are described. Chapter three contains the results of the maritime applications. Chapter four deals with the military applications and in Chapter five the agriculture and forestry applications are demonstrated. Chapter six contains the results on the data quality control and evaluation of the system performance, and includes a paper on the calibration of PHARUS. Chapter seven summarizes the main conclusions and recommendations of the report.

1.4 *References*

Ritt-Fisher, M.R., Halsema, D. van, Pouwels, H., and G.J. Wensink, 1997, PHARUS Market Assessment. Final report. BCRS-report 97-17, Delft, The Netherlands.

2. Cartographic application demonstration

The purpose of this group of demonstrations is to highlight the potential of PHARUS for cartographic applications. An important issue here is the geometrical integrity of the SAR imaging process, as well as the positioning of the image in a reference co-ordinate system. At the same time these demonstrations inform the potential users on the possibilities in swath width and resolutions.

2.1 *Land use classification*

2.1.1 Introduction

On 29 May 1997, a measurement campaign was conducted with the airborne PHARUS synthetic aperture radar of TNO-FEL/NLR/DUT. Polarimetric radar data were collected over Fochteloeërveen and over the Buitenland polder. The main part of these test sites consists of agricultural fields although the Fochteloeërveen site also contains urban areas and natural surroundings, mainly moor and forest. The aim of this section is to show that the PHARUS data can be used for a general land use classification (and even for a more detailed crop type classification as discussed in Section 5.1).

For a numerical verification of the classification results it is obvious that we need ground truth measurements. In case of the Buitenland test site (Section 5.1) such measurements were provided by Synoptics. The measurements were mapped onto a GIS data base so that fields (represented by polygons) could be created. The essence of the classification procedure then is to classify a number of agricultural fields into a selected number of crop types using some type of a Bayes classifier. With the Fochteloeërveen data, however, the ground truth was not known. Hence, no fields could be created and the land use classification scheme has to be based on pixels using the classifier of (Lee et al., 1994). Also, verification of the results has to be done by eye instead of numerically. For the land use classification in this section (as well as the crop type classification of Section 5.1) we prescribed the number of classes so that the classification procedure used here is that of supervised classification. Such in contrast with unsupervised classification where the samples are unlabelled (Duda and Hart, 1973).

2.1.2 PHARUS polarimetric radar data

The purpose of this section is to briefly describe the polarimetric radar measurements on which the classification scheme of the Fochteloeërveen test site as well as that of the Buitenland test site (Section 5.1) are based. The PHARUS data are fully polarimetric C-band radar measurements which means that full information on the complex scatter matrix S is obtained. Hence, a measurement at each pixel of the radar image may be written as:

$$S = \begin{pmatrix} S_{hh} & S_{hv} \\ S_{vh} & S_{vv} \end{pmatrix} \qquad (2.1.1)$$

With the elements of the scatter matrix, the indices h and v refer to horizontal and vertical polarization respectively. For instance, S_{hv} is measured by transmitting a vertically polarized radar pulse and receiving the backscattered signal with a horizontally polarized antenna. For a monostatic SAR, i.e. a radar system of which the positions of the transmit and receive antennas coincide, the scatter matrix may be shown to be symmetric (e.g. Groot, 1991).

Therefore, neglecting the unimportant absolute phase of the radar signal, the scatter matrix consists of five parameters of interest (three amplitudes and two relative phases). A set of parameters that is frequently used consists of the amplitudes of S_{hh}, S_{hv}, and S_{vv} , and the phases of S_{hv} and S_{vv} with respect to the phase of S_{hh}.

A covariance matrix P associated with the scatter matrix elements is obtained by performing the vector multiplication:

$$P = \begin{pmatrix} S_{hh} \\ S_{hv} \\ S_{vv} \end{pmatrix} \begin{pmatrix} S^*_{hh} & S^*_{hv} & S^*_{vv} \end{pmatrix} = \begin{pmatrix} S_{hh}S^*_{hh} & S_{hh}S^*_{hv} & S_{hh}S^*_{vv} \\ (S_{hh}S^*_{hv})^* & S_{hv}S^*_{hv} & S_{hv}S^*_{vv} \\ (S_{hh}S^*_{vv})^* & (S_{hv}S^*_{vv})^* & S_{vv}S^*_{vv} \end{pmatrix} \qquad (2.1.2)$$

For the matrix P there exists no commonly-used name. In this report, the matrix P will be referred to as the *polarimetric* covariance matrix; this to avoid confusion with the *class* covariance Σ introduced in Section 5.1. The polarimetric covariance matrix serves as input for the land use classification scheme while it also provides the feature vector for the crop type classification of Section 5.1. In the conversion from slant-range to ground-range co-ordinates, multilook images are obtained (number of independent looks is about 5) with a pixel size of approximately 3 m and a ground-range resolution of about 3.5 m. To obtain sufficient statistics and to reduce the effect of speckle in the radar measurements, the average of a number of covariance matrices over a certain area is used instead of (2.1.2):

$$\begin{aligned} C = < P > &= \begin{pmatrix} < S_{hh}S^*_{hh} > & < S_{hh}S^*_{hv} > & < S_{hh}S^*_{vv} > \\ < (S_{hh}S^*_{hv})^* > & < S_{hv}S^*_{hv} > & < S_{hv}S^*_{vv} > \\ < (S_{hh}S^*_{vv})^* > & < (S_{hv}S^*_{vv})^* > & < S_{vv}S^*_{vv} > \end{pmatrix} \\ &= \begin{pmatrix} \sigma_{hh} & 0 & \sigma_{hhvv}\exp[i(\phi_{hh}-\phi_{vv})] \\ 0 & \sigma_{hv} & 0 \\ \sigma_{hhvv}\exp[-i(\phi_{hh}-\phi_{vv})] & 0 & \sigma_{vv} \end{pmatrix} \end{aligned} \qquad (2.1.3)$$

In the above equation, "<>" denotes averaging over all pixels inside the area. Notice that the elements of the polarimetric covariance matrix C are in terms of power, i.e. are proportional to the squared amplitude of the scattering matrix elements. The σ terms are called the scattering coefficients (units of m^2) whereas the ϕ terms are referred to as the phases. Due to the averaging over all pixels, the off-diagonal elements of C (denoting the co-cross correlation) may be taken zero for extended natural objects (van den Broek and Groot, 1996). Inspection of a number of polarimetric covariance matrices confirmed the smallness of these terms. With the Fochteloeërveen data, the polarimetric covariance matrices were averaged over cells of 5 by 5 pixels so that a number of looks of approximately 50-100 is obtained.

2.1.3 Description of the Fochteloeërveen test site

The Fochterloeërveen site is situated west of the city of Assen. The geography of the test site is quite diverse in the sense that it contains agricultural fields as well as urban areas and natural surroundings. As shown in Figure 2.1-1, the Fochterloeërveen SAR data were processed in 3 parts which will be referred to as Focht_A, Focht_B, and Focht_C. The urban area in Focht_A and Focht_B is the city of Assen. The dimensions of the 3 test sites are given

in Table 2.1-1 from which it follows that each of the test sites measures approximately 8 km in x direction and 7 km in y direction (3.5 m resolution). The black spots in the plots are because of excessive aircraft movements during which the SAR lost track of site. Notice that besides agricultural fields and urban areas, the test sites also contain forest (e.g. middle of Focht_C) and moor grown with heather (e.g. bottom half of Focht_C).

test site	*x* by *y*	pixel size (m)
Focht_A	2520 x 2302	3.2
Focht_B	2660 x 2310	3.2
Focht_C	2580 x 2311	3.2

Table 2.1-1: Dimensions of Fochteloeërveen test sites.

2.1.4 Classification results

Before presenting the classification results it is important to realise that there is a principal difference between the classification of the Fochtelooeërveen data and that of the Buitenland data (Section 5.1). The difference is that in case of the Buitenland test site we know the exact ground truth and in case of Fochteloeërveen we do not. This means that the number of classes for the Fochteloeërveen test sites had to be determined by eye, i.e. by inspection of the plots in Figure 2.1-1 compared, e.g., with a topographic map. Because fields with the same vegetation can look slightly different, inspection by eye might raise the problem of introducing false classes. To avoid this problem we will only distinguish between broad variations in vegetation, like grass or forest, and not between different crop. Hence, in case of Fochteloeërveen, the number of classes will be limited and it is more appropriate to speak of a general land use classification in contrast with the crop type classification presented in Section 5.1. Not exactly knowing the ground truth also means that we do not know which pixels belong to one and the same field. Hence we cannot compute feature vectors x that are input to the Bayes classifier used in Section 5.1 which only have meaning if they are derived from a polarimetric covariance C (2.1.3) that was determined from a large number of pixels (typically a few thousand per field). Hence, in contrast with the Buitenland site, the Fochteloeërveen sites are not classified on a field basis but on a pixel basis. Obviously this means that we cannot use the Bayes classifier and thus need a different classifier for which we shall use that of (Lee et al., 1994). According to the classifier of (Lee et al., 1994), the discriminant in pixel x with respect to class k is given by:

$$g_k(x) = -\ln|C_k| - trace(C_k^{-1}P) \qquad (2.1.4)$$

where $P(x)$ is the polarimetric covariance of pixel x and C_k is the average polarimetric covariance pertaining to class k. Pixel x is assigned to that class with the largest value for the discriminant.

For each of the three Fochteloeërveen test sites we identified 6 classes as shown in Table 2.1-2. For each test site separately, the C_k were computed according to (2.1.3) from a training area (identified by eye) of a few hundred pixels. Because of the black spots caused by the excessive movements of the aircraft, only the left half of each test side was used for the classification (see Figure 2.1-2 to Figure 2.1-4). Figure 2.1-2 to Figure 2.1-4 also show the classification results of the three test sites where it should be mentioned that to reduce the effect of speckle on the classification results, the classification was not performed on individual pixels but on small cells of 5 x 5 pixels (16 m x 16 m areas). The classification results may be summarised as follows:

- some bare soil fields are confused with moor or with grass
- the outskirts of lakes are confused with moor and sometimes with bare soil
- shadow areas behind forests are confused with water and sometimes with moor or bare soil

An explanation of these results will be given in Section 2.1.5.

no.	class	colour
1	water	blue
2	urban	red
3	forest	dark green
4	grass	light green
5	bare soil	brown
6	moor	pink

Table 2.1-2 Land use classes of Fochteloeërveen test sites.

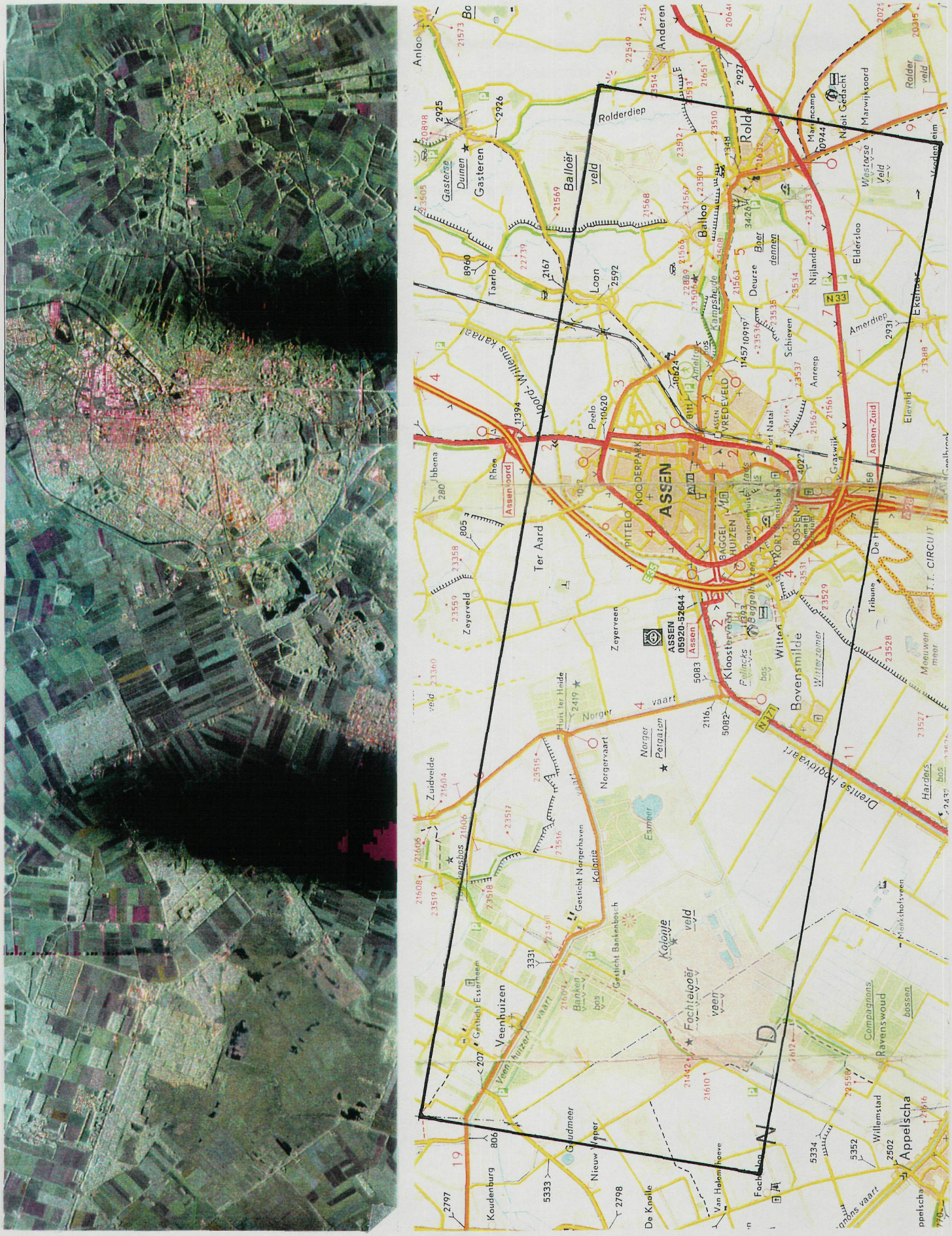

Figure 2.1-1: The three Fochteloeërveen test sites. With the polarimetric image (left) red=HH, green=HV, blue=VV. The right plot shows a map of the city of Assen (scale 1:100,000).

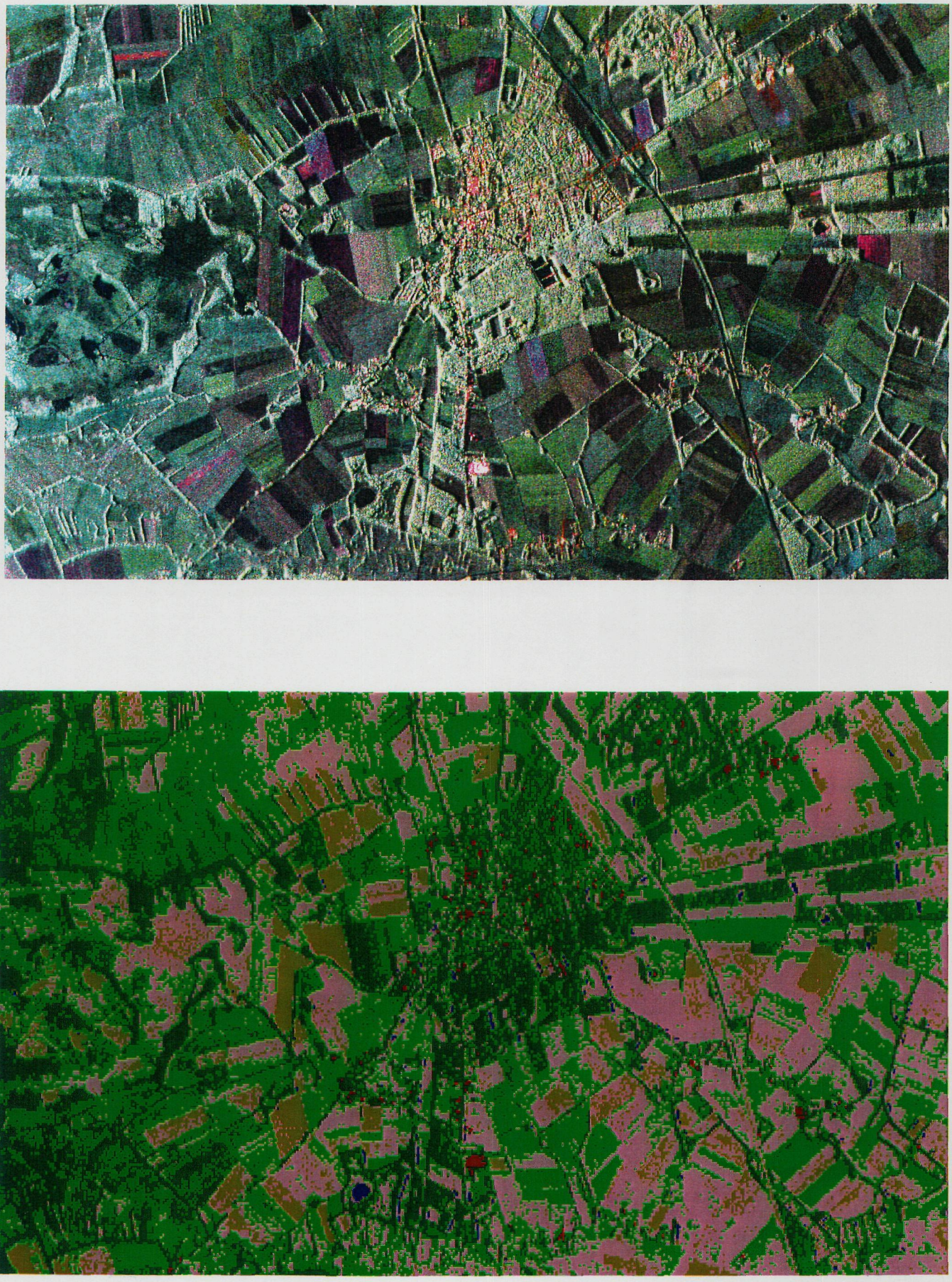

Top

Figure 2.1-2: Focht_A test site (top) and classification result (bottom). With polarimetric image red=HH, green=HV, blue=VV.

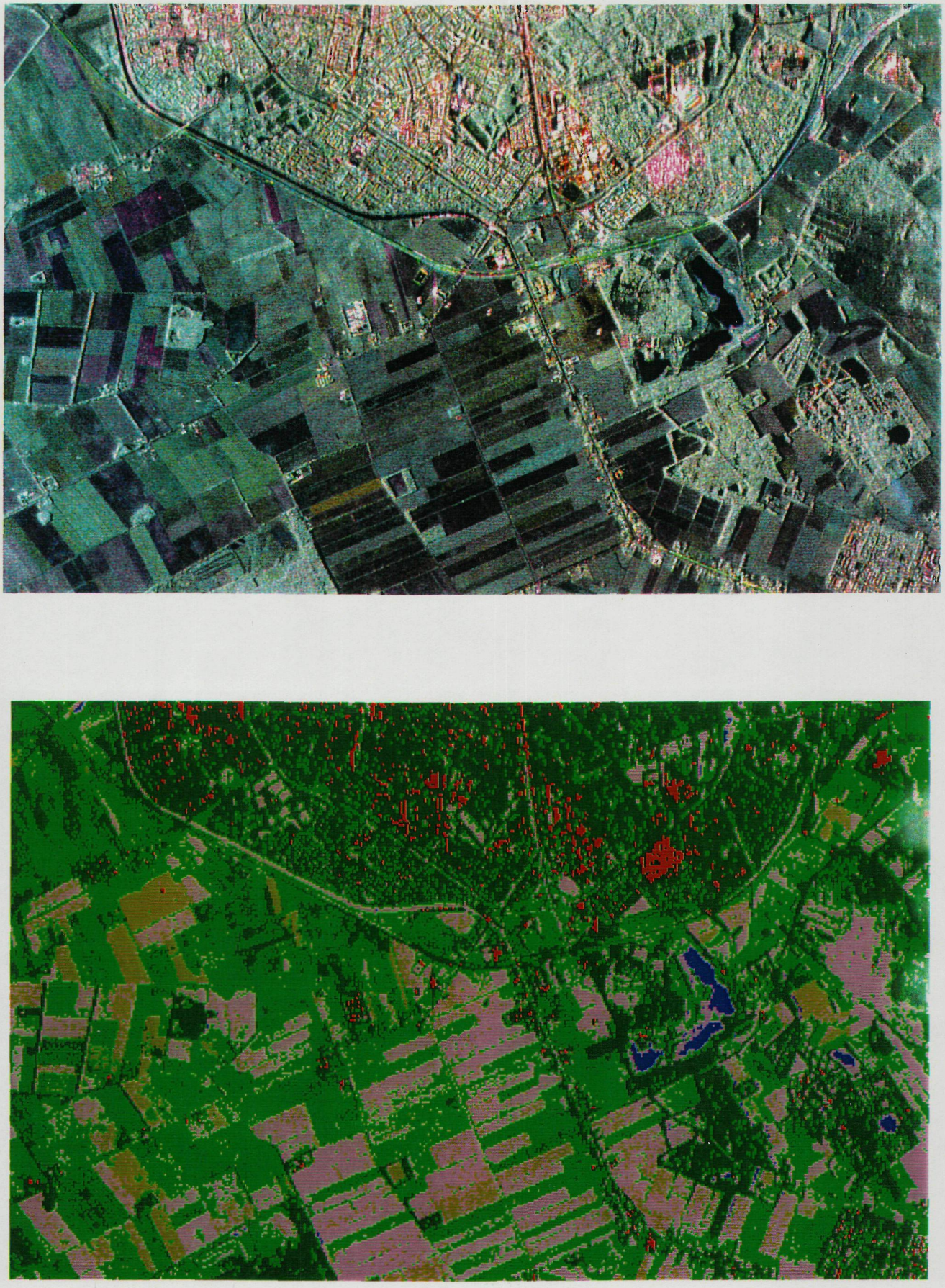

Top

Figure 2.1-3: Focht_B test site (top) and classification result (bottom).

Top

Figure 2.1-4: Focht_C test site (top) and classification result (bottom).

2.1.5 Analyses

The classification of a cell of pixels depends on the information contained in the polarimetric covariance matrix. This information consists of the channel intensities of the cell; $<S_{hh}S_{hh}^*>$, $<S_{hv}S_{hv}^*>$ and $<S_{vv}S_{vv}^*>$, the overall intensity (sum of the channel intensities), and the phase differences of the channels; arg($<S_{hh}S_{vv}^*>$) and arg($<S_{hv}S_{vv}^*>$). The overall intensity corresponds with the brightness of a polarimetric image like Figure 2.1-1. The proportion of the channel intensities is responsible for the colour in the image, e.g. if the *HH*, *HV*, and *VV* channels are fed to the red, green, and blue colour channels respectively, the image will appear red if *HH* is significantly larger than *HV* and *VV*. The phase differences do not appear in the image. Several experiments with the Lee classifier have shown that for a land use or crop type classification most of the polarimetric information is contained in the overall intensity. The channel intensities are less important although their proportion plays an important role in separating classes that have about the same overall intensity. This illustrates the importance of using polarimetric radar images for classification purposes. The phase differences contain very little information for a classification scheme.

To explain the results of the land use classification we will focus on the overall intensity. For each class of each test site, Table 2.1-3 gives the overall intensities derived from the C_k (characteristic for all polarimetric covariance matrices of a class k). This table shows that there are considerable differences between the class intensities within a test site so that the classes can be well separated which explains the success of the land use classification. Notice that although the intensity of one class may differ significantly with test site (e.g. the class "urban"; 68.1 for Focht_C and 241.2 for Focht_B). However, the importance for a correct classification are the proportions of the classes' overall intensities within one and the same test site. Also notice the low overall intensity of water which is caused by the small amount of back scattering from the flat water surface.

From Table 2.1-3 it is seen that the overall intensities of the classes "grass", "bare soil", and "moor" are close. However, it was found that the combined polarimetric information of overall intensity and channel intensities is enough to separate these classes. This is demonstrated by the fact that most fields of these classes are correctly classified and that confusion is only among a small number of fields. The reason why some of the bare soil fields were confused with moor or grass was found by a close inspection of Figure 2.1-2 to Figure 2.1-4 which showed that these fields were sparsely grown with meadow or grass.

The confusion of water with moor/bare soil in lake outskirts was found to be caused by the way the radar data are processed. The processing is based on an algorithm that tries to disentangle reflections from neighbouring pixels as well as possible. However, spill over of the reflected radar signal cannot be completely avoided so that a pixel will always contain part of the reflection of a number of neighbouring pixels. This explains the side lobes of the bright reflection that can be seen in the middle of Figure 2.1-3. Spill over usually occurs whenever there is a steep gradient in intensity, e.g. at the transition from land to water. As a consequence of spill over of pixels on the shore, the intensity of water in the outskirts was found to be slightly higher than that at the middle of the lakes and comparable to that of moor and bare soil. Notice that because of spill over, the smaller lakes, e.g. at the top-left of Figure 2.1-4, are entirely classified as moor/bare soil.

For shadow areas behind forests, the overall intensity was found to be comparable to that of water and in some cases to that of moor or bare soil so that shadow areas (for which no separate class was defined) are often mistaken for these three classes. The information offered by the channel intensities of these classes is apparently not strong enough to separate them. The obvious reason why shadow has the same intensity as water is that no reflections

are received back at the radar from shadow areas. In case there is spill over from the forest canopy, the shadow areas may be classified as moor or bare soil for the same reason as with the lake outskirts.

no.	class	Focht_A	Focht_B	Focht_C
1	water	0.3	0.2	0.2
2	urban	122.8	241.2	68.1
3	forest	8.2	6.8	10.5
4	grass	4.3	3.8	5.8
5	bare soil	3.2	4.2	4.1
6	moor	2.2	1.6	3.2

Table 2.1-3 Overall intensities (units of m^2) of the classes of the three Fochteloeërveen test sites.

2.1.6 Conclusions

Land use classification of the three Fochteloeërveen test sites gives good results for all six classes; water, urban, forest, grass, bare soil, and moor.

A small number of bare soil fields are grown with heather or grass so that the pixels in these fields are erroneously classified as moor or grass.

Spill over of radar reflection of a pixel to neighbouring pixels causes the lake outskirts to get an overall intensity comparable to that of moor or bare soil. As a consequence, the outskirts of lakes may be confused with these two classes.

From shadow areas behind forests no radar signal is scattered back. As a consequence, these areas are classified as water and in case of spill over from the canopy with moor or bare soil.

2.1.7 References

van den Broek, A.C., Groot, J.S., Results of the SIR-C/X-SAR 1994 campaign: Test site Flevoland, report 95-25, BCRS, February 1996.

Duda, R.O., Hart, P.E., Pattern classification and scene analysis, John Wiley & Sons, 1973.

Groot, J.S., Introduction to radar polarimetry, report FEL-91-B122, TNO Physics and electronics Laboratory, April 1991.

Lee, J.S., M.R. Grunes, R. Kwok, Classification of multi-look polarimetric SAR imagery based on complex Wishart distribution, Int. J. RS., vol. 15, no. 11, pp. 2299-2311, 1994.

2.2 *Cartography in tidal areas*

2.2.1 Introduction to mapping in tidal areas

The importance of mapping intertidal areas well

Intertidal areas are unique natural regions in the Netherlands. There are a small number of intertidal areas in (the southern province of) Zeeland, although the best known is of course the northern Wadden Sea. Like all other stretches of Dutch coast the intertidal areas are susceptible to change due to natural and human influences. It is important that these changes and their nature be observed quickly and accurately so that any correction steps can be taken as rapidly as possible. A sound general overview is also necessary if the area is to be managed efficiently and effectively.

To be in a position to monitor and manage an area it is necessary to survey its condition regularly. That is currently achieved by ships equipped with acoustics systems which sail for the lines of direction of points (for a detailed summary see 'Definition Study RWSBAS, 01/1996, MD-GAR, H2'). For these methods account has to be taken of ebb and flow and the limited depth at many places in the intertidal areas. For places which are inaccessible for shipping a field observer must measure the depth 'manually'. The difficulty of doing this and the time it demands means that such measurements are only carried out every three or five years. For the intertidal areas in particular this is too long an interval. Changes come much too fast.

Experiments with altimetry

Remote sensing methods have undergone a period of very rapid development over the past few years. If these developments continue the technical characteristics of the various methods will meet the demands and wishes of RWS in relation to mapping intertidal areas in the foreseeable future. For application analyses altitude shots have been made of the 'Groote Plaat' area west of Terschelling with the following technologies:

-aircraft laser altimetry,
-RWBAS with ERS,
-Terrestrial measurements,
-Conventional soundings,
-GPS soundings and
-Radar interferometry-altimetry (PHARUS).

This report is an evaluation of altimetry (the creation of a DTM) using radar images. These measurements are carried out from a aircraft, with the PHARUS radar sensor. PHARUS stands for polarimetric PHased ARray Universal Sar (specifications in section 2.2.2.1). The MD has one image from 27 August 1996 and one image from 2 June 1997.

OBJECTIVES OF THE STUDY

The objective of this study is to reach a judgement on the suitability of PHARUS images in the automatic production of a digital terrain model (DTM) for intertidal areas. The DTM could be produced by combining waterline maps for a specific moment with the water level at the same moment. We examine whether the images are suitable for automatic waterline detection. This must be carried out in a uniform, consistent manner bearing in mind demands as to precision.

2.2.2 PHARUS characteristics, recording conditions and data processing

2.2.2.1 **PHARUS characteristics**

The PHARUS sensor is a polarimetric SAR radar. SAR stands for Synthetic Aperture Radar. PHARUS hangs under an aircraft or satellite and looks 'to the side'. Polarized radar pulses are sent out by the sensor. When the returned (reflected) pulses are received note is taken of polarization, and differences in phase and amplitude. Modern orientation systems determine the position of the aircraft and the radar beam in relation to the aircraft. So the sensor views an area alongside the aircraft, which changes in a strip due to the movement of the aircraft. By processing the signal the strip is subdivided into pixels.

Different substances reflect the polarized beam in different ways. Water and land for instance, or different plants. By calculating the phase of the returned signal the distance between the aircraft and the reflecting substance can be determined. This makes it possible to create a DTM from a PHARUS image, for which all kinds of 'extra' characteristics, which are revealed by polarization.

The PHARUS system consists of three modules:
- The radar sensor on the exterior of the aircraft,
- The digitalisation, compression and photograph equipment on board of the aircraft and
- The flight data and radar data processing system 'on the ground'

These modules are in turn subdivided into (sub)modules. PHARUS' modular architecture means the system is simple to extend or adapt to specific user demands.

By combining a PHARUS radar image with current models for instance it is also possible to determine depth under water. This (extra) characteristic makes the system attractive as a system for intertidal areas and somewhat deeper waters (up to +/-10 meters).

Below the most important specifications of the PHARUS sensor have been bulleted (see PHARUS manual, 06/1996, TNO/NLR/TUD for complete specifications):

-Radar type:	Coherent pulse radar
-RF carrier wave:	5.3 GHz
-Pulsing frequency:	2000 to 5000 Hz
-Pulse length	3.2 to 25.6 μs
-Band width:	programmable
-Angle of photograph:	24^0
-Resolution:	up to 3 x 3 meter
-Maximum peak sending capacity:	960 watt
-Polarisation (sending + receiving):	horizontal + vertical
-Strip width:	26 km
-Strip length:	dependent on resolution and means of storage
-Maximum flight altitude:	12 km

2.2.2.2 **Weather and flight conditions**

To enable a good assessment of PHARUS images it is important that shooting or recording conditions be known. They can be subdivided into weather conditions and flight conditions. If there has recently been rain surfaces may have different reflection characteristics, while strip width has a bearing on the resolution used. Two PHARUS shoots have been carried out in the Groote Plaat area. The first was made on 27 August 1996 and the second on 2 June 1997.

Weather conditions
Not very important since radar is basically weather independent. Weather conditions are determined from the Dutch Met Office or Internet.
Dutch Met Office: NLG33,- a day + fixed once-only costs NLG25,-. Requests to dekkercg@knmi.nl stating familiarity with the costs and phenomena needed:-precipitation,-wind,-temperature,-visibility,-humidity,-etc.

Flight conditions
Not so very important. Flight data is available for use in further processing.

2.2.2.3 Data processing

The rough data from the PHARUS sensor can be processed in various ways to obtain an end result (grey value image). The manner in which the data is processed is dependent on the wishes / demands of the client the image is the image is being made for. The quickest version is a quick-look image, which can be generated very rapidly to check the photograph which has been made. Generating very precise images can sometimes take days. The 1996 and 1997 images were both processed in the same way. The method followed is described below.

The images have been given multi-look processing. This means that the antenna bundle (the aperture) is divided into a number of smaller bundles. Multi-looking is used to reduce the speckle (caused by the coherent character of SAR). For a homogenous area in a SAR image the number of looks $L = (m/s)^2$. Here m is the average and s the standard deviation. This relation is only valid for the linear power image and not for the scaled image. Span processing (HH+HV+VV) leads to doubling of the number of looks.

→The image is scaled with the function 10*log(I)*(1/A) to a division of 0 through 255 (1 byte). Here I is the original linear power of intensities image. A is the scale factor which indicates what the pixel values are in dB. with A = 0.25 dB/count. The original linear power image can be reconstructed with the above-mentioned formula.

→Once the values have been set the image is divided into pixels in the following manner:
a. Range (cross-track) compression (perpendicular to flight axis)
   - resolution 3.4 m
   - range weighing Cosine Squared 0.5 (= Hamming 0.75)
b. Azimuth (along-track) compression (flight path)
   - resolution 3.4 m
   - azimuth weighing Cosine Squared 0.5 (= Hamming 0.75)
   - number of looks 4.9 (span 9.8)

→A number of corrections are made to the division into pixels:
-range migration to correct mistakes which occurred perpendicular to the flight axis,
-line-of-sight phase, to correct mistakes in the flight path,
-antenna (platform) motion, this is a correction to compensate the motion of the aircraft,
-antenna elevation pattern: correction of the varying altitude of the antenna,
-sigma 0 variations, an estimate of the precision of the division into pixels.

→After the above-mentioned corrections the image is geometrically corrected via the cubic spline method

→Finally the image is scaled once more.

2.2.3 Analysis PHARUS data

The PHARUS data is supplied in digital and hard copy form. The digital images are processed with the IMAGINE programme and the hard copy images are examined manually.

2.2.3.1 **Visual analysis of the plots**

A number of phenomena are to be observed on the plots, which occur as a result of mistakes during shooting with the PHARUS sensor and during the data processing. Both plots are examined for curious elements and for each of these a possible cause and solution are examined.

Characteristic	Processing element	Natural morphological elements	Artificial elements	Possible explanation
Grey value leap between two images	û			Other histogram stretch
Geometric shift on the edge of two images	û			Not corrected properly geometrically
Line structures perpendicular to the aircraft path on the western edge	û			Processing artefact due to flight movements
Spreading of objects	û			Due to movement of objects
Spreading of objects in 2 perpendicular directions	û			Processing artefact
Grey dotted line for mutually equal distance	û	û		Musselbeds
Grey value course in channel		û		Concentrations floating substances
Rib patterns on wad plate		û		Various erosion processes ebb / flow
Sharp land / water border on the wad plate		û		Various reflection characteristics land / water
Grey value course on the plates		û		Various reflection characteristics from dry and wet sand

Table 2.2-1 Observed features in PHARUS images

Visual analysis 1996 PHARUS image

The plot of the 27 August 1996 shoot consists of 2 part images which run together (see Figure 3.2-1). There is a great difference in clarity and contrast between these two parts. This difference in contrast means that the same areas have different pixel values. In the lower half in some places the sea has the same value as the wad plate on the upper half. This can be interpreted with the human eye. The computer will have some difficulty however during automatic classification. One possible solution is to equalise pixel values in both images.

Besides the difference between the two parts there are some other elements to be found on the plot. In Table 2.2-1 these elements have been listed together with their nature / cause and

possible solutions.

It can be seen that a number of elements have natural morphological or artificial causes. But most mistakes occur during the image processing. This shows that PHARUS images are not up to standard on the following points:

- Equal histogram stretch in various images
- Geometric precision (also in relation to two images which run together)
- Homogeneity of images (lines perpendicular to the flight path
- Outshining (huge reflection 'spreads out' the object)

Visual analysis 1997 PHARUS image

The 2 June 1997 image was probably shot during high tide. The Wadden sandflat has the same reflection characteristics as the surrounding sea. In the image too few elements can be ascertained, the sandflat and the surrounding sea look the same (see Figure 2.2-1). A land-water line cannot be made out in this image (for the sandflat). There are black lines which indicate the contours of the flat. This is probably caused by patterns on the water by currents occurring at places where the (higher parts of the) flat are just below the surface of the water. In visual terms then, no land-water line can be made out in this image. This means that the image is also not suitable for processing by computer.

Evaluation visual analysis

The most important outcome is that flight schedules have to be well planned; if the sandflat is under water the data contain no significant cartographic information. The classification of the images will be influenced by a number of artefacts and phenomena, as mentioned in Table 2.2-1. The spread out objects, where large-scale reflection occurred will be classified in another high pixel value. The frames are also problematic around the edges; substantial light edges can be seen. This is also classified in the other high values.

2.2.3.2 Digital analysis of the PHARUS data

The PHARUS data was examined with the IMAGINE programme. The objective of the 'digital' examination of the images was to see if it was possible to automatically filter out a water line from the (various) images. As also concluded in the preceding section, scarcely any information can be gained from the 1997 image. This is probably due to high tide in combination with hard wind / current. As a result only the 1996 image has been digitally processed. The image is first classified, then 'edge detection' is applied. Three methods were used, two with manual classification and one with automatic classification. Due to the large number of graduations in the rough image it was not possible to apply 'edge detection' here.

Classification method 1; manual in 3 classes

The first classification was manual. The processing of the rough image is explained step-by-step below. The starting image was the vertically polarized image from 1996. The image covers the whole plate, but due to the difference in intensity over the image only the upper part of Figure 3.2-1 was used.

- Firstly the image is georeferenced on a Top25 halftone card. This directs the image to north and positions it in the RD system (see Figure 2.2-2 for a combination image)
- The second step was to take the training pixels, pixels which are representative of a specific class in the area. Three middle-large areas of training pixels were found, one in the water, one on the sandflat and one on the higher flat / land.
- The following step was to actually classify the image, with the high flat / land dark brown, the wad light brown and the water blue.
- The classified image was still quite speckled. This was improved using a 7x7 pixels nearest neighbourhood filter. the results can be seen in Figure 2.2-3.
- Automatic 'edge detection' was used on the classified image.

Classification method 2; automatic in 10 classes

For this classification the 1996 image was once again used as starting image. The following steps were applied:

- The rough image was first resampled to minimise peaks and speckling. After testing the various functions the choice fell on a 5x5 matrix focal filter with a median function.
- Then the image is automatically classified in 10 classes
- Colours are assigned to the various classes (sometimes the same colours to different classes). Dark blue for deep water, light blue for shallow water, light brown for sandflats and dark brown for dry/high flats. This is divided by personal interpretation using a plot of the area.
- With a 7x7 matrix and the nearest neighbour method the division of the image is reduced again. The result can be seen in Figure 2.2-4.

Classification method 3; manual in 4 classes

Basically all processes are the same for this last method as for the previous method, except for classification another procedure is followed. The image is not classified automatically but manually. This time there are not 4 large training pixel areas, but smaller more precise areas. This makes it possible to define very precise pixel values for the various classes. The result of this method can be seen in Figure 2.2-5.

After processing as below the images are compared and an examination is made of the way automatic 'edge detection' performed. In the following paragraph this is dealt with in detail and a judgement made on the applicability of the images.

Evaluation digital analysis

The three classified images appended show that there is little difference between the results of the various methods. In all three images a land-water border is clearly visible. This border is very dependent on the training pixels chosen.

- In every image a separate set of training pixels must be taken, as not every image has an equal histogram stretch.
- In the PHARUS images equal grey values have been given to various phenomena. Current in a channel is given the same grey value as low sandflat, as the reflection characteristics are the same. In this way a sandflat may be shown in the middle of a channel.
- As the image is divided in 10 classes, the water line can well be determined by selecting the colours assigned to the classes.

The difference in value per frame means that a univocal set of training pixels cannot be determined. It is also difficult to assign colours to automatically detected classes. A solution for this would be to give all images the same histogram stretch. Due to this there is a chance that information will be lost. Relations between grey values stay the same. The conclusion of the 'digital analysis' is thus that it is not at all easy to detect automatically to determine water lines from the sandflat images. Mediation by a human interpreter is necessary for assigning the training pixels and class colours. The method can be completely automated, by indicating the values between which the pixels in the images have to be set, but that leads to information (= loss of precision).

2.2.4 Estimate of possible applications and recommendations

After extensive study an univocal conclusion can be drawn. It is not easy to automatically extract a precise DTM from PHARUS images as the images are currently supplied. This is a consequence of the large numbers of characteristic elements in the individual images and the large differences between the images themselves.

If the images can be successfully put together geometrically (the images are slightly disformed by processing), which is made more difficult in the wad area by the lack of passing points, the images have first to be more or less 'smoothed out' in terms of pixel values. Then the irregularities and curious elements are filtered away. This is scarcely possible without the mediation of human interpretation.

The images processed with IMAGINE have been well classified for the plate. A small shift in the values of the training pixels can only result in a completely different water line. That means that the water line is determined by (human) interpretation of which pixels are water and which land / wad.

All things for which a DTM cannot be automatically generated are listed below:

- Lack of good geometric connection
- Grey value differences between various images
- Many curious (spread out) elements in the image

The above-mentioned points mean that human intervention is necessary for a good classification and water line detection.

There will have to be a standard sensor calibration for the sandflat shots, so that univocal pixel values occur in different images. These values may be influenced by the weather, like rain, mist, or wind causing waves on the water.

2.2.5 References

Wicherson, R. and J. v.d. Kraan, 1995, Het gebruik van remote sensing opnamen en kleinschalige luchtfoto's bij het actualiseren van kleinschalige wegenbestanden. Delft, Meetkundige Dienst, maart 1995.

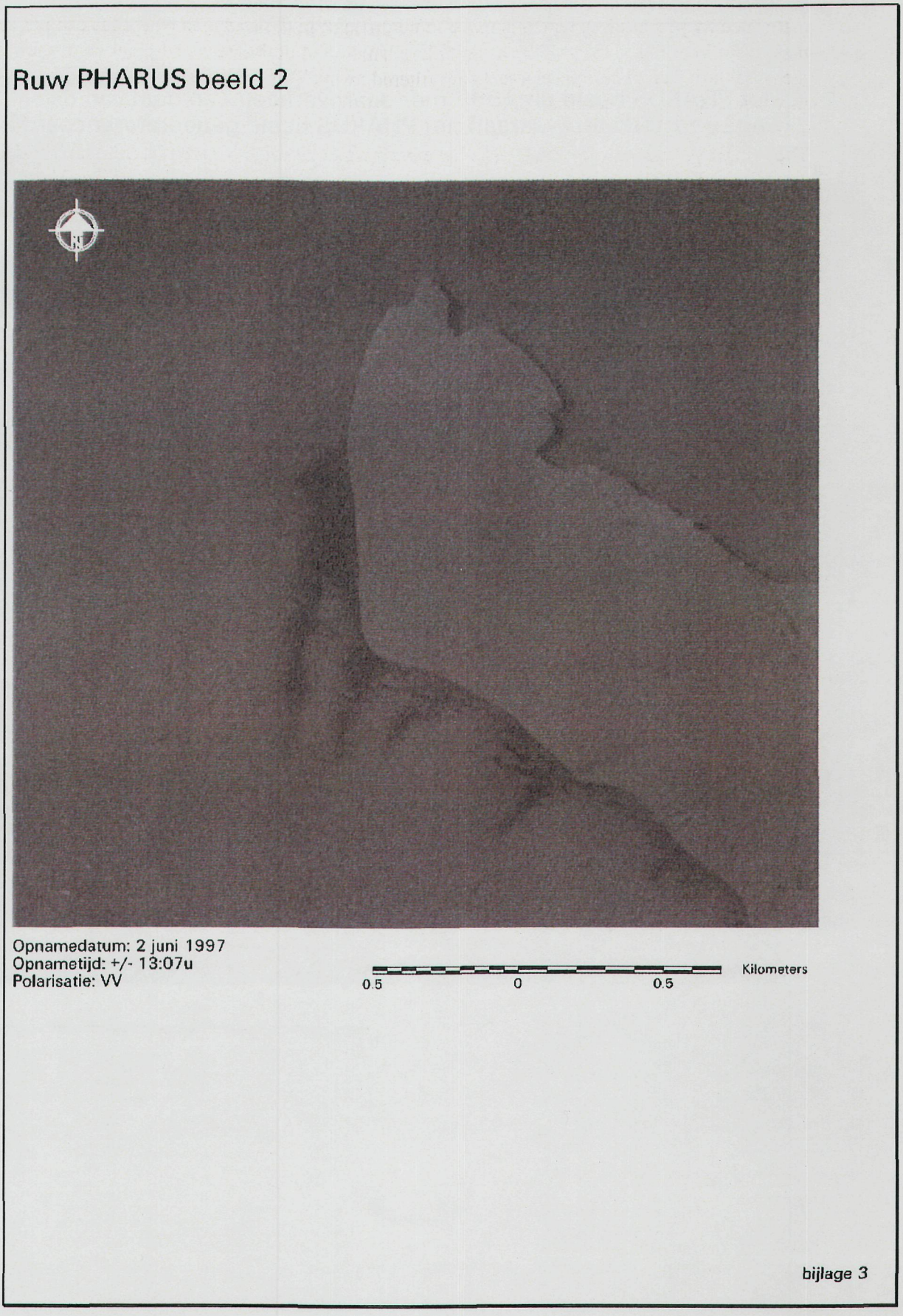

Figure 2.2-1 PHARUS SAR image of the "Groote Plaat" in June 2, 1997

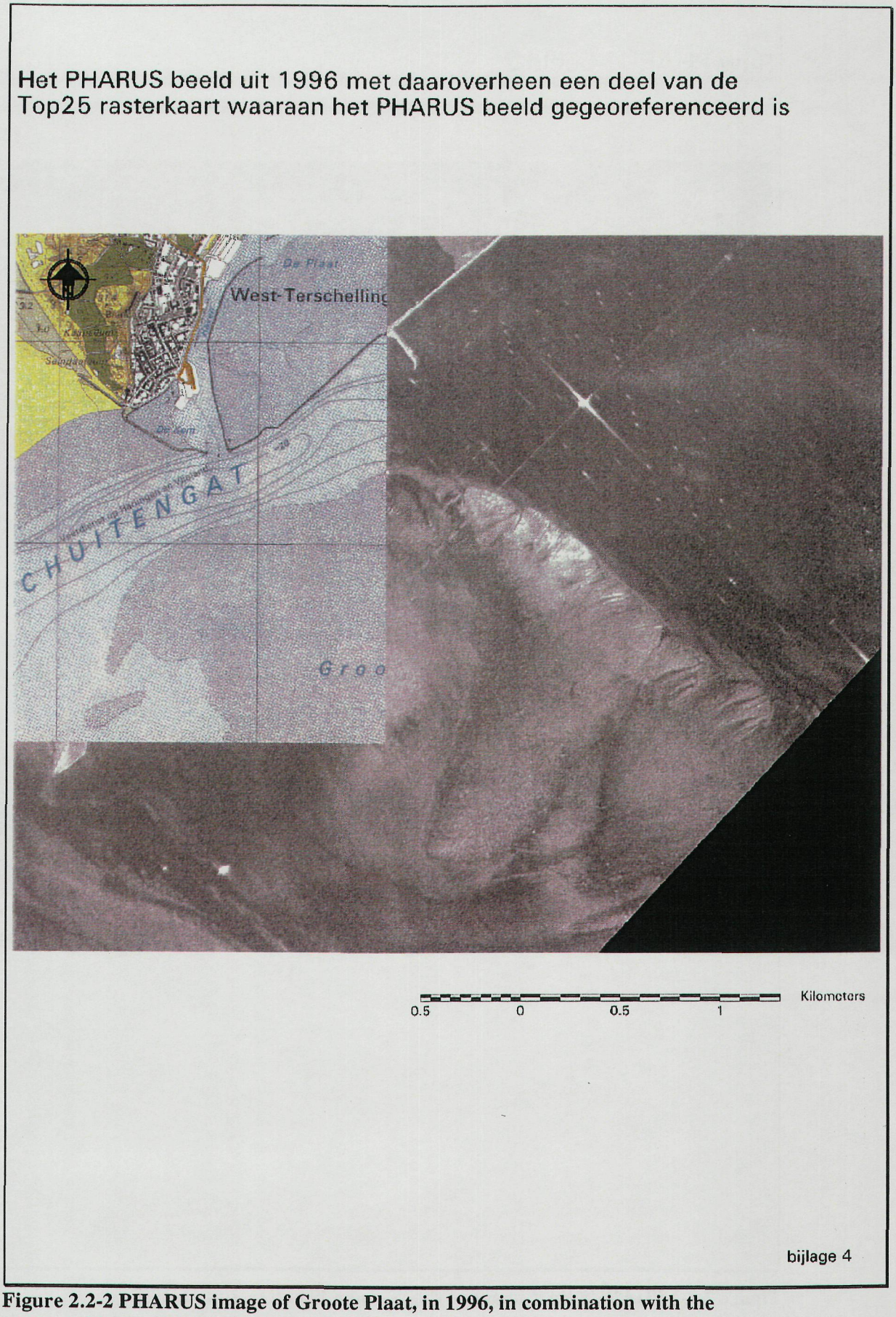

Figure 2.2-2 PHARUS image of Groote Plaat, in 1996, in combination with the topographic map 1:25.000

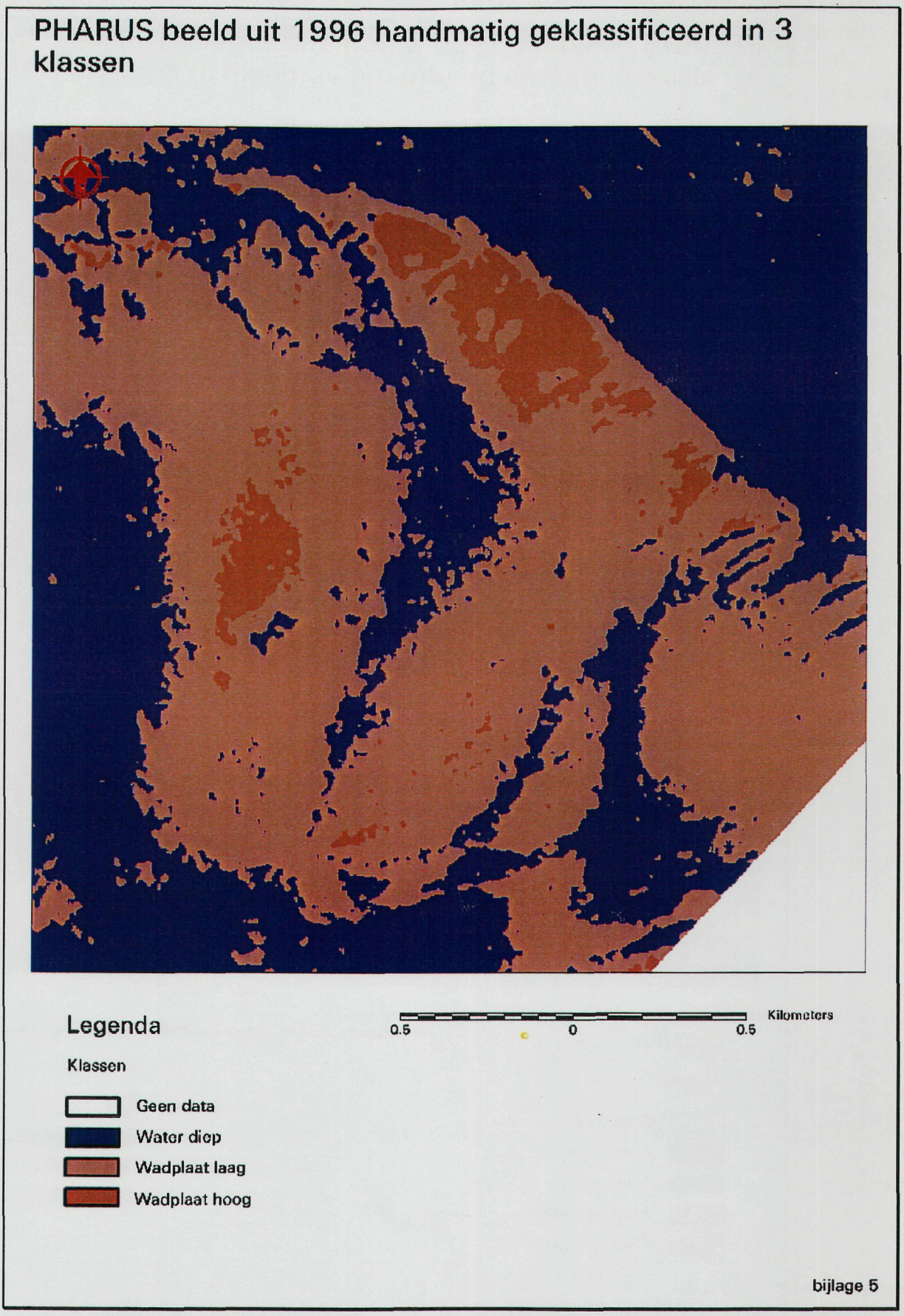

Figure 2.2-3 PHARUS image of 1996, manual classified into 3 classes.

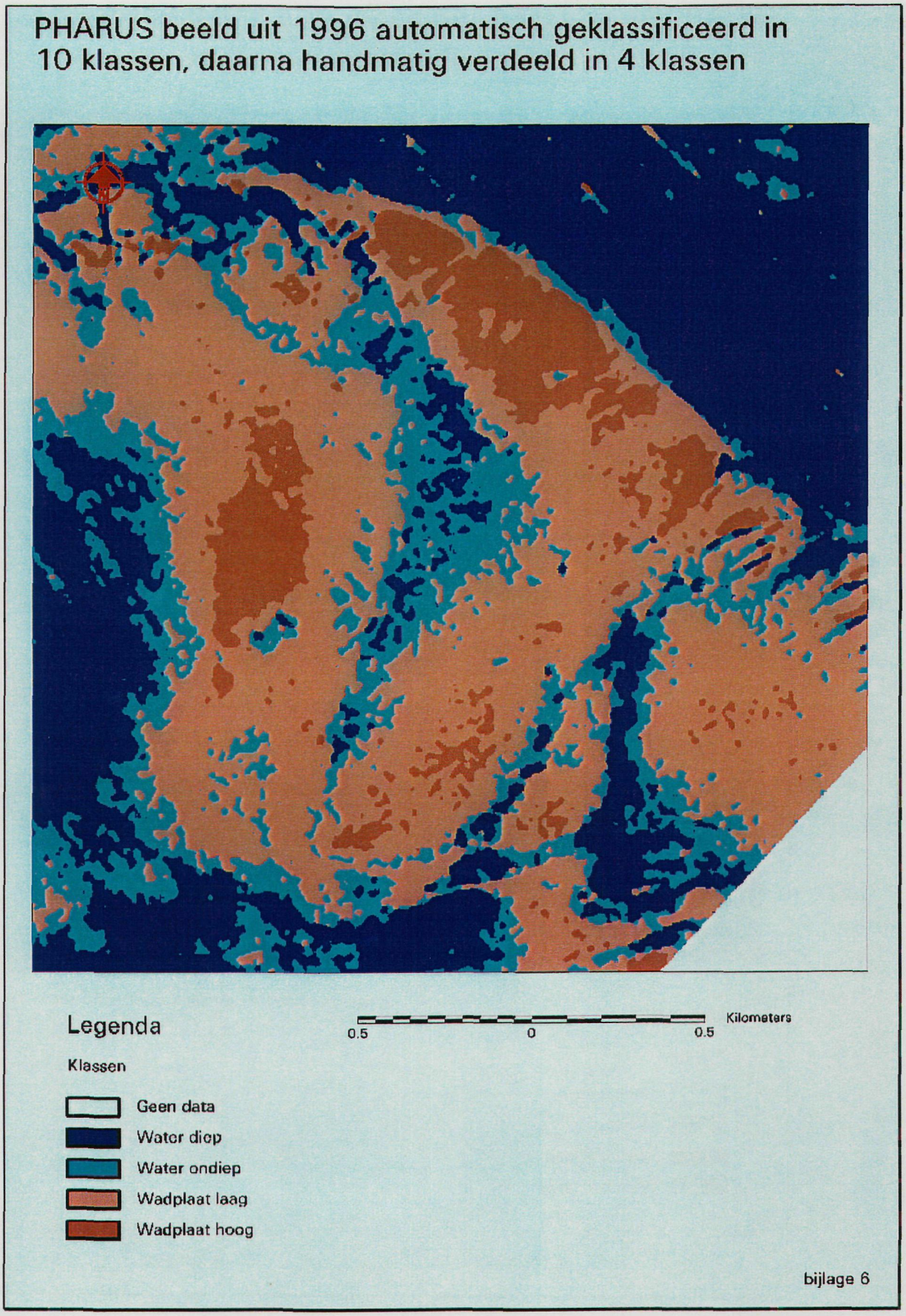

Figure 2.2-4 PHARUS image of 1996, automatically classified into 4 classes.

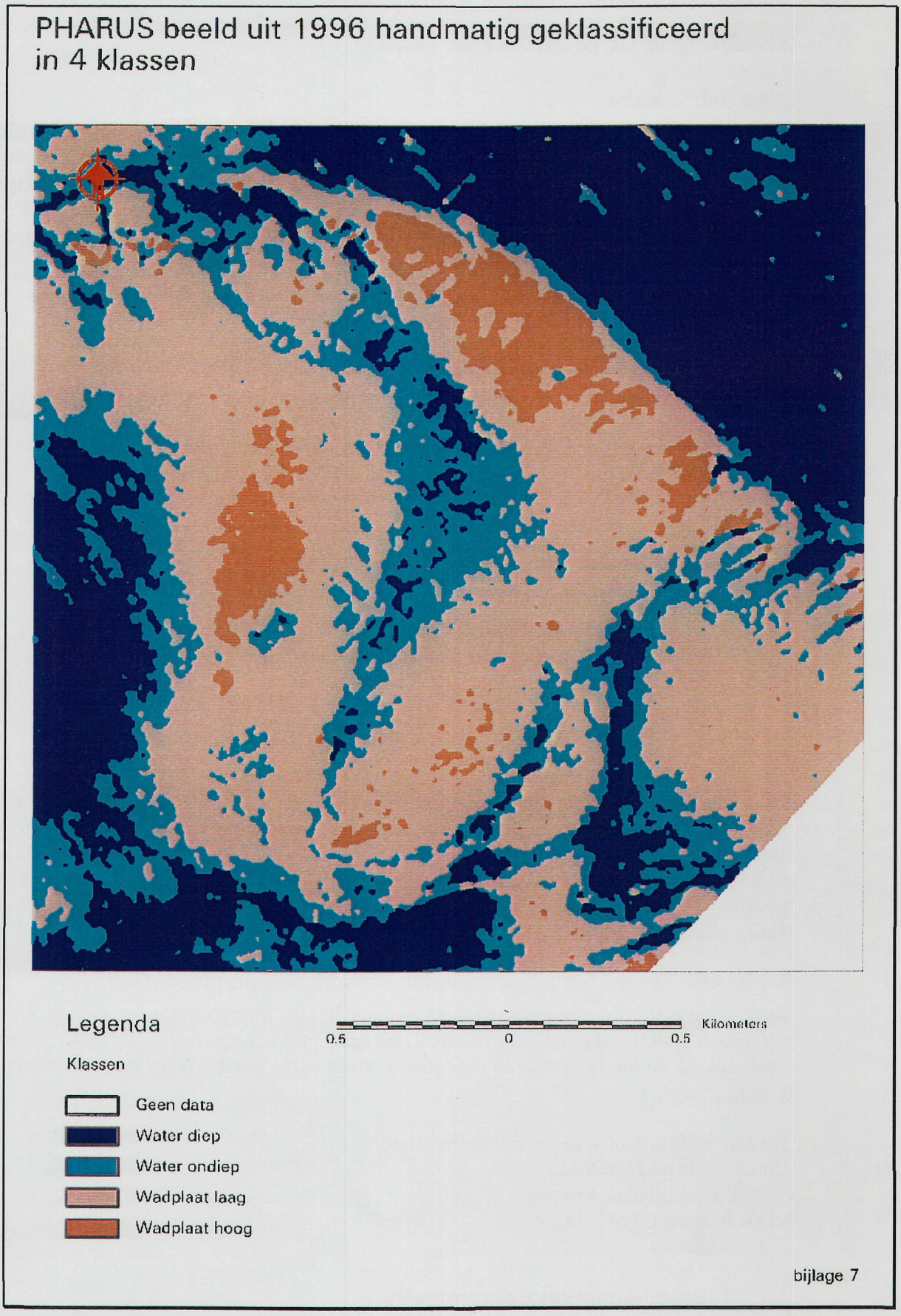

Figure 2.2-5 PHARUS image of 1996, classified manually into 4 classes

2.3 *CHANGE DETECTION FOR ROADS*

2.3.1 Introduction

The Traffic and Transport Advisory Service (AVV) at RWS supplies information on traffic and infrastructure on land and water. To facilitate this a great deal of information has been stored in databases. One example of this is the road database or the National Road Database (NRB). The database consists of a collection of polygons with administrative data on the roads. The database has to be updated regularly so it remains topical. This is realised using information which the AVV receives from the road maintenance authority (this can be government at various levels). The changes in infrastructure are not given to the AVV systematically or effectively however. This leads to 'holes' in the NRB.

Remote Sensing is a possible solution to this problem. Consider optical and radar imagery, to which simple image extraction or complex filter technologies are applied in order to remove the roads. Here however it is a case of detecting changes in the road structures from remote sensing images, also known as change detection. In this context change detection means

The detection of changes in the terrain from the change between two images or files following each other in time

Currently the AVV only wants to use change detection to localise the areas where the road structure has been (significantly) changed.

At least as important as the image-generating technology is the interpretation of images. The interpretation of data from one kind of sensor system is restricted by limitations and can be improved by combining information from various sources and / or sensors. An example could be the combination of SPOT images with radar images, where SPOT images are easier to interpret and the radar's high resolution is advantageous.

In the paragraphs below an explanation is given of the methods which could be used for the benefit of change detection on roads for the AVV. In section 2.3.2 various sensor systems for road detection are discussed. In section 2.3.3 change detection is explained further with 3 methods. In section 2.3.4 a system design is described using the components discussed for the benefit of change detection along with road measurement where necessary. The last section takes a peak at the future.

2.3.2 Alternatives for image material; sensors and preprocessing

There are numerous sensor systems which generate images from a satellite or aircraft. We distinguish optical and radar systems. In this paragraph the characteristics of various sensors are discussed. At the same time an indication is given of the suitability for road detection (change analysis).

The following sensor systems will be discussed:
- Small-scale photogrammetry
- SPOT-Panchromatic imaging
- SAR imaging (PHARUS)
- Laser altimetry

2.3.2.1 **Small-scale photogrammetry**

Small-scale photogrammetry means the generation of images of the terrain with an analogue or digital camera at average altitude. The images from analogue imaging should be scanned

as they will be processed digitally in the change analysis. In [Wicherson and v.d. Kraan, 1995] a scan resolution of 500 dpi (50,8 μ) is chosen, which is in agreement with a ground resolution of 91 cm. This resolution is not achieved with digital photogrammetry, but it is approximated.

Weather conditions are the greatest restrictions for photogrammetry. There has to be no cloud cover, the sun must be 'high' and there should not be too much overgrowth blocking the view of the road. There are often only a few days in the year on which all these conditions are present. An aircraft must also be available. For a scale of 1:18000 approximately 8000 photos are needed to cover the whole of the Netherlands. This is a very large amount compared to satellite images, especially if the costs are compared. It would seem too expensive to use photogrammetry only for localising changes in infrastructure.

For the manual measurement of roads a precision of circa 1 m can be achieved. The precision depends on the how the camera is fitted into the terrain system and the fitting points which are used for this (well defined or not well-defined points).

2.3.2.2 SPOT Panchromatic satellite images

SPOT images are (digital) satellite-generated images taken from an altitude of approx. 830 km. So the images do not have to be scanned. As optic sensors are present (0.30-0.70 μ), weather conditions have the same effects as for photogrammetry. A panchromatic SPOT image has a resolution of 10x10 m^2. This resolution is insufficient for road detection, as minor roads and roads in urban areas cannot be detected by it.

The costs of SPOT images for the whole of the Netherlands are not as high as for photogrammetry, as few images are needed (one SPOT image covers an area of 60 x 60 km^2).

The precision of road measurement is between 6 and 10 m. This is caused by the measuring flaw (several metres) due to the resolution and the adaptation flaw (~3 m) due to the geometric restoration. For this too a number of points – known in the terrain system - should be measured.

SPOT images are only suitable for grey value level comparison with each other if both images have the same grey value range. This can be effected by histogram matching. Differences in the grey value range may occur due to differences in the sun's altitude and clouds / mist. SPOT images are good for change analysis, although the resolution is not extremely good. In the future the resolution of TM scanners and panchromatic scanners will continue to improve with resolutions to 1 x 1 m^2. This development will mean an improvement in the detection of small and narrow objects in particular, such as roads in towns and villages.

2.3.2.3 SAR imaging (PHARUS)

Synthetic aperture radar (SAR) images are generated from a satellite or an aircraft, where the beaming source is also to be found, in this case the radar. The advantage of this is that the radiometry remains the same even if weather conditions change. The radar systems works independently of weather conditions, the radar waves (wavelength a few centimetres, X-band for example) are not troubled by the reflection on clouds etc. The radar image is affected by the physical characteristics of the reflection surface, such as coarseness.

PHARUS (Phased Array Universal SAR) is a new kind of aircraft radar system that can transmit and receive with various polarisations (SAR is an active system). A combination of the various polarisation images generates an image with high resolution (3 x 3 m^2 at approximately 8 km altitude) see Figure 2.3-1.

Figure 2.3-1 PHARUS image (HH +HV +VV), Amersfoort 26 April 1996

One limitation radar systems have is the interpretation of the images. As radar has different reflection characteristics than sunlight the interpretation of radar images is different to that of images generated by optical systems, like SPOT. Still little is known of the reflection of radar waves on various kinds of surfaces. It can be expected that asphalt (roads) has a different reflection characteristic than vegetation for instance. On the other hand a system that does not need to rely on weather conditions has a great advantage.

The precision of road measurement is circa 5 meters and corresponds with the precision of the Topographic Department's TOP10Vector maps. The lack of precision is chiefly caused by the geometric characteristics of radar images.

The geometric correction must be carried out precisely for change detection. This is the most important correction for SAR images, as radiometric corrections are not needed for histogram matching, provided the images to be compared have not been taken too far from each other. In that case shadows fall differently in both images, which hampers comparison.

2.3.2.4 **Laser altimetry**

Laser altimetry is a measuring technique, in which laser pulses are transmitted to the earth's surface from an aircraft. The reflection time allows calculation of the distance between terrain and aircraft. Wavelengths of approx. 1micron are used for measurements. The reflection is dependent on weather: it must be sufficiently clear if laser measurement is to be successful. There should also be little overgrowth in the terrain.

Laser altimetry can be suitable for road detection, as the laser produces a data set with a high density (the laser measures in a zigzagging motion with a frequency of circa 5000 Hz). Besides laser measurements video footage is often shot too. There are actually three measurements then: the range measurement (which indicates the altitude), the signal strength (degree of reflection) and the video footage. A combination of these 3 measurements make very good standard of road extraction possible.

As the laser measurements are not three dimensional they have to be translated into a grid in which the altitudes are represented as grey values for example. Roads are often at a different level than the rest of the landscape, so that roads are recognisable in the altitude component due to the contrast. This is especially valid for rural areas. In urban areas many problems are caused by the reflection of the laser pulse via buildings, which means that too great a range is measured. The solution to this could be to measure with greater point density.

Laser has a different reflection for asphalt/ cement than for vegetation. This has to be expressed in the signal strength, although little research has been done into this. Furthermore, the video image can provide a lot of extra information on the lay-out of roads in towns. Fitting in the video images geometrically is a problem here.

There is no experience with road recognition in laser altimetry, so we are unable to say anything worthwhile about the precision. What can be said is that the precision of the road detection is dependent on the point density in the terrain. With a higher point density the grey value plot can be better interpreted. Measuring and processing of a set of laser altimetry data of high density is also an expensive.

2.3.3 Types of change detection

Three types of change analysis can be distinguished:
1. change detection by means of edge detection filter [de Wit, 1997]
2. change detection by means of image extraction [de Wit, 1997]
3. change detection as overlay with old NWB vector information and edge detection

2.3.3.1 Change detection by means of edge detection filter

In this technique an edge detection filter, which is not direction dependent, for instance a Prewitt filter, is used on the old and new image. This means that edges are found in all directions. To find significant edges, a threshold value can be installed, for instance 20. In this an edge is only denominated when the gradient exceeds the threshold value at both sides.

This method has as condition that the images which are compared must adequately fit to each other, in order to prevent detection of faulty road slides.

The disadvantage is that edges are not only detected on roads (but for instance vegetation changes). An extensive visual interpretation must be carried out to be able to interpret the changes adequately.

2.3.3.2 Change detection by means of image extraction

In this method the change is directly calculated by subtracting the grey values of the images per pixel and by then calculating the difference. Again a threshold value is installed to detect significant changes only. In [de Wit, 1997] a change value greater than 20 or smaller than -20 is also considered as significant.

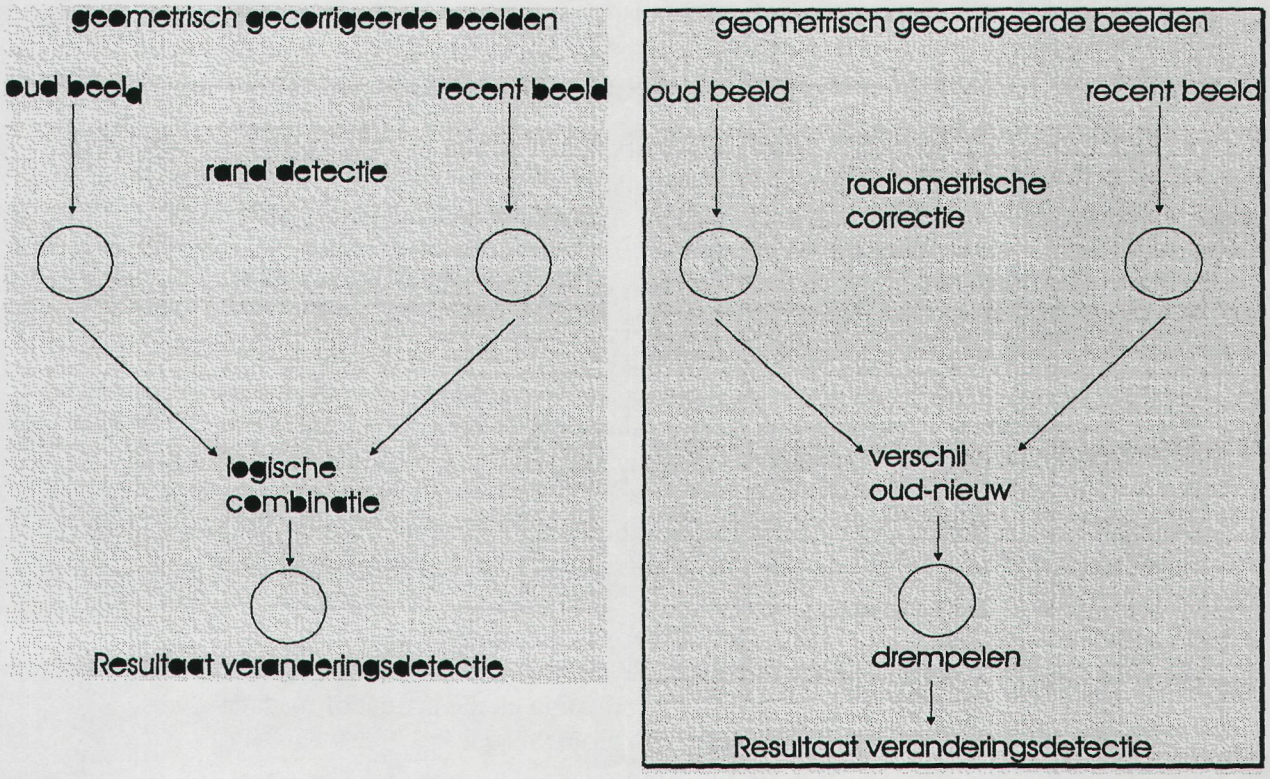

Figure 2.3-2 2 types of change analysis: edge detection at the left, pixel differences at the right.

This technique presupposes the condition , that both images are radiometrically corrected, especially for reason of possible differences of solar position and other weather conditions. In addition, the images must again fit together well.

Again other changes are detected. In this method, however, those other changes are often discernible as planes, whereas road changes are discerned as lines. The road changes are

therefore clearly distinguishable from for instance vegetation change or building developments.

2.3.3.3 Change detection as overlay with old NWB and edge detection.

An alternative method of change detection is the detection of changes on the basis of a single image, i.e. correcting the latest image geometrically and making an overlay with the latest version from the NWB. With aid of an edge detection filter the edges can be extracted in the image. Because disappeared roads are considered as 'not valid' (after all, a road often continues to exist), this can provide a good update: new roads then emerge form the vector file. Because new roads always must connect somewhere to the old road network, all that remains to be done is checking via the old NWB whether there are new edges. Subsequently, a decision rule can be formulated (threshold value for grey value), which determines whether or not the newly connecting edge is a new road.

2.3.4 A system for change detection of roads

2.3.4.1 The system

In order to develop a good system for the benefit of change detection, the requirements made on the final product must be considered. After all, the product is the update of the NWB. Change images can be used to roughly determine the location of the changed infrastructure. Original images can also be used in combination with the latest topical vector information of the NWB, form which changes can be derived.

In regard of the first method it is important that the source images of the change image correspond in terms of grey value range (histogram matching) This is often problematic in optical sensors, such as SPOT; numerous factors affect the radiometry of the SPOT image. The change image becomes difficult to interpret because of this. The definition of a significant grey value change differs for each situation. This problem does occur with radar images, because the sensor intrinsically contains the radiation source. With radar, however, the geometry can sometimes pose problems.

All sensors have more trouble with recognising road (change) in urban areas than in rural areas. The greatest cause for this is resolution. With radar, effects such as relief displacement, shadow effect and hyper radiation play a role.

New, not yet registered roads often occur at city edges, on the border of urban and rural areas. On radar images, roads in such areas are only recognisable from the building pattern. this poses problems with complex patterns. The resolution plays a great role in optical systems. The resolution is highest in photogrammetry, which can recognise the city roads to a reasonable degree, while SPOT images leave many minor roads unrecognisable. In regard of laser altimetry I expect that the reflection of the signal via buildings will cause flaws. this can be anticipated by choosing a higher resolution in those areas. This increases the chance on 'correct reflection' of a laser pulse and roads will be recognised better in the interpolated grey value area (grey value ~ height). Because roads are often on a different level than the surroundings, roads must be adequately detectable from the relief image. In this a altitude accuracy of 15 cm is assumed.

The costs for the various processes. Photogrammetry is the most expensive, because many pictures have to be taken at a limited number of flying days per year. Analogue pictures all have too be scanned before they can be digitally processed. It seems convenient to use for instance digital pictures for urban areas. These have a slightly lower resolution than analogue pictures, but are cost reductive. Furthermore, fixed fitting points must be selected.

SPOT images cost the least. Only digital images must be bought which must be geometrically fitted in the terrain. the quality of SPOT images depends of the weather conditions during the shot. this means that not every SPOT image can be used.

SAR images from a plane (PHARUS) give reasonable resolution and radiometric characteristics. The collection and processing costs are between those of SPOT and photogrammetry. Because the interpretation of radar images is not as self-evident as that of optical images, this will take extra time, resulting in relatively higher labour costs. Laser altimetry is expensive, particularly where shots are concerned. An advantage is that the images made for the Topical Altitude File Netherlands can be used. However, this file is renewed every four years, so no new images are available every year. A great advantage is that per flight three sorts of information are gained (altitude, signal, video).

Because each collection technique has its limitations, it seems logical to combine two techniques into a single system. To bring together the advantages of radar shots (resolution) and the interpretation facilities of optical shots, possible combinations are SPOT-PHARUS and Laser-PHARUS and (Digital) Photogrammetry-PHARUS , in which respect laser and photogrammetry have more possibilities in urban areas. Laser altimetry is a relatively novel method, still wanting investigation of the influence of faulty causes. Considerable more experience has been obtained with photogrammetry.

The latter option seems to provide a good system with the advantage that with the combination roads can also be measured, making field surveyors obsolete. A change analysis is also very well possible because of the easily comparable radar images. This way the detection of change areas can be carried out, after which a digital picture can support the interpretation for the measurement of roads. An important factor is the availability of programs that can compare the different measurements and connect them geometrically. A good package for this purpose is Erdas Imagine, partly because it is already available at the Geometrical Service of the Department of Public Works (so there is already experience with the package). A problem, however, is that little radar technique experience is available in regard of road detection. This problem will probably be left behind in the course of time. The process development in the new system is indicated in the figure. It is indicated which step is taken automatically and at which steps an operator is needed (semi-automatic and manual).

2.3.5 Post-change detection measurement

After the change detection the roads should be able to be measured from the images. Presently this would have to be done by an operator. For change detection in the context of the Traffic and Transport Advisory Service this is not insurmountable, because the number of roads still to be measured is often limited. In addition, the road measurement is an addition to the localisation of road changes).

The automatic detection of roads from digital images is however an investigation item which has received a lot of work. In this light, roads can be detected by means of multiple shots and templates and Geometrically constraint multiphoto matching. Furthermore, so-called snakes can be a means for that. In this method points are given which are in the vicinity of the road. By following the road with a template, an optimal polynome (snake) can be drawn through the detected road points.

Advanced edge detection filters are developed to detect edges which are actually a border in the terrain. A problem with roads is that they occur in so many states that, that no unique edge or template can be defined. [M. de Gunst, 1991/Förstner, 1997]. In reality, hardly any generally applying training samples can be defined for the object 'roads'.

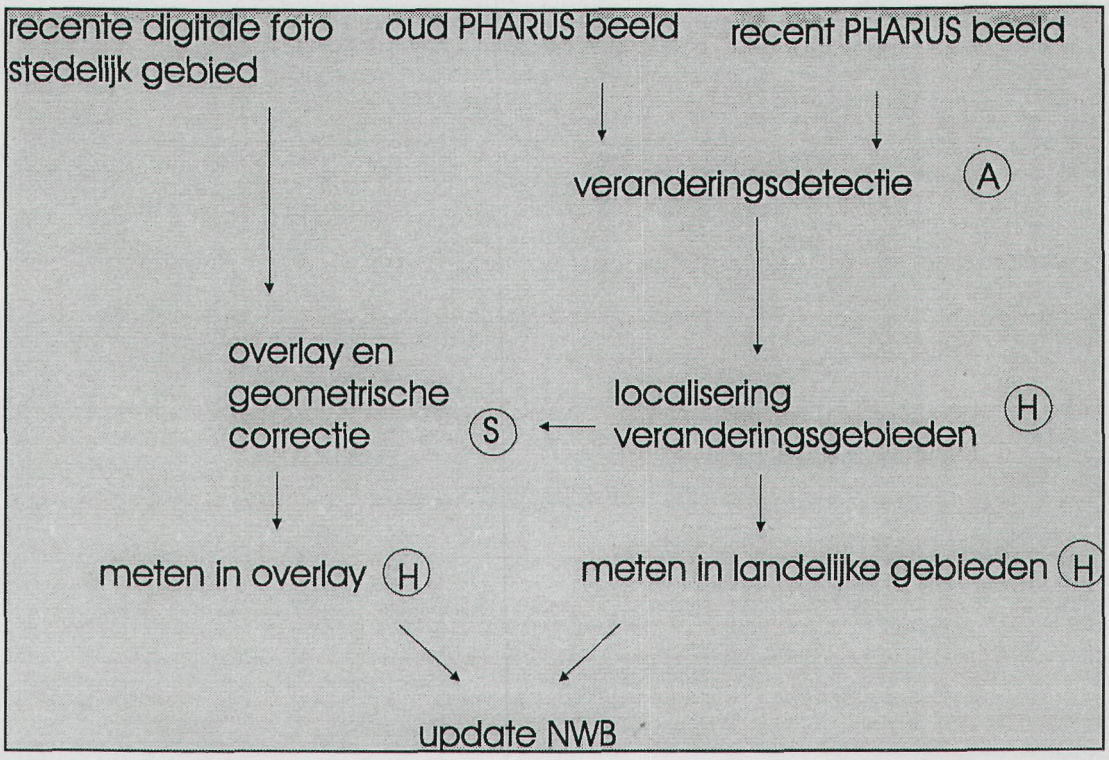

Figure 2.3-3 The System: M = Manual processing, S = Semi automatic, A = Automatic processing

2.3.6 Use of PHARUS images for road detection

From PHARS to PHARUS

During past years the Geometric Department has investigated the possibilities of remote sensing and photogrammetry for the collection of geographic road information and the revision of digital road files. One of the possibilities under investigation, is the use of PHARS images for road detection. The spatial resolution of the images which were made with PHARS is approximately 6 metres. The general conclusion was the PHARS images were difficult to interpret because of the specific characteristics of the radar, but that nevertheless 60 to 70% of the roads in urban areas could be detected. In rural areas a 90% could be achieved. (Wicherson and van der Kraan, 1995). In the meantime the successor of the PHARS sensor has become available: PHARUS (PHased ARray Universal SAR). Because of the improved resolution of PHARUS (3.5 at 3.5 metres) it is to be expected that road detection in urban areas can be greatly improved. Because PARUS has the option to make polarimetric shots, the added value of the polarimetric information can be evaluated. For the benefit of the road detection experiment a polarimetric image was acquired of a part of the Dutch town of Amersfoort as part of the PHARUS Familiarization program. This image depicts the same area as the PHARS image, acquired some years ago.

Geometry

To be able to assess the internal geometry of the PHARUS image, the image was geometrically corrected with the aid of the TOP10 Vector data in which only that part was used where the houses are delineated. With aid of approximately 8 checkpoints a first grade geometric correction was carried out. The RMS flaw could be reduced to ± 1.3 pixels. Figure 2.3-4 shows the PHARUS image with the TOP10Vector file superimposed on it. Even though there is no independent check, an impression can be obtained of the internal geometric precision.

Figure 2.3-4 PHARUS image of Amersfoort with overlay of VECTORTOP10 data set

Figure 2.3-5 PHARUS image with overlay VOR data set (see text for explanation)

Figure 2.3-6 PHARUS image with overlay VOR data set (see text for explanation)

Despite the low RMS flaw with which the PHARUS image was corrected, there proved to be small shifts between the PHARUS image and the TOP10Vector that were not constant over the picture. The cause of this shift could be sought in an inaccuracy in the radar image. It is also possible that a typical radar characteristic such as relief displacement contributes to this shift. After a more accurate inspection of the image the deviations proved to be mostly between 3 and 6 metres with extremes of 10 metres. This range lies between the accuracy boundaries of the TOP10Vector, making worthwhile assertions about the geometric accuracy difficult. the geometric accuracy can be said to be sufficient for the envisaged application, the collection of geographical road information.

Collection of road information with PHARUS
For the estimation of the usefulness of PHARUS images for the collection of road information, the VLN (VOR Location Network) file of Amersfoort from the Traffic and Transport Advisory Service was used. This file contains, besides the geographic location of roads, further information which was not used in this study. Furthermore, a list was compiled with characteristics that can be recognised in the PHARUS image. This way it is possible to come to a reasonably objective estimate of the information in the PHARUS image. A PHARUS image was used that was obtained with the aid of 'span-processing'. This way of processing involves three different polarimetric bands combined into a single image offering with less interference. After a first evaluation, it is estimated that an image with less interference has more value for this application than a single polarimetric image.

Comparison PHARUS and VLN
In comparing the PHARUS image and the VLN file it is immediately evident that clear shifts exist between the two files. Particularly at the east side of Figure 2.3-6 it is clearly visible that the highway in the VLN file has shifted in comparison to the PHARUS image. These shifts can for the greatest part be attributed to the inaccuracy of the VLN field (Wicherson and Van der Kraan, 1995).

Within the urban area the roads in the PHARUS image are in many cases not directly recognisable, but can be deducted from the structure of the buildings surrounding the roads. This indicates that road detection from a PHARUS image corresponds to the complexity of the buildings. It is tricky to distinguish roads in the image (Figure 2.3-5) of the town centre of Amersfoort although the street pattern is easily recognisable in the district east of the city centre. The street pattern is not only difficult to recognise in the complex buildings in the old city centre, but also in residential districts with many free-standing houses. (Figure 2.3-5, south-west corner).

An additional problem is that often no uniform street pattern can be derived from the building structure; main roads can mostly be clearly indicated, but street patterns in residential districts often allow for multiple interpretations. Once experience has been gained with the interpretation of a road pattern from PHARUS images this disadvantage will probably be of more limited significance.

Conclusions
It can be concluded that a PHARUS image contains a lot of information about building structures and consequently also about road patterns. Direct collection of road information will be possible in areas with sparse buildings, but in areas with complex building structures this will prove to be difficult or even impossible. With the reference data sets employed (TOP10Vector, VLN) is impossible to make a worthwhile conclusion about the geometric accuracy of the PHARUS image, but it is at least comparable to the accuracy of the reference files. The differences found can not be univocally traced back to specific characteristics of the PHARUS image.

2.3.7 General conclusion on road detection

The high resolution optical systems and the radar (especially SAR) systems will be increasingly important over the coming years. Similarly, the laser scanning systems will be further developed - mostly form geometric perspective. Optical systems resolution will continue to improve and the radar images will continue to convey information about the earth, which we normally could not obtain. (e.g. sea current measurements in the oceans). The polarimetry in PHARUS also supplies more information than a regular SAR.

This also means an improvement for road detection. High resolution satellite scanners (up to 1x1 m2) supply much information in high detail. Possibly these images will allow adequate road detection from the optical satellite measurements.

The system design that was described in section 2.4, is a design that will be subject to change in the future. Especially the developments in the field of radar are moving fast. But in all of this, the budgets will have to be carefully considered.

2.3.8 References

Wicherson, R. and J. v.d. Kraan, 1995, Het gebruik van remote sensing opnamen en kleinschalige luchtfoto's bij het actualiseren van kleinschalige wegenbestanden. Delft, Meetkundige Dienst, maart 1995.

A. de Wit, 1997, Application of SPOT-PAN imagery for detecting changes in road networks. Delft: Survey Department, Rijkswaterstaat, 1997.

A. de Wit, Gebruik van sateliet remote sensing voor actualiteitsbepaling van het nationaal Wegenbestand van RWS-AVV. Delft: Meetkundige Dienst, Rijkswaterstaat, September 1997.

M. de Gunst, 1991, Automatic extraction of roads from SPOT images. Delft: Faculteit der Geodesie, 1991.

W. Förstner and L. Plümer, 1997, Semantic modelling for the acquisition of topographic information from images an maps. Basel: Birkhäuser Verlag, 1997.

3. Maritime applications

Maritime applications like the detection of oil spills have been operational in the Netherlands for many years now. Also an advanced application like the mapping of the sea bottom topography with SAR has been developed in the Netherlands. This second application has proven to save ship's time (and therefore money) during conventional mapping programmes. The purpose of these demonstration applications is to emphasise the improved features of PHARUS especially in terms of the implications of the increased swath, increased sensitivity and reduced speckle.

3.1 *Oil spill detection*

The demonstration of oil spill detection with PHARUS did not provide satisfactory results. The followed procedure in the data acquisition is briefly described in this section.

Oil spills are detected regularly by the patrol aircraft of RWS-DNZ. It has originally been proposed to have PHARUS stand-by for a period of a week during which the patrol aircraft of RWS-DNZ is patrolling the North Sea. Once an oil spill is detected, PHARUS was to be called in and a combined flight with PHARUS and the RWS-DNZ aircraft would be made over the oil spill. However, RWS-DNZ planned a controlled experiment during which an oil spill was made and a SLAR image and a SAR image were acquired, allowing for a clear indication of SAR- versus SLAR performance. Unfortunately, due to technical problems the quality of the SAR data was too bad. A second experiment with PHARUS participating in the Bonnex trial at Helgoland where also the RWS-DNZ SLAR was flown was cancelled, again because of technical problems.

The BCRS preferred to finish the Familiarization program on 31-5-98. Therefore, it has been decided to omit the oil detection experiment from the Familiarization program. It has been agreed that it will be investigated how a new oil spill experiment can be performed, taking into account the gained experience on the logistic problems which occurred during the Familiarization program. A new oil spill detection trial is planned in the submitted PHARUS ASAR demonstrator proposal.

3.2 *Bottom topography*

3.2.1 Introduction

Accurate and reliable depth maps (in digital format) are required for the purpose of monitoring and control of the seabed and inter-tidal zone. In the Netherlands depth information in the coastal zones is collected operationally on a routine basis by Rijkswaterstaat. At this moment this is done by a traditional technique using ship-borne echo sounders, which is expensive and time consuming.

In a previous study a depth map of the Groote Plaat area was constructed using ERS SAR images, which have a spatial resolution of 25 m x 25 m (pixel size being 12.5 m x 12.5 m). The ERS satellite is orbiting the earth at an altitude of approximately 785 km. In this study a depth map will be constructed using PHARUS SAR imagery, which has a spatial resolution of 3.4 m x 3.4 m (pixel size being 3.0 m x 3.0 m). The PHARUS sensor is mounted on an aircraft which flew at a height of about 6 km.

3.2.1.1 **Aim**

The aim of this project is to obtain the complete bottom topography of the project area by using the Bathymetry Assessment System (BAS). The Bathymetry Assessment System will be applied to airborne radar images (SAR) and combined with sounding data of the project area. These results will be compared with those obtained previously using ERS SAR images, which have a coarser resolution.

3.2.1.2 **Project area**

The project area is the Groote Plaat tidal flat located South West of Terschelling. The size of the area is about 3.0 km x 4.5 km. The corner co-ordinates of the area are presented in Table 3.2-1. The co-ordinates are given in the Rijksdriehoek co-ordinate system (origin in Paris).

corner points	X	Y
North	145,000	597,000
East	148,500	594,000
South	146,000	592,500
West	142,500	595,500

Table 3.2-1 Corner co-ordinates of the project area Groote Plaat.

3.2.2 Data

In order to calculate the depth in the project area with the Bathymetry Assessment System the following information is required:

1 Radar images,
2 Hydrological and meteorological data at the time of image recording,
3 Sounding data,
4 Geo-referencing data.

SAR images are the main information source for BAS. Local depth changes are calculated from the SAR images; the other data are needed to fix some parameters in the BAS. Field measurements of windspeed and direction, and the tidal phase are needed to calculate the water level and current. No corner co-ordinates are provided with the PHARUS SAR image. Therefore additional geographical data are required.

3.2.2.1 Radar images

A single PHARUS SAR image covering the area was obtained through TNO-FEL. Four ERS SAR images covering the project area were obtained previously from Rijkwaterstaat. All images were recorded mid 1996. A list of the images is given in Table 3.2-2.

Platform	orbit	frame	date	time (GMT)	time (MET)
ERS-1	25797	1071	June 20, 1996	21:38	22:38
ERS-2	06124	1071	June 21, 1996	21:38	22:38
ERS-1	25962	2529	July 02, 1996	10:37	11:37
ERS-2	06289	2529	July 03, 1996	10:37	11:37
PHARUS			August 27, 1996	8:37	9:37

Table 3.2-2 List of PHARUS and ERS SAR images.

The PHARUS SAR image is shown in Figure 3.2-1 and covers the project area completely.

The PHARUS SAR images have been processed by TNO-FEL as follows:

1. Range (cross-track) compression
   1.1. resolution 3.4 m
   1.2. range weighing: Cosine Squared 0.5 (= Hamming 0.75)
2. Azimuth (along-track) compression
   2.1. resolution 3.4 m
   2.2. azimuth weighing: Cosine Squared 0.5 (= Hamming 0.75)
   2.3. number of looks 4.9.
   2.4. Span processing (HH+HV+VV) results in doubling of the number of looks, i.e. 9.8.
   corrections:
   - range migration
   - line-of-sight phase
   - antenna (platform) motion
   - antenna elevation pattern
   - σ_0 variation, due to the incidence angle (θ) dependence have been removed by assuming a sine dependence: $I \approx 1/\sin(\theta)$
3. Conversion to ground range (geometry)
   3.1. cubic spline interpolation
4. Scaling
   4.1. image scaling to the byte range of 0-255 using the function 10*log(I)/A, where I is the power count value of the original image and A is the scale factor (A=0.25 dB/count)

The radar backscatter intensity along a single line in range direction in a SAR image is calculated using information over a certain distance in azimuth direction. If the size of the area in azimuth direction is too small the calculated radarbackscatter is incorrect. Therefore, processing of SAR data of a specific area should be based on information including also a sufficiently large area outside the image area. The PHARUS image has been processed in two parts, because the data volume was too large to be handled in a single processing run by the SAR processor of TNO-FEL (the situation in 1996). Figure 3.2-1 shows a transition between the two separately processed image halves, which can be contributed to this leading/trailing effect (personal communication with R.J. Dekker, TNO-FEL).

Other relevant technical parameters are:

Polarisation:	VV
Altitude	6150 m
Near range (ground) distance	3340 m.
Incidence angle at near range	28.5^0
Incidence angle at mid swath	52.4^0
Incidence angle at far range	64.0^0
Pixel size (ground)	3.0 m x 3.0 m
Flight direction	132 (from NW to SE)
Radar look direction	left
Swath width	9300 m

3.2.2.2 Hydrological and meteorological conditions

The hydrological and meteorological conditions at the time of image recording are shown in Table 3.2-3 and Table 3.2-4. The water level information in Table 3.2-3 is based on field measurements and on "De Getijgenerator", a program provided by RWS to calculate water levels at a large number of positions in Dutch waters. The wind data shown in Table 3.2-4 were taken from the "Monthly Bulletin North Sea 1996." The position of the three stations is given in Table 3.2-5.

Date	time (GMT)	time (MET)	Vlieland haven	West-Terschelling	Harlingen
June 20, 1996	21:38	22:38	+57	+47	+41
June 21, 1996	21:38	22:38	+41	+31	+16
July 2, 1996	10:37	11:37	+26	+53	+93
July 3, 1996	10:37	11:37	+74	+96	+116
July 3, 1996	10:37	11:37	$+63^m$	$+88^m$	$+108^m$
August 27, 1995	8:37	9:37	+16	+42	+78

Table 3.2-3 Water levels in cm with respect to NAP at three locations in the Dutch Wadden Sea. Values are calculated using "De Getijgenerator". ^{m} indicates a field measurement.

Comparison of Table 3.2-3 and for instance the image in Figure 3.2-1 shows that the water levels are clearly related to the position of the shore line. Of July 3, 1996 field measurements of the water level were available (row 5 of Table 3.2-3). Comparison with the sixth row of the same table shows a set up effect of -8 cm, which may have been caused by the strong wind of 9 m/s on July 3, 1996.

Date	time (GMT)	time (MET)	wind speed [m/s]	wind direction	tidal phase Hook of Holland	tidal phase Harlingen
June 20, 1996	21:38	22:38	8	300	+5h06	-1h51
June 21, 1996	21:38	22:38	9	300	+4h33	-2h22
July 02, 1996	10:37	11:37	7	285	-3h48	+1h07
July 03, 1996	10:37	11:37	9	210	-4h35	+0h18
August 27, 1996	8:37	9:37	5	150	-5h43	+1h39

Table 3.2-4 Hydrological and meteorological conditions. Wind speed and wind direction represent the conditions at West-Terschelling, a station closest to the project area. The tidal phase is with respect to High Water. The wind direction is in degrees true north, i.e. measured in degrees clockwise from the geographical north.

The PHARUS image and the ERS images of July 2, and July 3, 1996 were recorded after high tide at Harlingen (falling tide), so the current direction in the tidal channel is from South to North. The ERS images of June 20, and June 21, 1996 were recorded before high tide at Harlingen (rising tide), so the current direction in the tidal channel between Ameland and Terschelling is from North to South.

The hydrological and meteorological conditions during acquisition of the PHARUS SAR image are rather different from those during the previously recorded ERS SAR images. The windspeed is significantly lower and the wind is coming from the opposite direction.

The general flow pattern is determined by the tidal phase.
Figure 3.2-2 shows the flow pattern in the area about 1h30 after high water at Harlingen, which corresponds to the flow conditions at the time of recording of the PHARUS SAR image (assuming no wind effect).

	Vlieland haven	West-Terschelling	Harlingen
X(RD)	135,280	143,870	156,480
Y(RD)	590,000	597,420	576,550

Table 3.2-5 Position of three locations in the Dutch Wadden Sea. Co-ordinates are with respect to RD.

3.2.2.3 Sounding data

Sounding data were obtained from Rijkswaterstaat. The sounding data consist of 19 section lines sailed mid 1996.
Figure 3.2-3 shows the bottom profile along each section line in a quasi three dimensional display. The sampling interval along a section line is on average about 32 cm. The bottom level is relative to NAP and has been measured using a Real Time On The Fly Differential GPS. Therefore, the depth measurements have not been reduced to NAP using the standard methods of water level correction!

3.2.3 Bathymetry Assessment System

Under favourable meteorological and hydrodynamic conditions (moderate winds of 3 to 8 m/s and significant tidal currents of about 0.5 m/s), air- or spaceborne Synthetic Aperture Radar (SAR) imagery shows features of the bottom topography of shallow seas.

The imaging mechanism of mapping sea bottom topography by imaging radar consists of three stages:

(1) Interaction between (tidal) flow and bottom topography results in modulations in the (surface) flow velocity. This relation can be described by several models with an increasing level of complexity: continuity equation, shallow water equations, and/or the Navier Stokes equations.

(2) Modulations in surface flow velocity cause variations in the surface wave spectrum. This is modelled with the help of the action balance equation, using a relaxation source term to simulate the restoring forces of wind input and wave breaking.

(3) Variations in the surface wave spectrum cause modulations in the level of radar backscatter. To compute the backscatter variations a simple Bragg model can be used, but also available are two-scale and first iteration Kirchoff (Holliday) models.

Based on the above three stage mechanisms (see Figure 3.2-4), a suite of computer models has been developed and operationalized at ARGOSS. Models with different levels of complexity and physical detail are available for each step. These models describe the flows, waves and electromagnetic backscatter and can be used for a quantitative analysis of radar imagery.

This suite of computer models generates the radar backscatter given the (initial) bathymetry and the wind. In order to invert this depth-radar backscatter relation, a data assimilation scheme has been developed, minimising the difference between the calculated and the measured radar backscatter by adjusting the bottom topography. The radar backscatter differences are part of the input for a penalty function which integrates the differences between model predictions and measurements. Note that also the difference between measured and calculated depth is part of the penalty function. At present a data assimilation scheme using one-dimensional models is implemented. The selection of the linear model which is most appropriate has been automated.

3.2.4 Method

The Bathymetry Assessment System is described in detail in section 3.2.3. Given the sounding data the bottom topography will be determined for the area of interest by applying the Bathymetry Assessment System. In order to realise the aims of this project, the following activities have been carried out:

1 The required data have been collected, such as the PHARUS SAR image, soundings, hydrological and meteorological data.
2 Pre-processing of the PHARUS SAR image: geometric correction, image classification, distortion correction.
3 Determining an initial bathymetric map based on the sounding data.
4 Calculation of the depth in the project area "Groote Plaat" using the sounding data and the PHARUS SAR image.
5 Making available the calculated bathymetry in digital format.

3.2.5 Results

3.2.5.1 Geometric correction

The PHARUS SAR image was loaded into the system and geometrically corrected using suitable land marks visible in the SAR images and the most recent topographic map of the area [Topografische kaart van Nederland 1:25.000, blad 5A, Terschelling, uitgave 1994]. The result is shown in Figure 3.2-5 and Figure 3.2-8.

3.2.5.2 Radiometric correction

The radiometric correction of the PHARUS SAR image involves two steps. The first step is somewhat *ad hoc* and was executed before the image was entered into the BAS system. The second step involves the standard BAS procedures. Here, only the first step will be discussed.

The PHARUS SAR image was processed in two halves, which resulted in a small intensity transition (see Figure 3.2-1).
Figure 3.2-9 shows the intensity profile of the two horizontal lines at both sides of the transition, as well as the difference. The difference is almost zero at the left side and increases to 20 dB at the right hand side of the figure. Fortunately, the larger differences are located outside the area of interest. The intensity change was removed by fitting a low order polynomial through the difference. This fit was used to modify the image. In Figure 3.2-5 and Figure 3.2-8 it can be observed that the change has been removed successfully.

3.2.5.3 Depth calculation

Using the PHARUS SAR image, the sounding data, the hydrological and the meteorological data the depth was calculated with the Bathymetry Assessment System. Calculations were made at two grid resolutions: 5.0 m and 12.5 m. The result for the 5.0 grid calculation is shown in Figure 3.2-10. The accuracy of the result at the section lines is shown in Table 3.2-6. The computed depth at each sounded position has been extracted from the depth matrix using bilinear interpolation and was compared to the actual measurement. As an example the depth profile along three different section lines is shown in Figure 3.2-11. The comparison in Table 3.2-6 is based on four quantities:

- bias the average depth difference
- rms the root mean square depth difference
- abs the average absolute depth difference
- 5% the five percentile difference

The results presented in Table 3.2-6 represent a lower bound on the accuracy which can be achieved. The differences presented can be attributed to the natural variability in the sea bed within a grid cell, which is as expected larger within a 12.5 m grid cell than within a 5.0 m grid cell. Furthermore, the soundings used to assess the accuracy were also used for calibration.

The largest absolute error is 39 cm and is found in at the last depth sample of section line 2. At this point the depth increases rapidly from the tidal flat towards the channel (see Figure 3.2-3). The depth change occurs within a distance of 1.5 m, which is much smaller than the resolution of the imagery which is 3.4 m.

		5.0 m grid			12.5 m grid			
Section line	bias [cm]	rms [cm]	abs [cm]	5% [cm]	bias [cm]	rms [cm]	abs [cm]	5% [cm]
1	0.1	2.1	1.5	4.8	0.3	2.5	1.8	5.0
2	0.1	2.3	1.1	3.5	0.0	2.6	1.6	4.2
3	0.1	2.5	1.8	5.4	-0.0	2.9	2.2	5.7
4	0.0	1.5	1.1	3.2	0.1	1.9	1.4	3.9
5	0.0	2.2	1.4	4.8	0.0	2.4	1.8	4.9
6	0.0	1.3	0.9	2.8	-0.1	1.6	1.2	3.1
7	0.0	1.8	1.3	4.0	0.0	2.0	1.5	4.2
8	0.0	1.4	1.0	2.9	0.0	1.6	1.3	3.3
9	-0.0	1.3	0.9	2.9	0.0	1.5	1.2	3.2
10	0.0	1.1	0.8	2.3	-0.0	1.3	1.0	2.4
11	0.1	1.4	1.0	3.2	0.2	1.7	1.2	3.4
12	0.0	1.2	0.9	2.7	0.1	1.5	1.1	2.9
13	0.1	1.9	1.3	4.2	-0.0	2.1	1.6	4.2
14	-0.1	1.6	1.1	3.5	-0.1	0.2	1.5	4.1
15	-0.0	2.3	1.6	4.7	0.1	2.7	2.0	5.8
16	0.1	1.5	1.1	3.0	0.2	1.8	1.4	3.8
17	0.1	2.2	1.5	4.4	0.0	2.4	1.8	4.9
18	-0.0	1.7	1.1	3.2	-0.0	2.5	1.7	4.8
19	-0.1	1.8	1.2	3.5	-0.1	2.2	1.5	4.2
Overall	0.03	1.74	1.19	3.63	0.04	1.97	1.52	4.11

Table 3.2-6 Depth accuracy of the Groote Plaat depth map at the section lines.

		5.0 m grid				12.5 m grid			
Section line		bias [cm]	rms [cm]	abs [cm]	5% [cm]	bias [cm]	rms [cm]	abs [cm]	5% [cm]
1	x	-0.5	3.3	2.5	6.4	4.4	8.0	5.2	18.5
2	*	-0.4	5.1	3.1	9.7	-0.6	5.0	3.3	10.3
3	x	0.1	4.3	3.0	8.5	0.0	5.3	3.2	8.5
4	*	-0.1	2.9	2.2	5.8	-0.0	2.9	2.2	5.9
5	x	0.1	3.2	2.5	6.8	0.0	3.3	2.6	6.8
6	*	-0.3	2.2	1.7	4.4	-0.3	2.2	1.7	4.3
7	x	0.2	2.2	1.7	4.4	0.2	2.2	1.8	4.4
8	*	0.0	1.9	1.5	3.9	0.2	2.2	1.6	4.0
9	*	-0.2	2.4	1.8	5.1	-0.3	2.6	1.9	5.3
10	x	-0.0	2.1	1.6	4.4	0.0	1.9	1.5	3.8
11	*	0.4	2.7	2.1	5.3	0.7	2.7	2.2	5.2
12	x	-0.1	3.5	2.5	7.9	-0.4	3.6	2.7	7.8
13	*	0.0	4.7	3.8	10.0	0.2	4.7	3.8	8.7
14	x	0.3	4.5	3.3	8.8	0.4	4.4	3.3	8.1
15	*	-0.1	3.7	2.8	8.0	-0.1	3.8	2.9	8.3
16	x	0.1	3.2	2.5	6.3	0.2	3.3	2.5	7.0
17	*	-0.3	4.1	3.2	8.4	-0.4	4.2	3.3	8.3
18	x	-0.3	4.7	3.4	8.7	-0.2	5.2	3.6	9.3
19	*	-1.2	3.9	3.0	7.2	0.0	3.2	2.3	5.8
Overall		-0.05	3.8	2.7	7.5	0.28	4.3	2.9	8.0

Table 3.2-7 Depth accuracy of the two Groote Plaat test depth maps based on half of the section lines.

To get an independent estimate of the accuracy the sounding data were split into two sets of section lines, denoted by "x" and "*" in Table 3.2-7. Based on each set of section lines a (test) depth map was constructed. A comparison with the depth samples in the other data set yields an independent estimate of the accuracy and is shown in Table 3.2-7. The errors presented in Table 3.2-7 are larger than those presented in Table 3.2-6, but still quite small. It is expected that the actual accuracy of the two depth maps is much better, because the comparison is made as far as possible from the calibration data. Table 3.2-7 is a worst case estimate for the accuracy of the two depth maps. Furthermore the accuracy of the depth map using all sounding data is expected to be even better because the distance between the section lines is 200 m, which is halve of the distance in the two test maps.

Note that the results of the section line 1 and 19 have been obtained by "extrapolation" of the model parameters. The result of the 5.0 m grid is obviously much better than the result of the 12.5 m grid which indicates that a finer image resolution may improve the BAS results considerably.

3.2.6 Discussion and conclusions

A map of the sea bed of the Groote Plaat area has been constructed at 5.0 m resolution using a PHARUS SAR image and depth soundings along 19 section lines. The depth was calculated using BAS. The reduction level of the sounding data was determined using the satellite based DGPS method. Estimates on the lower and upper bound of the accuracy are shown in Table 3.2-8.

	bias [cm]	rms [cm]	abs [cm]	5% [cm]
lower bound	0.03	1.7	1.2	3.6
upper bound	-0.05	3.8	2.7	7.5

Table 3.2-8 Lower and upper bound on the accuracy of the 5 m resolution depth map constructed using the Bathymetry Assessment System.

Inspection of the results at the individual section lines shows that no effects are due to the intensity transition in the original images. Apparently the somewhat ad hoc method used to remove it was adequate.

The accuracy of the constructed depth maps has improved considerably as compared to the maps based on the ERS SAR data constructed previously. For this purpose the overall results of the PHARUS based and the ERS based depth maps have been compiled in Table 3.2-9 and Table 3.2-10.

	bias [cm]	rms [cm]	abs [cm]	5 % [cm]
PHARUS 5.0 m	0.03	1.74	1.19	3.63
PHARUS 12.5 m	0.04	1.97	1.52	4.11
ERS 12.5 m	0.08	1.98	1.46	3.99

Table 3.2-9 Overall depth accuracy of depth maps constructed of the Groote Plaat area using all sounding data for calibration.

	bias [cm]	rms [cm]	abs [cm]	5 % [cm]
PHARUS 5.0 m	-0.05	3.8	2.7	7.5
PHARUS 12.5 m	0.28	4.3	2.9	8.0
ERS 12.5 m	0.81	7.34	5.84	14.48

Table 3.2-10 Overall depth accuracy of depth maps constructed of the Groote Plaat area using half of the sounding data for calibration. Accuracy is determined at the location of the other sounding data.

Table 3.2-9 shows that an improved resolution results in a more accurate depth map at the calibration lines. The accuracy of both the 12.5 m resolution ERS and PHARUS based depth maps is comparable. Therefore the improved accuracy can be attributed to the resolution and is not the result of using a different radar system. An improved accuracy is expected, because the same soundings are used for both calibration and testing. In Table 3.2-10 the soundings are split in a set used for calibration and a set used for testing. The 12.5 m results based on the PHARUS radar image are more accurate than the ERS result. Although the hydrometeorological conditions differ, it seems likely that the improved PHARUS result can be attributed to the lower speckle level of the PHARUS image. The accuracy is further improved by using higher resolution data, 5 m instead of 12.5 m. The latter was not expected beforehand.

Comparison of the depth maps of ERS and PHARUS shows that the depth accuracy has improved considerably (Table 3.2-10). Three reasons can be given:

1 The speckle level of the PHARUS data is lower, enabling better calibration of the model. The lower speckle level is easily observed by comparing Figure 3.2-6, Figure 3.2-7, and Figure 3.2-8.
2 The spatial resolution of the PHARUS data is better making it possible to position the radar data more accurately.
3 The spatial resolution of the PHARUS data allows for more detailed calculations which may improve the results. This is substantiated by the "extrapolation" results for the first and last section line.

Results show that high resolution SAR imagery may considerably improve the quality of calculated seabed topography. In order to increase the value of the PHARUS imagery, as used in this study, for quantitative interpretation the following improvements are suggested:

- Processing of a complete image in a single run, to avoid intensity transitions.
- Processing of sufficient data outside of the area visible in the imagery to avoid the edge effect.
- Addition of a "leader file" similar to the ones used in case of for example ERS SAR. Such a "leader file" should include information about resolution, pixel size, absolute image intensity, noise level, corner co-ordinates, time of recording, aircraft heading, altitude, incidence angle (at near of far range), radar look direction (left or right), etc.
- Use of 16 bit format instead of the 8 bit format. Although use of 8 bit format reduces the file size, this advantage is only minor. The size of the PHARUS images used in this study was about 10 Mbytes. Even if this size were doubled, these files are still very small compared to, for example, ERS SAR images which measure about 130 Mbytes. On the other hand the disadvantages are considerable: loss of accuracy and truncated signals at low intensities.
- The change in image intensity as a function of incidence angle, this image transformation has to be inverted in order to interpret the data quantitatively.

Figure 3.2-1 PHARUS SAR image of the "Groote Plaat" of August 27, 1996.

platform	PHARUS	
orbit/frame		
date | time (GMT)	August 27, 1996	8:37
HW wrt Harlingen	+1h39	
water level Harlingen (NAP)	+78	
water level West-Terschelling (cm NAP)	+42	
U10 | direction	5 m/s	150

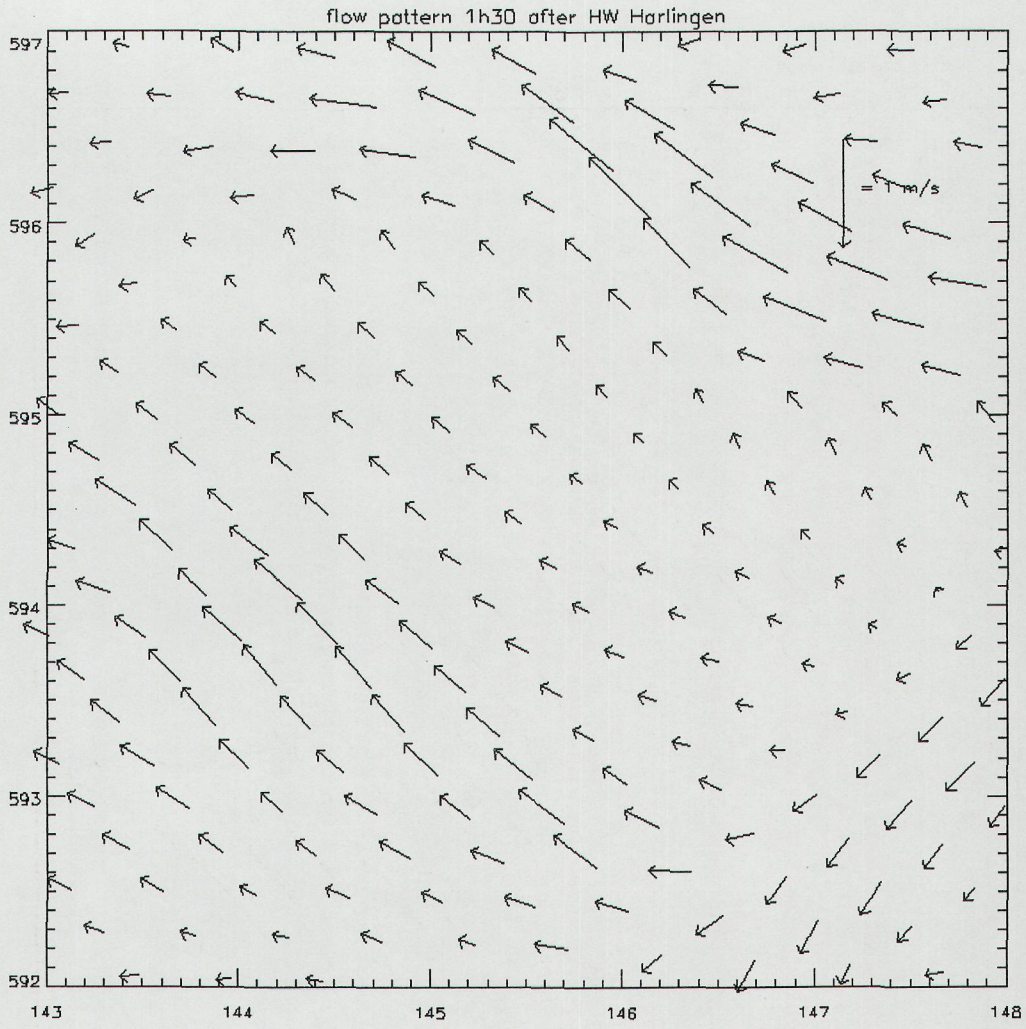

Figure 3.2-2 Flow pattern in the Groote Plaat area about 1h30 after high water at Harlingen.

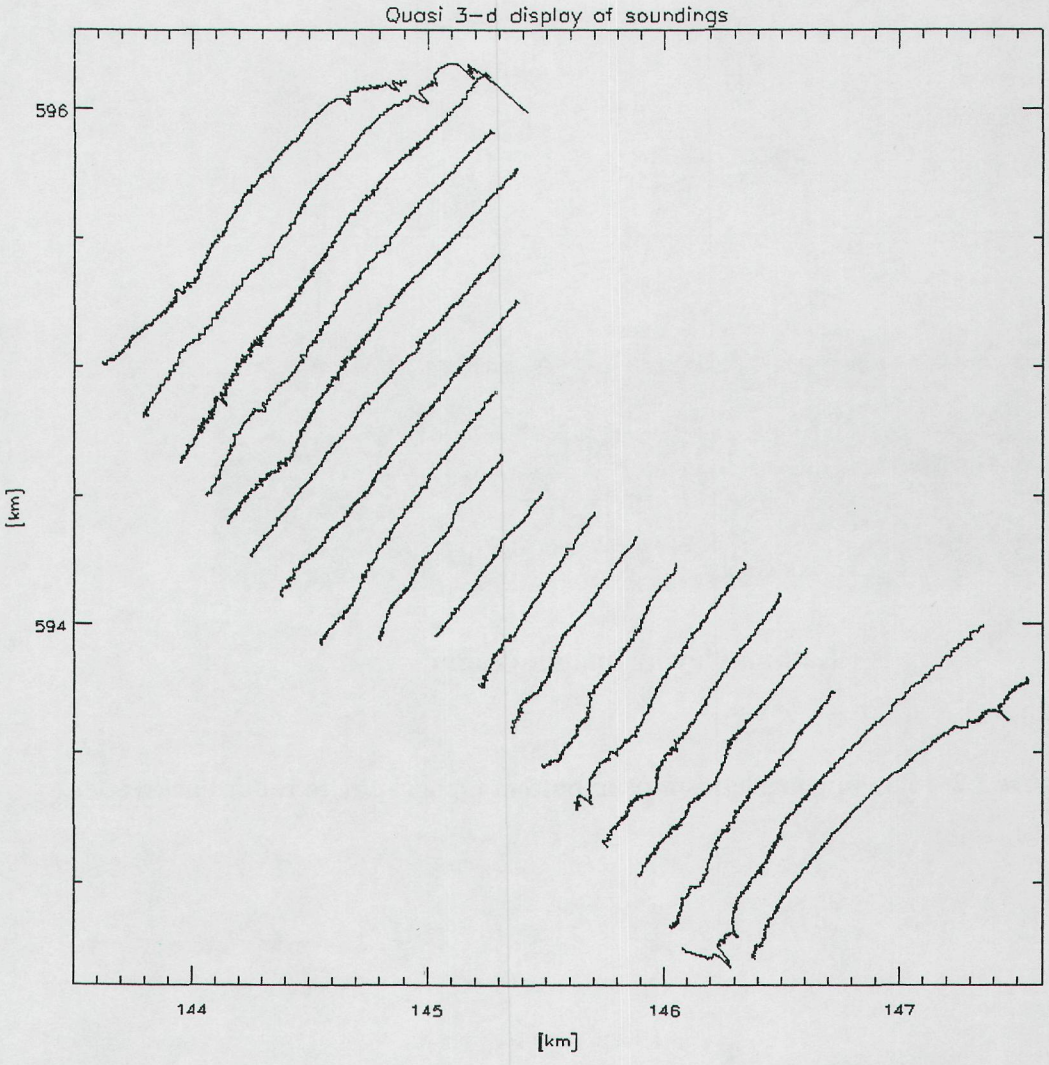

Figure 3.2-3 Quasi 3d display of depth profiles measured in the Groote Plaat area in mid-1996. One km in the horizontal plane corresponds to 5 m in the vertical direction.

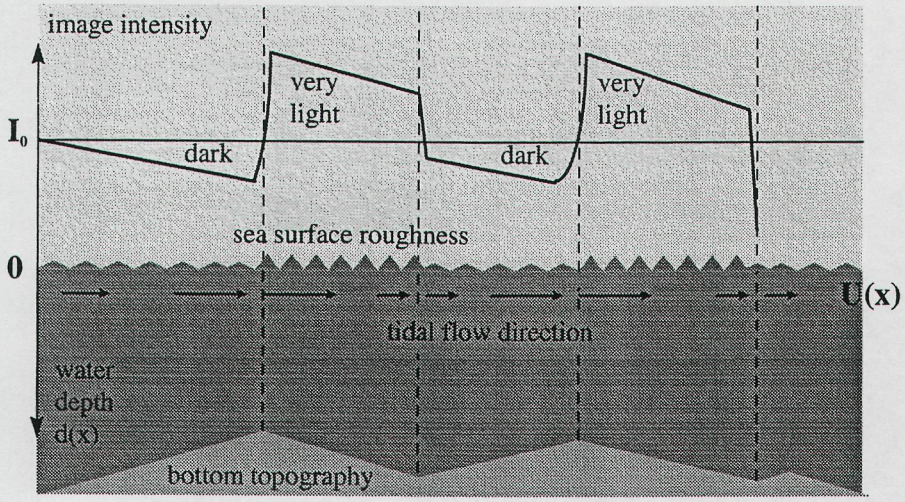

Bathymetry by imaging radar

Figure 3.2-4 Imaging mechanism from bottom topography to radar backscatter.

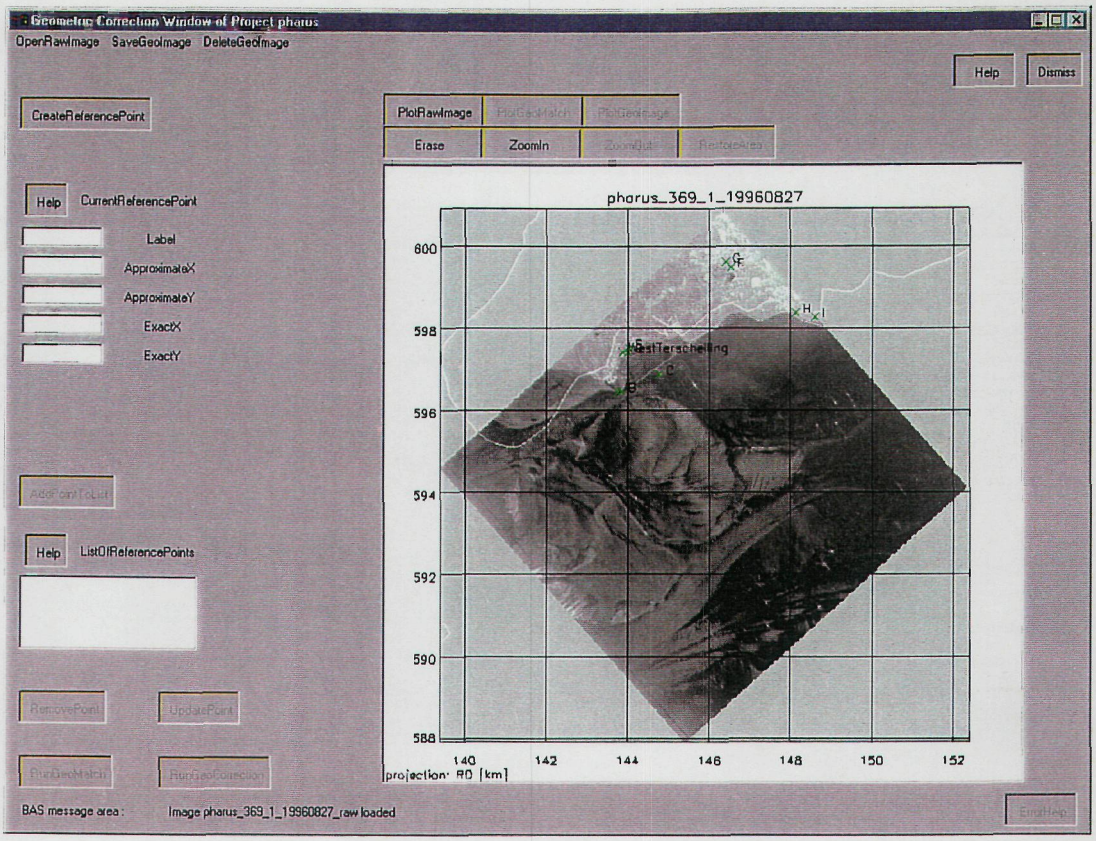

Figure 3.2-5 Geometrically corrected PHARUS SAR image of the project area recorded August 27, 1996 (whole image).

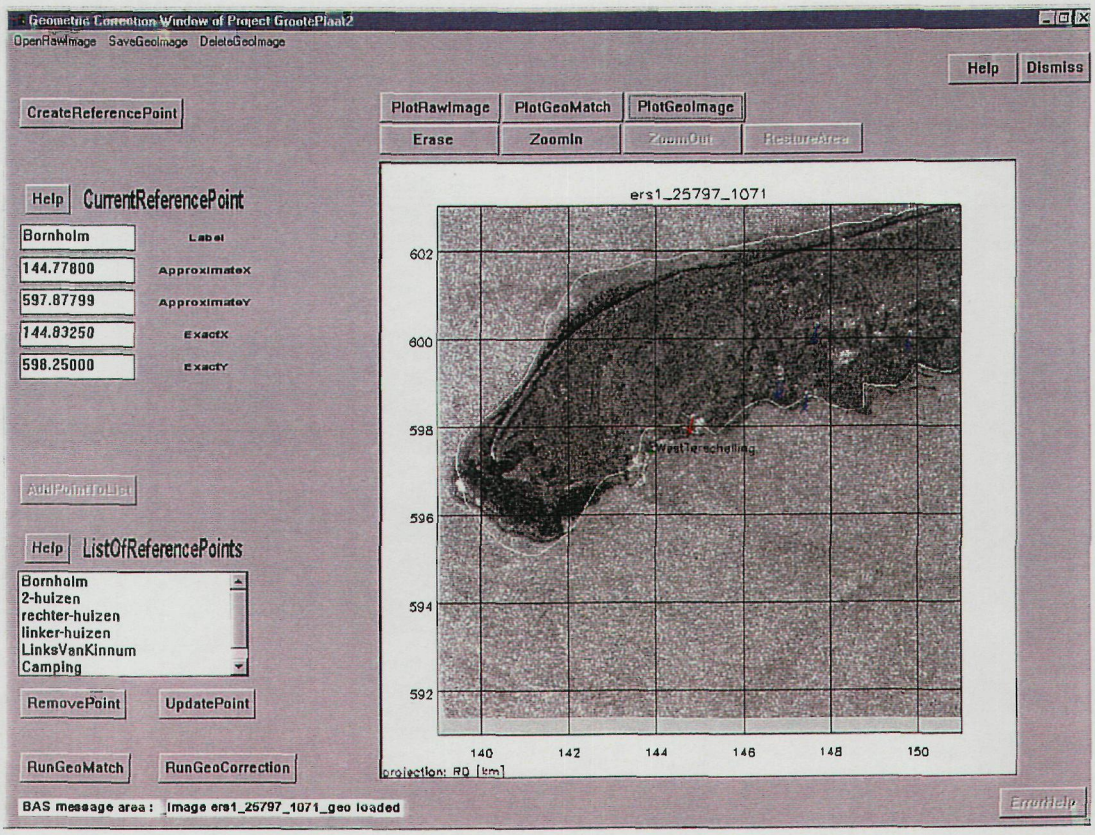

Figure 3.2-6 Geometrically corrected ERS SAR image of the project area recorded June 20, 1996.

platform	ERS-1	
orbit | frame	25797	1071
date | time (GMT)	June 20, 1996	21:38
HW wrt Harlingen	-1h51	
water level Harlingen (cm NAP)	+41	
water level West-Terschelling (cm NAP)	+47	
U10 | direction	8 m/s	300

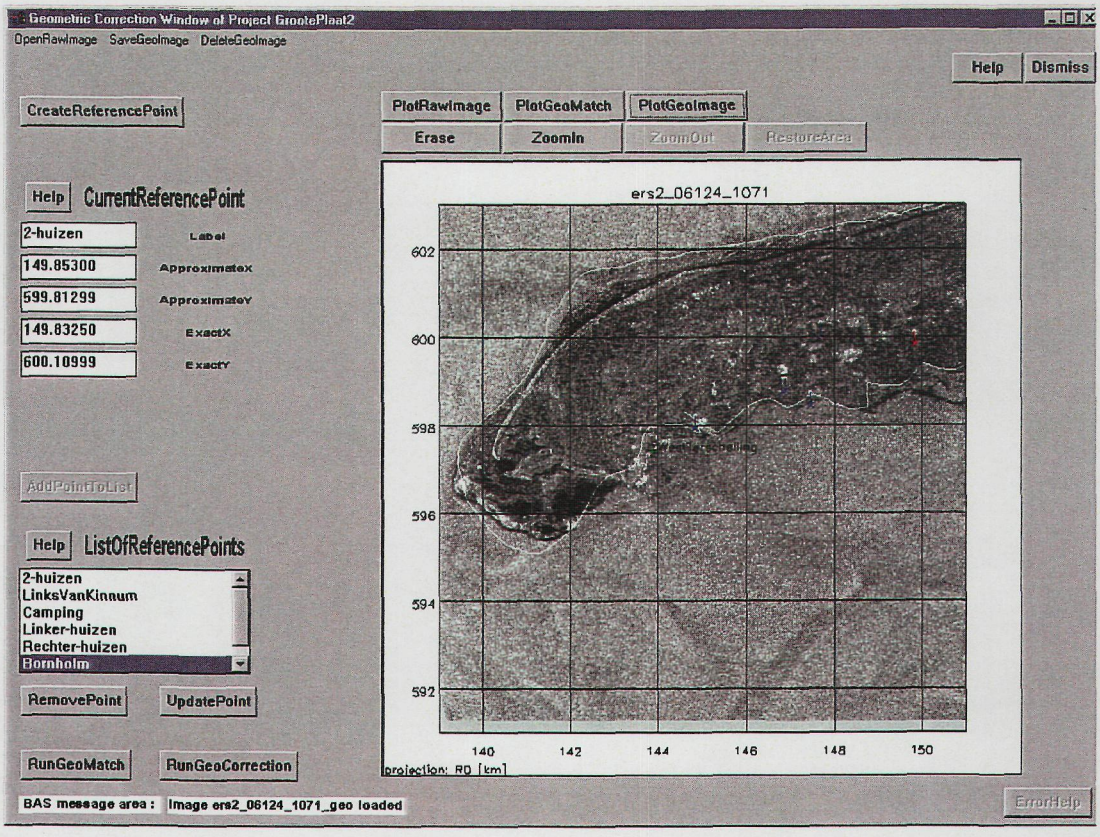

Figure 3.2-7 Geometrically corrected ERS SAR image of the project area recorded June 21, 1996.

Platform	ERS-2	
orbit I frame	06124	1071
date I time (GMT)	June 21, 1996	21:38
HW wrt Harlingen	-2h22	
waterlevel Harlingen (cm NAP)	+16	
waterlevel West-Terschelling (cm NAP)	+31	
U10 I direction	9 m/s	300

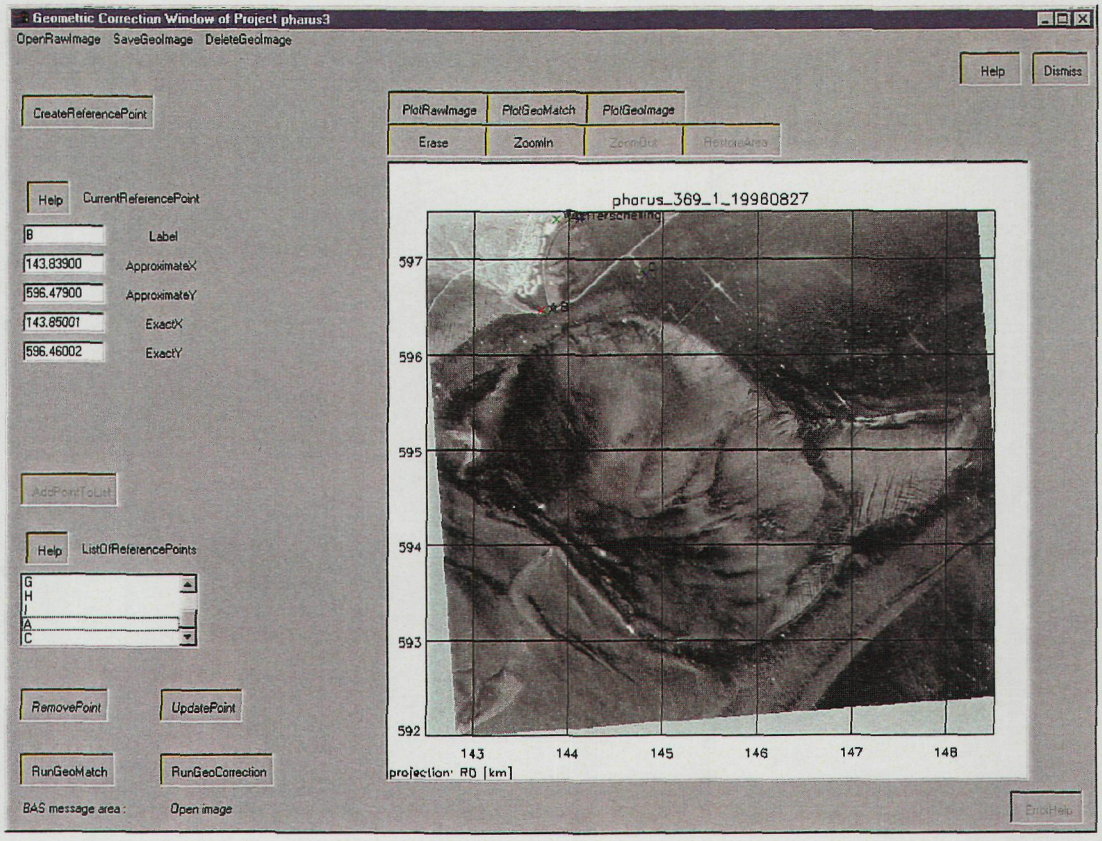

Figure 3.2-8 Geometrically corrected PHARUS SAR image of the project area recorded August 27, 1996 (part of the image).

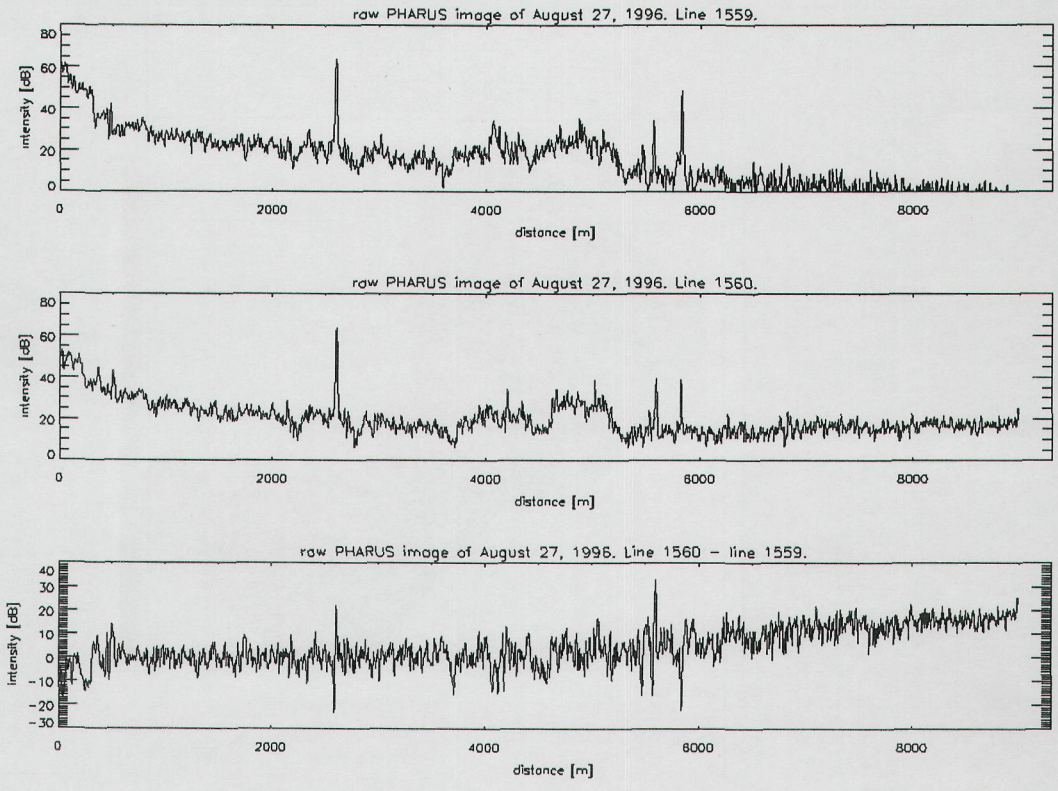

Figure 3.2-9 Intensity profiles of the PHARUS SAR image of the project area recorded August 27, 1996. Top: line 1559, middle: line 1560, bottom: difference of line 1559 and line 1560.

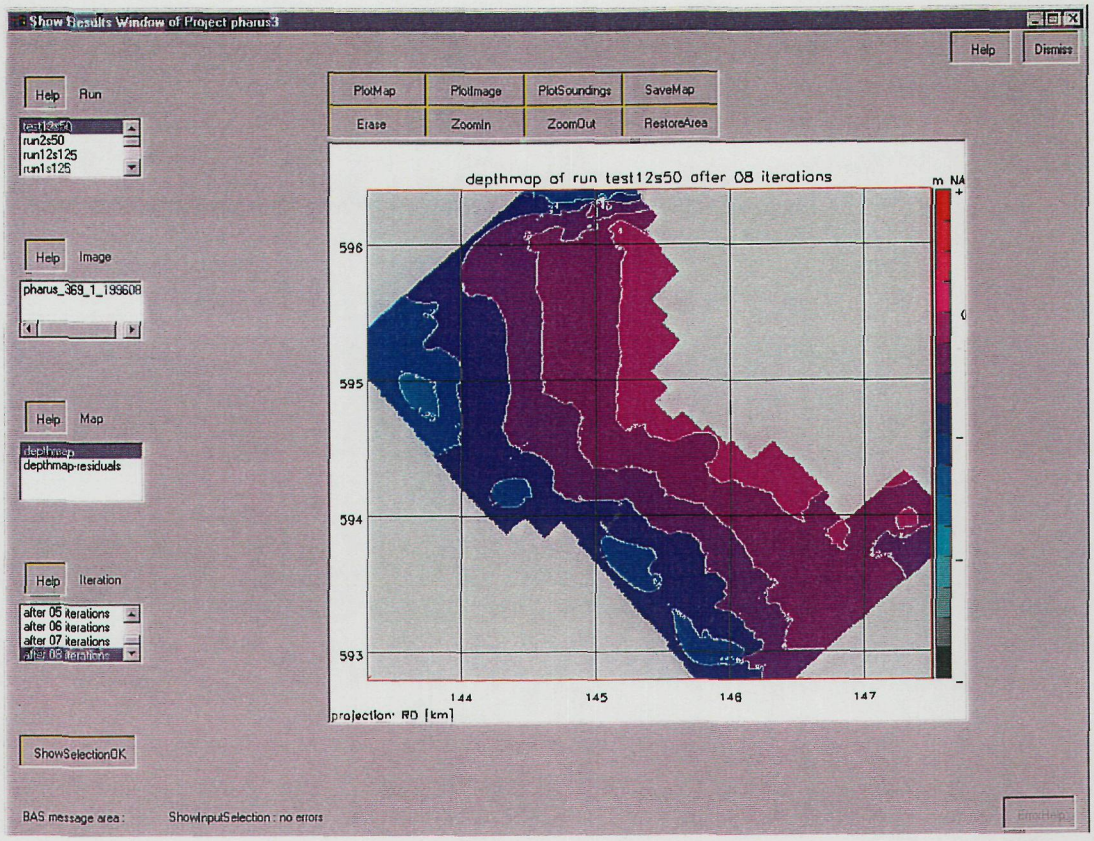

Figure 3.2-10 Map of the sea bed topography of the Groote Plaat area, based on the PHARUS SAR image and all sounding data.

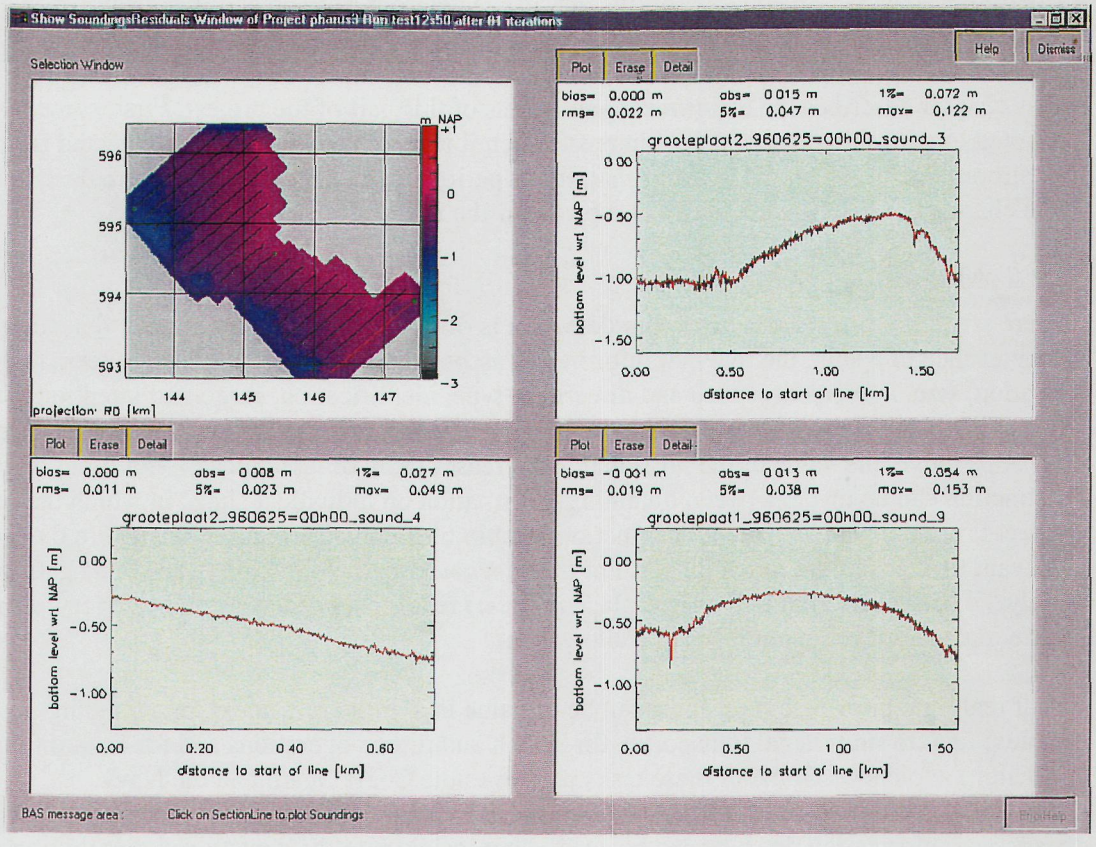

Figure 3.2-11 Three depth profiles of the sea bed topography of the Groote Plaat area, based on the PHARUS SAR image and all sounding data. Upper left picture gives overview of measurements. Both the measurements and the calculations (which coincide almost completely) are shown for line 1, 10 and 19 (lower left, upper right and lower right respectively). Lines are numbered from 1 to 19 starting in the upper left.

3.3 *Ship and ship wake detection*

3.3.1 Introduction

One of the oldest radar applications is the detection of ships at sea. Airborne SAR (Synthetic Aperture Radar) is also suitable for this purpose. Therefore, ship detection constituted one element of the PHARUS Familiarization program.

This chapter describes the experiment and results of this part of the project. First, some text is devoted to why ship detection is of interest. Then it is reviewed what can be expected from an airborne polarimetric SAR. After that, the experiment and the data analysis are described. The chapter concludes with results and plans for the future.

3.3.2 Motivation

There are numerous reasons why ship detection is of interest. Apart from merely detecting the presence of a ship, the relevant information associated with ship detection concerns location, size, movement (speed and direction), type, identification, cargo and intention of the ship. This list is approximately ordered by ease of obtaining this information from radar data. As ships move, the value of the information decreases more or less quickly with time. A distinction can be made between obtaining information on individual ships, in which the time aspect is crucial, and statistical information on ship traffic in a certain region, where the relevant time scales are much longer. For the first category, information needs to be gathered, analyzed and transferred to the right place in (near) real time. For the second category, a time lapse of days or even months may be allowable.

Near real time information on ships can be of value in a military context, in a policing context (e.g. to find illegal transports), for search and rescue operations and for hazard (e.g. collision) avoidance. Some of these tasks pertain to the Coast Guard and the Navy.

Statistical information on ships can be used to get insight into the density and distribution of ship traffic and shipping routes, which, for example, can be the basis of policy decisions on implementing traffic control schemes. Information on the operations of fishing vessels can be used in verifying or policy making of fishing restrictions. Information on the behaviour of ships with a potentially dangerous content (oil, chemicals) can be used to assess pollution dangers and possibly implement environmental protection measures. Some of these issues are relevant to Rijkswaterstaat and the Netherlands Ministries LNV and VROM.

3.3.3 The use of PHARUS

PHARUS, being an airborne polarimetric SAR, has a number of properties that make it suitable for the purpose of ship detection. Being a radar, it can operate by day or night, unhindered by clouds, fog, rain or smoke. This compares favourably to the performance of optical or infrared sensors, although the latter have in general a higher spatial resolution. The typical amount of spatial detail that can be discerned by PHARUS is of the order of meters (more specific numbers are given below).

Being a SAR means that it can image a large field of view ("swath"), keeping the same high spatial resolution over the full field of view; as opposed to conventional radars, which quickly lose spatial resolution at larger distances. The instantaneous field of view is of the order of 10 km (like the spatial resolution, this imaging parameter is adjustable).

Being airborne implies that PHARUS can cover large areas in a short time, and that it can be quickly and flexibly deployed and directed to areas of interest. This provides much greater flexibility than the use of a satellite, which has a fixed revisiting schedule, or a shore-based radar, which only covers a limited area.

As PHARUS is an imaging radar, it not only detects targets but also images the earth (sea) surface. Thereby, it is also able to detect disturbances on the sea surface. Actually, many kinds of sea surface disturbances are seen in SAR images; many are natural, but some are created by the moving ships. These are referred to as "ship wake signatures". The wake signatures can be used as an aid in the detection process, and can be the source of additional information on the ship. The kind of information that might, in principle, be extracted from the wake signature is ship motion (speed and direction), ship size and draught. It should be noted, however, that this information is not easily obtained at present.

The polarimetric capability of PHARUS is expected to be of added value in ship detection, since the polarimetry of the ship's signature is expected to be different from that of the water. This is especially of relevance to the detection of small ships; as the sea surface itself also produces a radar echo, the radar echo of a target needs to be discernible from that of the surrounding sea. In non-polarimetric radars, this distinction can only be made on the basis of radar echo strength alone. In a polarimetric system, a different polarization signature will also lead to target detection.

On the basis of the present development status and parameters of PHARUS and results described in the literature, we may expect that PHARUS is able to detect relatively small ships (> 10 m), find ships' locations with high accuracy, estimate speed, heading and size with reasonable accuracy, and obtain some limited information on ship type (tanker, frigate, cargo, fishing). Ship identification and draught are not expected to be feasible from PHARUS data (yet). Two effects are beforehand expected to lead to a lower detection performance. One is sea state, because the radar echo of the sea increases with sea state, making it more difficult to discern small targets in the background. The other is ship motion (heave, roll, pitch and yaw), since this will lead to a defocusing of the ship in the SAR image construction; this effect is expected to be more important in far range. This defocusing effect, however, may be actually turned into an advantage by applying so-called Inverse-SAR (ISAR) processing to the data, where use is made of the ship's motion to construct a very-high resolution image of the ship. This type of processing is presently not yet available for PHARUS.

Concerning real time information, at present PHARUS is not equipped for that facility. The processing needed to go from recorded radar data to a SAR image, and subsequently to extract information on ships and transmit the information to where it is needed, necessarily needs some time. With the proper infrastructure and processing power, delays induced by this can be minimal. A real time SAR processor for SAR image production is currently being developed at TNO. For now, however, the PHARUS data are recorded on the aircraft, and, after the flight, processed on the ground. Present capabilities provide for a turn-around time of within a day at best.

3.3.4 Experiment

Three experiments for ship detection have been carried out under the Familiarization program. Originally, only one was planned, but the first two attempts failed due to technical problems. The first two were controlled experiments, with valuable support from the Navy and from Rijkswaterstaat.

In the first (failed) experiment, a Navy ship was directed to navigate at a certain location, with a fixed speed and heading, logging its navigational data. The ship was especially equipped with a GPS receiver and an air band radio for communication with the PHARUS aircraft. The logistics of the experiment worked out well, since the ship was imaged by the aircraft and all relevant ship information at time of imaging was logged. Unfortunately, the system did not perform successfully.

In a second (also failed) attempt, it was planned to image the Hoek van Holland area. At the scheduled time, the harbour radar at Hoek van Holland was manned by personnel from Rijkswaterstaat, who logged the positions, movements and identifications of ships in the area. In this way, the performance of PHARUS could be compared to the actual situation. Unfortunately, the PHARUS flight was cancelled due to technical problems.

On the basis of these experiences, it was decided to use ships of opportunity in following attempts, and to postpone controlled experiments, which require considerable support effort, to a later time when PHARUS would be more reliable. In the third experiment, again the Hoek van Holland area was imaged, this time, however, without in-situ data. The third experiment was successful. An area of approximately 22 by 16 km was imaged in two adjacent east-west strips of approximately 22 km length near Hoek van Holland, where the presence of ship traffic is nearly assured, on the morning of May 29, 1997. PHARUS was used in mode "BCRS-3" at 4.8 km altitude, 100 m/s aircraft velocity, leading to a fully polarimetric data set with a nominal single look spatial resolution of 3.5 m in slant range by 1.0 m in azimuth, a strip width of 8 km, and incidence angles varying between 49° and 71° (near range to far range). The parameters of this data set are listed in the table below. On account of the expected lower backscatter level in the cross-polarized (HV, VH) channels, the receiver gain of these channels was set 10 dB higher than that of the co-polarized (HH, VV) channels.

Strip	1	2
Date	29-5-1997	
Flight	460	
Polarimetry	Quad	
Nominal resolution (m)	3.5 m slant range × 1.0 m single look azimuth	
Time (UTC)	09:31	09:21
Scene top right	52° 04.4' N, 4° 00' E	52° 08.8' N, 4° 00' E
Scene bottom left	52° 00.0' N, 3° 40' E	52° 04.4' N, 3° 40' E
Track angle	89° N	-91° N
Altitude (m)	4780	4720
Scene size (km)	22.5 × 8.1	22.5 × 8.1
Incidence angle	49°-71°	50°-71°
Yaw	-5°	8°

Table 3.3-1 Parameters of the acquired data set.

3.3.5 Processing and analysis

The data were processed on the GSP (Generic SAR Processor), correcting for aircraft motions, into multi-look images (5 looks without overlap) at 5 × 5 m ground resolution. (Multi-look processing is done to lower the speckle noise in the image.) Four polarimetric channels were produced (HH, HV, VH and VV). Particular steps in the processing were:
(a) Interference due to clock frequencies was filtered out of the data at range compression;

(b) The variation of backscatter level with incidence angle was removed, in order to obtain images with a constant background level;
(c) The images were logarithmically scaled. The resulting, as yet uncalibrated, images were visually inspected using contrast enhancement on a computer monitor.

In order to be able to correctly interpret the polarimetric signatures, and use the polarimetry as a tool to discern the ships from their background, polarimetric calibration of the data is necessary. As polarimetric calibration is not yet implemented as an automatic tool in the GSP, this had to be done separately, which is very time consuming. For that reason, only a subset of the data was selected for this. This subset (of strip 1) was processed into a polarimetric covariance matrix format. Its imaging parameters are listed in the table below.

Scene top right	52° 04.4' N, 3° 59.8' E
Scene bottom left	52° 00.0' N, 3° 50.0' E
Image size (Ground range × Azimuth)	8120 × 11200 m ; 4080 × 5700 pixels
Pixel size (Ground range × Azimuth) (m)	1.965 × 1.965
Resolution (Ground range × Azimuth) (m)	6 - 5 (near to far) × 4
Number of looks	6
Multilook by	Spatial averaging in azimuth
Tapering (range and azimuth)	Cosine squared, 6 dB
Incidence angle	49.0° - 70.7°
Format	Calibrated polarimetric covariance matrix

Table 3.3-2 Parameters of the calibrated image.

The subset selected for calibration was completely re-processed, on a newer version of the GSP.
The following steps were included in the processing of this subset:
(a) Interference due to clock frequencies was filtered out;
(b) The DC level of the I and Q channels was removed;
(c) Correction for the antenna elevation pattern was applied;
(d) Receiver gain correction was applied (to correct for the 10 dB gain difference between co- and cross-pol channels);
(e) The residual variation of backscatter level with incidence angle was removed.

The polarimetric calibration consisted of the following steps:
1. Phase calibration;
2. Cross-talk calibration, by symmetrization of the covariance matrix;
3. An estimated gain imbalance correction.

For all these calibration steps, use was made of the recorded sea clutter data itself in combination with assumptions about the behaviour of the clutter, without any external calibration devices. No radiometric calibration (i.e., calibration of the absolute radar backscatter level) was performed (nor indeed foreseen); this is not necessary for the application.

The calibrated image is suitable as input for polarimetric detection routines. However, after the double re-execution of the experiment and the, larger than foreseen, effort to calibrate the data, within the project no more time was available to further pursue this aspect, and it has to remain for future work. From the calibrated polarimetric covariance matrix data, three power images (HH, VV and HV) were extracted and visually analyzed after logarithmic scaling. By definition, the VH channel is equated to the HV channel as a step of the calibration process, so these two "cross-polarized" channels contain the same information after the calibration.

Polarimetric information not contained in the three power images concern phase differences between the (complex) channels.

3.3.6 Results

First, the results from the uncalibrated data will be given. Then the calibrated data will be discussed in some more depth.

Visual analysis of the uncalibrated images of strip 1 yields a total count of 12 targets (assumed to be ships) within the 180 km^2 processed area. One of the ships has a wake signature. Of one range line in strip 1 the image quality is very poor; the cause of this is unknown. In strip 2, 22 targets and 4 wakes are found within the 140 km^2 processed area. This strip contains a number of localised disturbances which take the form of thin, short lines in azimuth direction. These features are not seen in strip 1. Their origin is unknown; possibly interference by other radio emissions might be a cause. It is expected that this kind of disturbances can easily be filtered out if necessary, without affecting ship detection performance.

For the calibrated data, the subset of strip 1, an evaluation of the data quality was performed. Analysis of the raw data I- and Q- values shows that there are no overflows, and that quantization noise is unimportant. Raw I and Q signal levels in the HV and VH channels are higher than in the VV and HH channels. Also from the raw data, an average signal-to-noise ratio is estimated in the VV channel of 12 dB, in the HH channel of 8 dB and in the HV and VH channels of 0 dB (3 dB after symmetrization). It can be concluded that the received cross-polarized radar backscatter was at a level comparable to the system noise. A higher receiver gain would not have improved the data quality of the cross-polarized channels. S/N ratios here refer to "background clutter to system noise", not "target to noise".

The polarimetric power images resulting from the calibration are shown in Figure 3.3-1. The figure consists of three parts, viz. the HH (a), VV (b) and HV (c) channels.

The VV channel shows a lot of structure on the sea surface, with ships as bright targets, mostly clustered in the bottom centre and bottom right part of the scene. A visual count within this image yields a total of 8 targets. One of these (second from the right, just right of a brighter target) is uncertain. Its weakness and nearness to a bright target at the same range make it suspect of being a side lobe or alias effect. Although this calibrated scene only shows ships at near range, the uncalibrated data contain many ships also at medium and far ranges because the uncalibrated scene is larger than the calibrated scene.

In far range, the structure on the sea surface becomes more fuzzy. This is due to the longer synthetic aperture time at far range in combination with the fact that the sea surface is not stationary but in motion (waves, etc.). The synthetic aperture time is the time needed for the SAR to collect the data, which is longer for the far ranges. The full synthetic aperture time, needed to reach the 1 meter single look resolution, varies between 4 and 8 seconds in the present situation. At far range, details on the sea surface become significantly replaced during the synthetic aperture time, and become thereby smeared in azimuth direction. Also, most of the ships are elongated in the azimuth direction. This may mean that a ship is actually oriented in that way, but it may also be due to motion of the ships (including heave, roll, pitch and yaw) during the synthetic aperture time. Part of the elongation is also due to side lobes. One of the ships (the one at nearest range) shows a wake. The dark-bright-dark cross cut of the wake some distance behind the ship points to a wake of the turbulent type (as opposed to e.g. a Kelvin wake), indicating the direction of motion of the ship. In this case, it is evident that the elongation of the ship image must be due to azimuth smearing, no attempt has been made to further analyze the wake for velocity information. The other ships have no clear

wake signatures, which makes it plausible that they are not moving. The sea surface is overall characterized by stripes, which are probably older wakes from ships that have passed earlier.

The HH channel shows essentially the same features as the VV channel, except that at the far range the image becomes featureless. This is due to system noise; at far range, the HH backscatter of the sea drops below the system sensitivity. This is in accordance with the fact that sea surface backscatter drops off with incidence angle, and is lower for HH than for VV. Inspection of spectra of the raw data (discussed above) confirms that in far range no signal from the sea surface is detected, and that the smooth grey background is merely system noise. The same 8 ships are seen as in the VV image, plus 4 weak targets at bottom centre. In HH, the ships stand out higher above the sea clutter, as can be seen from the fact that weak side lobes in range (fuzzy, vertical lines through the centre of the targets) can be seen in HH, while not in VV. This is according to expectation.

The cross-polarized channel (HV=VH) is characterized by a still weaker signal from the sea surface. Here, most of the image background is just system noise (as discussed above). Only at very near range, the same sea surface features as in VV and HH are weakly visible. (Note that also the wake from the ship at nearest range shows up in the cross-polarized channel.) This is as expected; cross-polarized backscatter in general has a much lower level than co-polarized. Because of the relative weakness of the cross-polarized signals, these are very susceptible to contamination from co-polarized backscatter. The calibration procedure, however, has reduced cross talk to better than -50 dB, so the HV image can be regarded as reliable to that extent. The ships have again higher contrast to the background, as can be deduced from the still more prominent side lobes. (Lacking a detailed analysis of the actual side lobe levels in the various channels, this is only a preliminary conclusion.) The 4 weak targets at bottom centre, which were visible in HH but not in VV, are also found in HV.

Combining the results from the 3 channels, we find a total of 12 targets within the 91 km^2 of the calibrated scene, one of which is uncertain (possible side lobe or alias effect).

3.3.7 Conclusions

Based on visual analysis of the HH, VV, VH and HV polarimetric channels (calibrated and uncalibrated), it can be concluded that ships are easily detected by PHARUS. Also ship wakes are readily imaged. The ships appear to have the highest contrast with respect to the sea clutter in the HV channel, indicating that the cross-polarized channels are best suited for this purpose. Of the co-polarized channels, the contrast between ship and background is larger in HH than in VV, so that of these two HH is better suited. However, if information from the ship wakes is required (e.g., ship velocity), then the VV channel contains most information, also out to the far ranges.

On account of the lack of in-situ information in this experiment, the PHARUS results cannot be verified. There is no indication of the completeness of the set of ships that PHARUS detected. Also, it cannot be verified whether all targets detected by PHARUS were indeed ships (and not, e.g., large waves). This applies particularly to the uncertain / weak targets. (The reasons for the lack of in-situ data were explained in the section "Experiment".)

The ship signatures seem to be subject to considerable azimuth smearing, making it difficult to extract information on ship size and heading. Different processing techniques, however, might alleviate this effect.

The analysis of the raw data signal levels has shown that the cross-polarized radar backscatter at the receiver is of a level comparable to the receiver noise. Only at the very near ranges is the cross-polarized backscatter detectable. Therefore, if the cross-polarized radar backscatter

of the sea surface needs to be imaged over most of the swath, a different PHARUS mode is required, with steeper incidence angles and/or lower altitude. To a lesser extent, the same applies to the HH backscatter. (Note that the sea surface backscatter level is also dependent on wind velocity.)

Due to lack of time in the project (for reasons explained before), the analysis has been only preliminary. In particular, only the polarimetric power channels were visually interpreted. It is expected that much can be gained by subjecting the complete polarimetric covariance matrix to a classification scheme for optimum distinction between ships and background sea clutter. Also only then, the maximum benefits from PHARUS' polarimetric capability can be demonstrated.

3.3.8 Future work

The polarimetric data set obtained from this experiment can be analyzed further, by applying automated detection algorithms to the polarimetric data as outlined at the end of the previous paragraph.

While this project has shown that PHARUS can be used successfully for ship detection, and that its polarimetric capability is of value, no quantitative conclusions on the performance of PHARUS could be drawn (in terms of detection rates and false alarm rates). For this, it is necessary to perform a controlled experiment with a complete set of in-situ data. Especially small targets are of interest, as are situations of higher sea state and the performance at far range. At present, PHARUS is deemed reliable enough to invest effort in such a verification experiment. Possibly, such an experiment can be combined with a future ENVISAT-ASAR experiment. An investigation into the performance of PHARUS should also take into account other modes (e.g., modes with a larger swath but less polarimetric information) so that conclusions may be drawn as to the operationally or economically optimal mode for the application of ship detection.

The possibilities for processing the data in ways to counter the azimuth smearing of the ship signatures should be addressed. Possibly, ISAR techniques may be used.

In the longer term, ship detection is one of the applications to benefit from the real time SAR processing capability presently being developed. For full real time benefits, also a data link to the ground should be implemented.

Figure 3.3-1 (next 3 pages). Power images of the calibrated part of strip 1; ref. the table in the section "Processing and analysis". (a) VV image. (b) HH image. (c) HV image. The long side is azimuth direction, the short side ground range. The images are logarithmically scaled, and sub-sampled by a factor of 3 to fit on the page.

(a)

Noordzee. 29 May 1997. PHARUS single channel (VV). data by TNO-FEL/TUD/NLR.

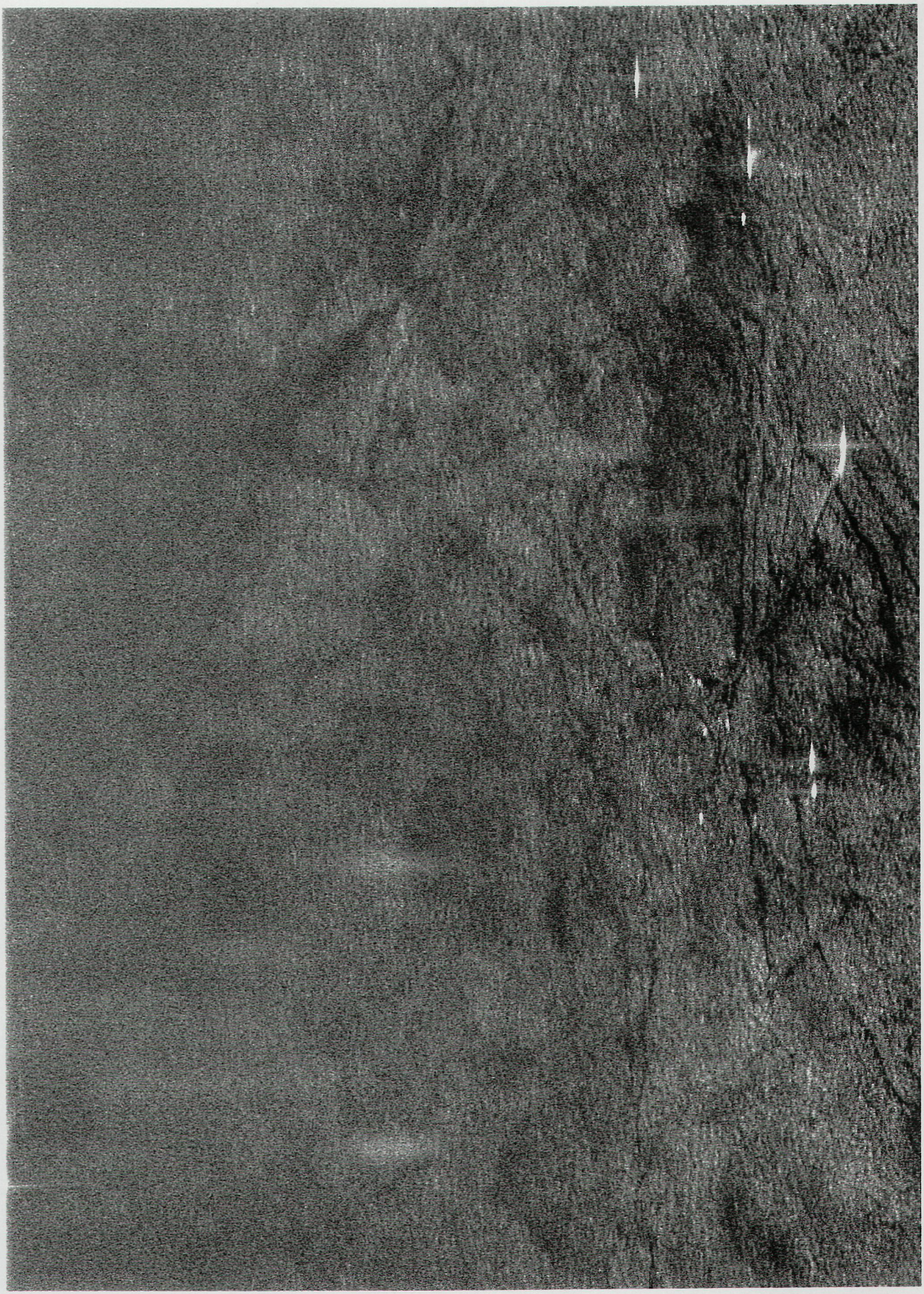

Noordzee. 29 May 1997. PHARUS single channel (HH). data by TNO-FEL/TUD/NLR.

(b)

Noordzee. 29 May 1997. PHARUS single channel (HV). data by TNO-FEL/TUD/NLR.

(c)

4. Target Detection with PHARUS

SAR has been used, and is being used increasingly for military applications. Obviously, the capability to observe during night and day, and through fog, rain and clouds is a very significant military advantage over other sensors. The same goes for the radar ability to observe over very long distances. Therefore, SAR is already an important military surveillance and reconnaissance tool in several military forces in the world. In the PHARUS Familiarization program, the main objective of WP 7, named 'Target Detection' was to demonstrate some of the PHARUS capabilities for military applications. Since a number of polarimetric data takes with PHARUS of static military installations and vehicles had already been made on an earlier occasion, it was decided to focus on *moving* targets in this WP; as an additional experiment, a recording was made under the influence of a jamming signal directed at PHARUS from the ground. The military relevance of SAR jamming is obvious; it is a means of preventing or misleading the observation with SAR, by transmitting interfering signals at the SAR.

4.1 *The MTI experiments*

The main experiment consisted of trying to demonstrate the ability to detect moving targets with PHARUS. To reduce the preparation effort and risk for this first MTI experiment, an area was chosen where there would with certainty be moving targets with a reasonably large velocity; the chosen area was around the major traffic junctions near The Hague, with several main highways in different directions. The technical preparations mainly consisted of defining suitable imaging settings for an MTI-experiment, as the pre-defined basic PHARUS modes were not usable for this purpose.

The detection of moving targets is based, in the first place, on the additional Doppler shift of the echo signal caused by the motion of the target. In the normal imaging modes, on-board Doppler filtering is applied, for the purpose of data rate reduction while preserving received energy. This filtering also removes echoes from Doppler-shifted moving targets. Consequently, an imaging mode without pre-filtering had to be defined, which, because of the very much higher data rate, was defined as a single polarization mode. In this 'MTI-mode', a recording was made with PHARUS of a part of the A12 highway near Zoetermeer.

The processing of data was done in three steps:

1. The data was first processed as normal SAR data, providing a normal SAR image of the imaged area. This image, though in one polarization only, was even of slightly better quality than the usual single-polarization image, due to the fact that no on-board data reduction was applied. This means that the azimuth ambiguity level is extremely low, which results in improved image contrast.
2. After viewing the SAR image, the Doppler shifts of expected targets were predicted, and the SAR/MTI processing was performed, focused on the predicted Doppler shifts. In a real MTI system, target Dopplers can not be predicted, so that a bank of Doppler filters must be applied to cover a range of possible target velocities. The approach used for the experimental data is a simply shortcut with respect to the more general-, more time consuming approach, which, in the end, would yield the same results for this case.
3. After SAR/MTI processing, moving target detections could be made, which were translated to target positions on the highway and their velocities

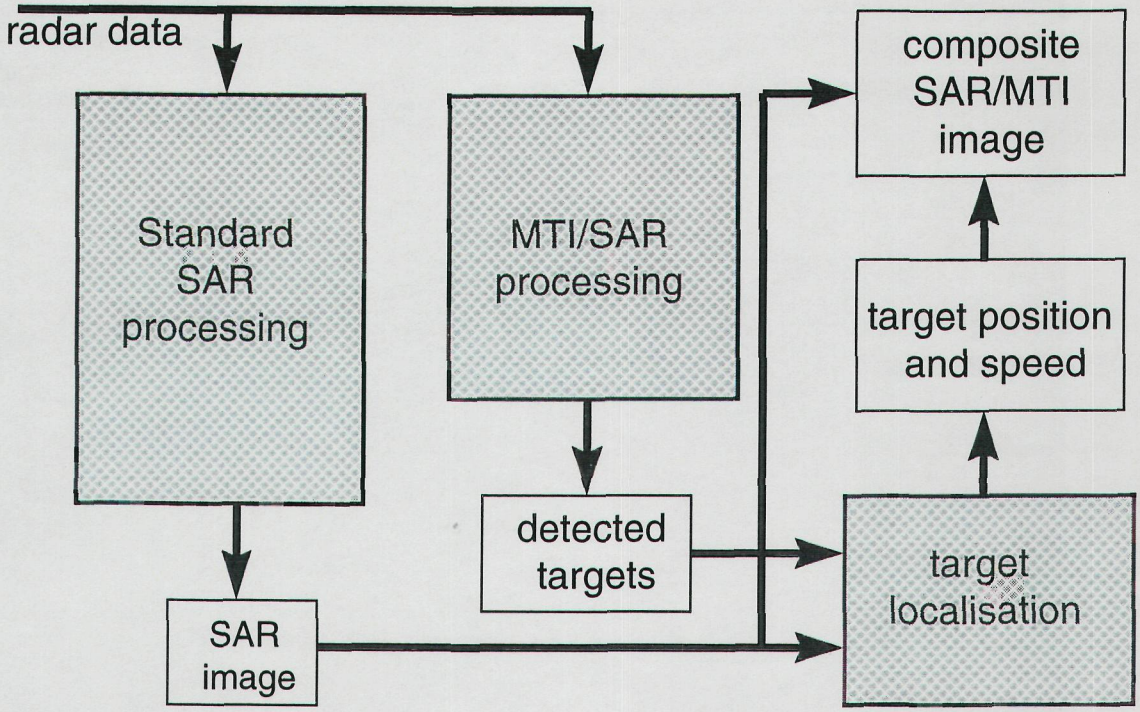

Figure 4.1-1 SAR MTI processing scheme

The SAR and MTI processing approach is schematically shown in Figure 4.1-1. The first product that is produced is the SAR image itself. This is shown in Figure 4.1-2. It clearly shows part of the A12 with Zoetermeer mostly on the left. When the same raw data is processed with shifted Doppler Centroid, which is the basic MTI/SAR processing, the image shown in Figure 4.1-3, appears. Clearly, most of the image is dark, since all reflections from static objects have now been strongly suppressed by the MTI processing. The slightly slanted bright spots are objects which apparently move with approximately the assumed velocity. These are now easily detected. Since, the velocity is *approximately* known, from the fact that they are detected in a particular Doppler band, and from the slanted shape of the response, it can be concluded that these targets must move along the A12. This additional information then makes it possible to calculate not only the position on the A12, but also their velocities with much higher accuracy: this is done by making use of the fact, that the moving targets are displaced in the SAR image from their actual position. The amount of displacement is proportional to their radial velocity. By assuming that the real target positions are on the A12, the displacement can be determined, which leads to the radial velocity estimate. Since the direction of motion is also known from the road orientation, the complete velocity vector of the target can be derived. Note that these deductions can only be made by using the MTI detections together with an interpretation of the SAR image! In this way a composite image can be made using the SAR image, on which the detected targets are superimposed with symbols. This was done twice; both for targets moving towards the radar, and those moving away from the radar. The results are shown in Figure 4.1-4 and Figure 4.1-5.

Figure 4.1-2 SAR image from the PHARUS MTI experiment

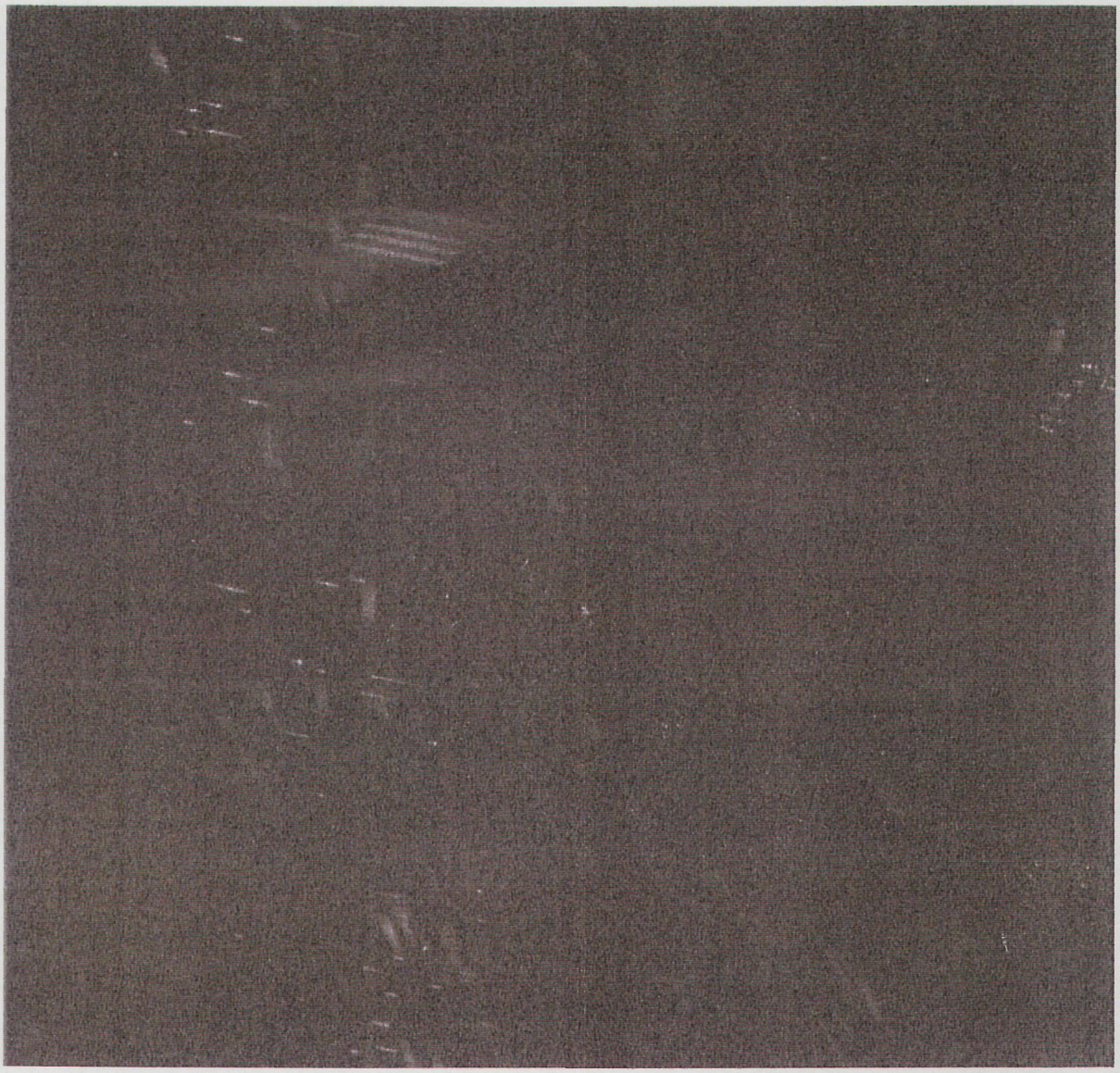

Figure 4.1-3 PHARUS data after MTI/SAR processing

Figure 4.1-4 Composite SAR/MTI image showing moving targets on the left (in the image) side of the A12. Velocities are indicated in km/h.

Figure 4.1-5 Composite SAR/MTI image showing moving targets on the right (in the image) side of the A12. Velocities are indicated in km/h.

4.2 *Conclusion regarding MTI with PHARUS*

With these results it has been demonstrated that it is possible to detect fast moving targets with PHARUS. Since this technique is based on Doppler separation between the SAR image signal and the moving target signal, it is possible to calculate what radial velocity is approximately required for targets to be detectable with this technique. The lower limit depends on several factors such as the target direction, and radar cross section, the incidence angle, and the velocity of the aircraft carrying PHARUS. As a rule of thumb, one can say that this technique works well if the radial target velocity Vr is well above the limit given below:

$$V_r > \frac{V \cdot \lambda}{2 \cdot d_{ant}}$$

where V is the aircraft velocity (100 m/s), λ the radar wavelength (0.057 m), and d_{ant} the antenna length (1 m). This gives a lower limit of 10 km/h. However, the radial velocity is the projection of the actual ground velocity towards the radar, onto the line of sight. At, say, 45°, the lower limit on the ground is 14 km/h. In practice, the lower limit is about 20 km/h. Detection of much slower targets requires more sophisticated MTI techniques, which make use of 2 of three SAR antennas along track, or antennas with multiple phase centres such as monopulse antennas or phased arrays with separate subpanels. Such experiments can be carried out with the PHARUS system: on the short term, experiments are foreseen without significant hardware changes, making use of the fact that different parts of the antenna can be switched on and off, thus 'simulating' two antennas. The next step would be to modify the radar, so that it can receive of different parts of the antenna simultaneously, but through separate receiving channels. In this way, very powerful SAR/MTI modes could be realised with the PHARUS system.

4.3 *PHARUS jamming experiments*

The jamming experiment was carried out in co-operation with NLR to validate a power budget link calculation model for jammers (NLR), and to try out interference removal techniques (TNO-FEL). The power budget calculation is part of NLR's contribution to the determination of possible ECCM (Electronic Counter Counter Measures) activities in space based SAR systems (Project EUCLID RTP 9.3). To this end it is, among others, necessary to determine what power is required to jam a space based SAR. By doing a jamming test with the airborne PHARUS SAR, and predicting the effects with the same model, at least a partial validation of the model could be executed. The outcome of the model is the Jam-to-Signal ratio (J/S) for an object on the ground with a certain radar cross section.

In the test, the jammer consisted of a ground-based 20W C-band CW generator connected to a 16 dB horn antenna. This antenna was located at a cross-track distance of 10 km with its boresight axis in a plane perpendicular to the aircraft track. The polarization of the jamming signal was horizontal. It was predicted that this power should be able to blur the (unprocessed) PHARUS image. The result of the test is shown in Figure 4.3-1.

Figure 4.3-2 shows the prediction, in terms of Jam-to-Signal ratio, where the jammer is located at 1.2 km along track and 10 km cross-track. It displays the jam-to-signal ratio encountered by PHARUS as it flies its track while mapping the terrain. The picture shows that even rather low J/S values result in severe disturbances.

Judging from the images, the following conclusions can be drawn:

- enough power was applied to hide ground features;
- the image is degraded around the main beam.
- there is a reasonable resemblance between prediction and test outcome. In comparing the two figures one should take into account that the real image shows processed data, the prediction shows only the raw data.

As these were the expected effects, it has been concluded that the calculation model is correct, at least for this simple scenario and jammer configuration. The execution of the jamming test with the airborne PHARUS system has -at least partially- validated the model which will be used in the EUCLID RTP 9.3 Space Borne SAR technology study.

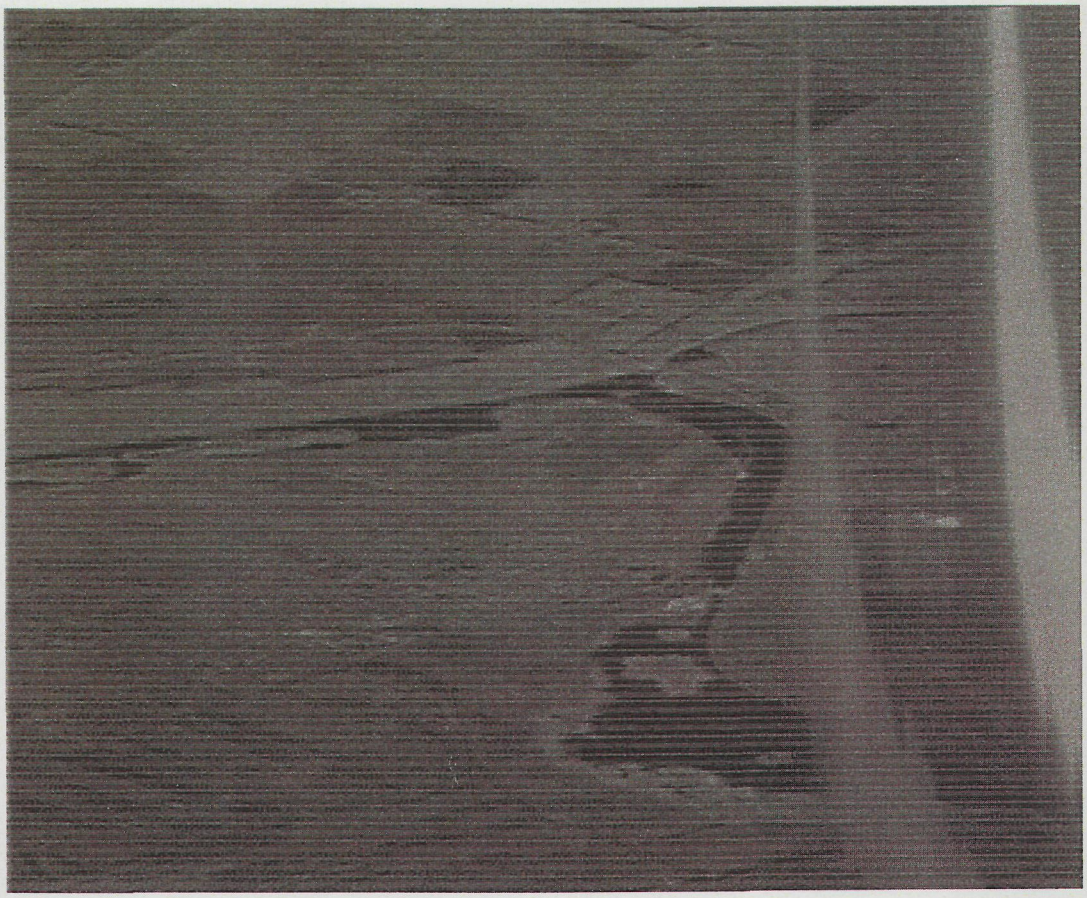

Figure 4.3-1 C-band airborne SAR image with jamming

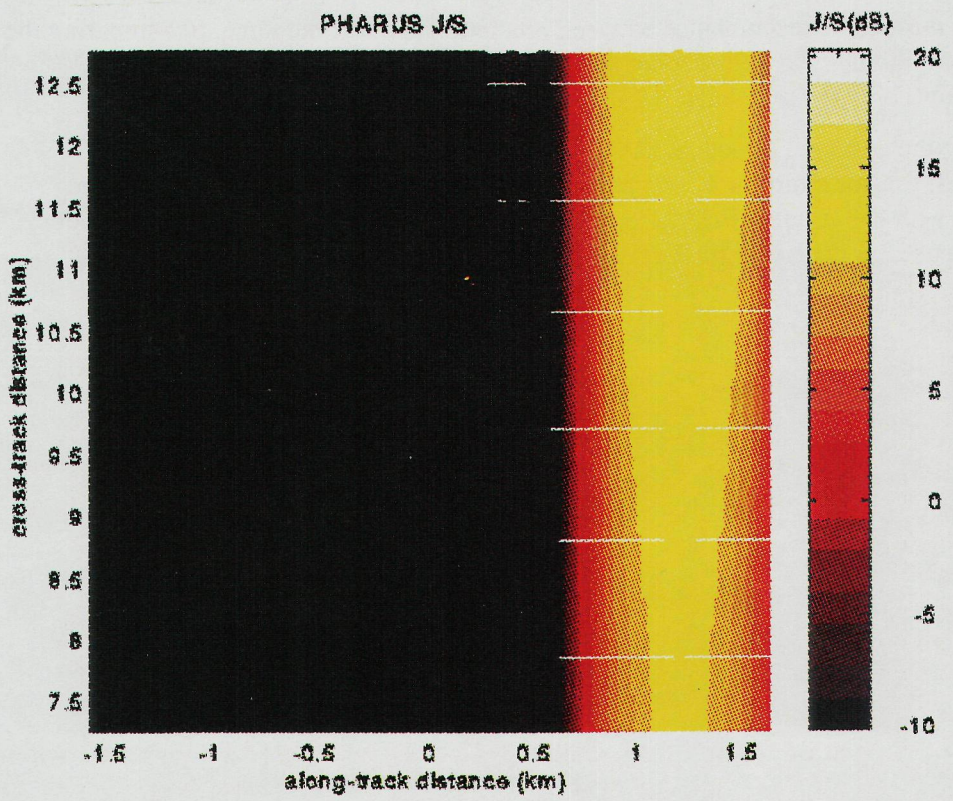

Figure 4.3-2 Predicted J/S for the C-band airborne SAR image

Measures against jamming

Apart from the model validation undertaken by NLR, TNO-FEL investigated some means to mitigate the effects of jamming.

First of all, since the experiment was done in a polarimetric mode, and the jammer was a single polarized (H) transmitter, the effect of the jammer is only apparent in the H-receive channel of PHARUS (HH and HV). HV is most severely affected, since the wanted signal (the image) has a lower level than HH. The remaining channels are virtually unaffected (VV and VH). Figure 4.3-3 shows the effects of jamming in different polarizations. Note that in fact *any* fixed jammer polarization can be effectively nulled by using the orthogonal polarizations. This means that half of the polarimetry is lost, due to the jamming.

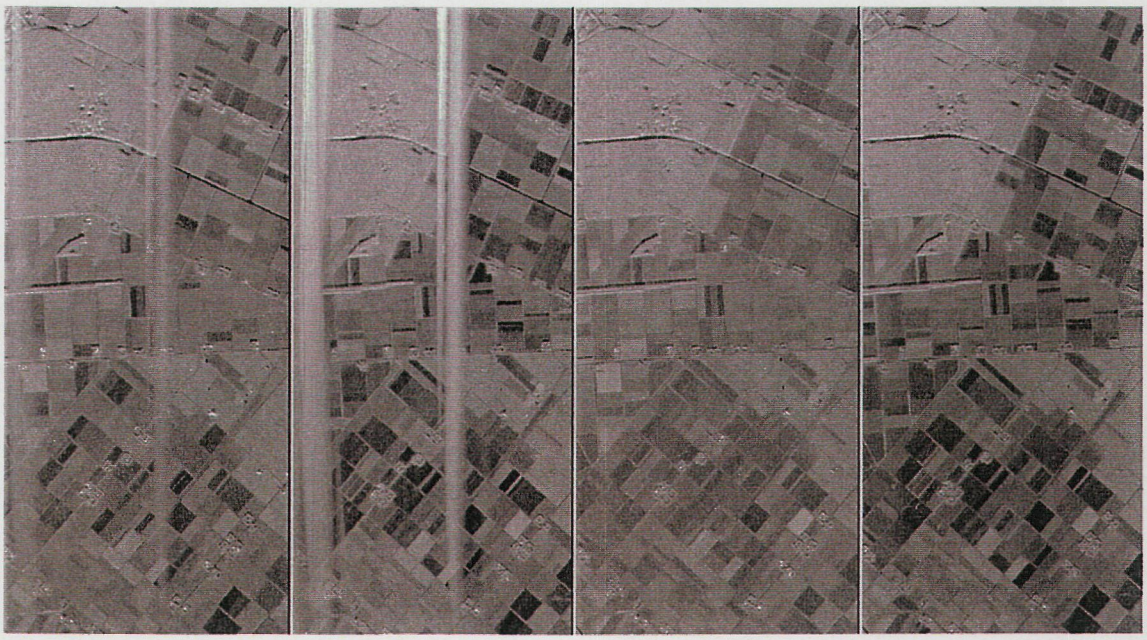

Figure 4.3-3 Jamming effect in 4 polarizations (HH,HV,VH,VV)

Secondly, it was tried whether the effects of jamming can be removed by appropriate filtering. The transmitter was a CW transmitter emitting a single frequency, which could therefore be easily identified in the received signal spectrum. A very narrowband filtering was implemented by modifying the pulse replica used in the SAR image processing. Taking out a small part from the replica has the effect of suppressing a narrow signal band, while there is no additional computation required! The results is shown in Figure 4.3-4. Though the filtering has affected the overall image quality somewhat, it has succeeded in revealing the part of the image that was initially screened by the jammer. More sophisticated filtering techniques are likely to improve the result. On the other hand, larger jamming power will complicate this task, due to saturation (i.e. non-linear) effects that will occur in the receiver and in the digitisation. Also, noise- or pseudo-noise jammers will be more difficult to remove, since their spectrum is spread out, and cannot be filtered out; this type of jamming does, however, require more jamming power.

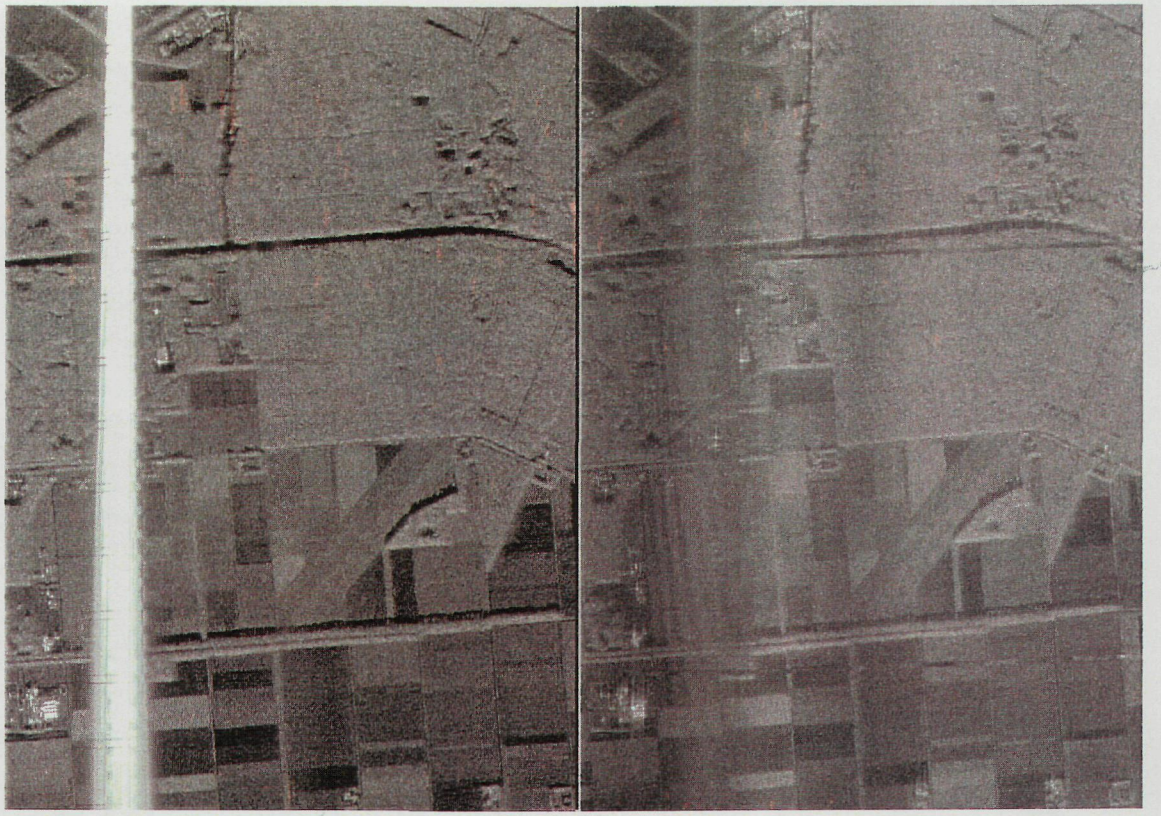

Figure 4.3-4 A jammed PHARUS image (left) and the result of interference filtering (right)

4.4 *Conclusions from the jamming experiment*

The results of the jamming experiment were in accordance with the model predictions made by NLR; the model could be partially verified this way. The image is degraded in the area around the main beam of the radar.

Furthermore, it was shown that a very simple jammer has limited effectiveness against the PHARUS system, due to the fact that 1) a small image region is affected, 2) only 2 out of 4 polarimetric channels are affected, 3) the signal can be detected and removed. The latter will become more difficult when the jamming power is increased, and the signal is randomised in some way, giving it a wider spectrum.
The jammer filtering technique that was applied can also be used against effects of interferences which are not intentional, as long as they are relatively narrowband.

5. Agriculture and forestry

It is known that in agricultural applications and forestry the use of polarimetric SAR has many advantages over single polarized data. Two selected applications are aimed at demonstrating the advantages of polarimetric radar in the fields of agriculture and forestry. These are respectively, crop classification and forest monitoring.

5.1 *Crop classification*

5.1.1 Introduction

In this section the crop type classification results of the Buitenland test site are presented. The polarimetric PHARUS radar measurements on which this classification is based have been described in section 2.1.2. Ground truth measurements as provided by Synoptics were mapped onto a GIS data base so that fields (represented by polygons) could be created. With the crop type classification of the Buitenland data a selected number of 194 agricultural fields were classified into 8 crop types using a Bayes classifier (supervised classification).

5.1.2 Description of the Buitenland test site

The Buitenland test site is located between the river Oude Maas and the city of Rotterdam. In Figure 5.1-1, part of Rotterdam can be seen as the urban area at the top whereas the river Oude Maas is visible at the bottom of this figure (the right plot gives a landmap of Rotterdam with the test site indicated by the box). The test site, mainly consisting of agricultural fields, measures 2260 pixels in x direction by 2550 pixels in y direction which, with a pixel size of 2.8 m (ground-range resolution of about 3.5 m), corresponds to approximately 6 by 7 km in distance.

5.1.3 Ground truth measurements

Ground truth measurements were provided by SYNOPTICS to TNO-FEL. These measurements consist of a digital landmap and a crop index file obtained by a land survey. The landmap gives the Buitenland site divided into a number of 225 agricultural fields represented as polygons. The top plot of Figure 5.1-2 shows the boundaries of these polygons whereas in the right plot a colourscale is mapped over the index range of 1 to 225.The 225 fields may be divided into 13 crop types such as onion, grass, or bare soil. With each field, the crop index file associates with a number in the range from 1 to 253. Of the inventory of 225 fields, a number of 14 fields had to be removed because of incomplete crop type information. More specifically, of 9 fields, the index was absent from the crop index file provided by Synoptics. Of 5 other fields Synoptics could not determine the crop type and labelled these fields invalid. Hence, 211 fields, which could still be divided into 13 classes, remained for classification. However, besides the above-mentioned 14 fields, we decided to reject 17 more fields of which it was clear that the classification would lead to problems. Of these 17 fields, 5 fields were rejected either because they contained a mixture of different crops or because a pylon dominated the field's radar reflection. Also, crop types with less than five fields were excluded from the crop type classification assuming that at least five fields are needed to construct a reliable class covariance pertaining to a 5-element feature vector (Section5.1.4). This removed 5 crop types associated with 12 fields. Table 5.1-1 gives an inventory of the remaining 194 fields divided over the remaining 8 crop types (13 minus 5) denoted by *A* to *H*. The numbers between brackets in this Table correspond with fields that were rejected from the crop type classification. The dashes in the third column indicate the crop types that were rejected because they contained less than 5 fields, i.e. crops 3, 6, 9, 11, and 13. A detailed specification of Table 5.1-1 is given in Table 5.1-3 of section 5.1.5.

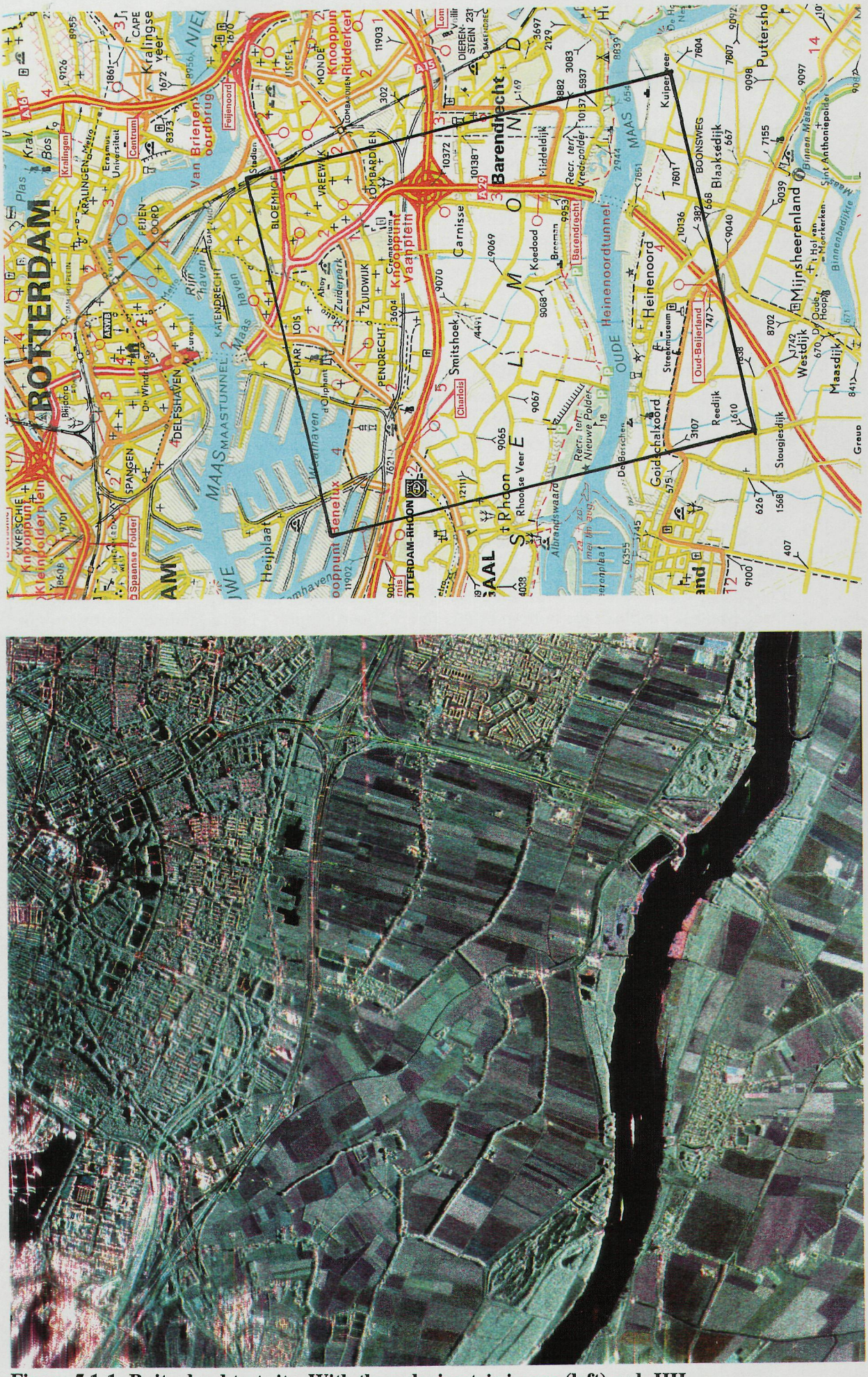

Figure 5.1-1: Buitenland test site. With the polarimetric image (left) red=HH, green=HV, blue=VV. In the right plot (landmap of Rotterdam, scale 1:100,000), the test site is indicated by the box.

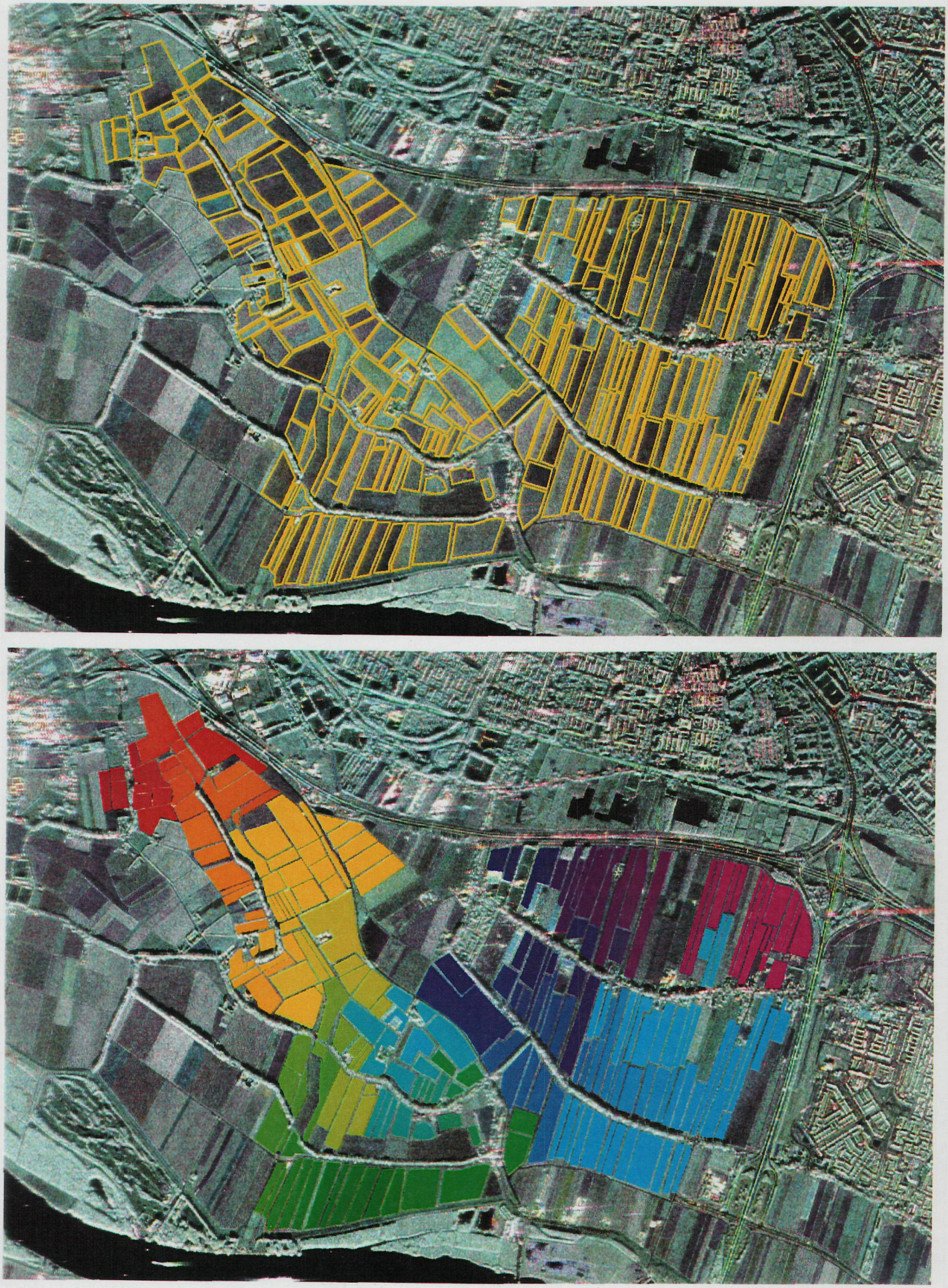

Figure 5.1-2: The 225 agricultural fields of the Buitenland test site represented as polygons. In the bottom plot a colourscale is mapped over the 1-225 index range.

Table 5.1-1: Inventory of 225 agricultural fields. Numbers between brackets denote fields that were excluded from the crop type classification.

crop number	crop type	class	number of fields
1	onion	*A*	6
2	beet	*B*	13
3	orchard	---	(4)
4	cabbage	*C*	35 (+2)
5	bare soil	*D*	13
6	grain	---	(1)
7	grass land	*E*	26
8	barley	*F*	28 (+1)
9	peas	---	(1)
10	potato	*G*	44 (+1)
11	spinach	---	(2)
12	wheat	*H*	29 (+1)
13	maize	---	(4)
	unknown crop		(14)
total			194 (+31)

5.1.4 Feature vector extraction

All pixels inside a field were used to set up the field's average polarimetric covariance matrix C (Equation (2.1.3) in section 2.1.2) resulting in a number of looks well over 100. From each polarimetric covariance matrix C, the vector $x^t=(\sigma_{hh}, \sigma_{hv}, \sigma_{vv}, \mathrm{Re}[\langle S_{hh}S^*_{vv}\rangle], \mathrm{Im}[\langle S_{hh}S^*_{vv}\rangle])$ of a field was constructed which served as the feature vector for the crop type classification. Because the five components of the feature vector comprise all relevant elements of the polarimetric covariance matrix, the constructed feature vector gives full information on the polarimetric information of a field.

5.1.5 Classification results

All feature vectors x inside a class i (i=A to H) were used to set up the class mean: $\mu_i=\langle x\rangle=(\langle\sigma_{hh}\rangle, \langle\sigma_{hv},\rangle, \langle\sigma_{vv},\rangle, \langle\mathrm{Re}[\langle S_{hh}S^*_{vv}\rangle]\rangle, \langle\mathrm{Im}[\langle S_{hh}S^*_{vv}\rangle]\rangle)^t$, and the class covariance matrix: $\Sigma_i=\langle(x-\mu_i)(x-\mu_i)^t\rangle$ which are both required in the discriminant function on which the classification is based. The "<>" in the expressions for μ_i and Σ_i denote averaging over all fields (each field provides one feature vector) of a class. Assuming, as is usually done, that the feature vectors x are normally distributed, the following discriminant or Bayes classifier function g may be used to assign a feature vector to one of the 8 classes (Duda and Hart, 1973):

$$g_i(x) = -\left(x-\mu_i\right)^t \Sigma_i^{-1}\left(x-\mu_i\right) - \ln\left|\Sigma_i\right| \qquad (5.1.1)$$

In the above Equation, μ_i and Σ_i are the mean and covariance matrix of the i'th class (i=1 to 8) while $|\Sigma_i|$ denotes the determinant of Σ_i. The field is assigned to that class which gives the largest value of g (notice that if , e.g., g_i=-3 and g_j=-4 that $g_i>g_j$).

The confusion matrix summarising the classification results of the 194 fields is given in Table 5.1-2. The top matrix shows the number of classified fields. Each row in the matrix represents a class. The totals give the total number of fields in each class and thus correspond with the numbers in Table 5.1-1. For example, of the 13 fields of class *B*, 9 fields were correctly classified as beet while 4 fields were erroneously classified: 3 as bare soil (class *D*)

and 1 as wheat (class *H*). The bottom half of Table 5.1-2 gives the results expressed as a percentage of the total number of fields. As can be seen from the matrix, most fields are correctly classified with exception of class *C* (cabbage) of which 17 out of 35 fields were classified as bare soil (class *D*). The reason is that the cabbage plants in some of the fields had recently sprouted when the site was overflown. Obviously, such hardly vegetated fields may easily be mistaken for bare soil fields. A more detailed analysis of the classification results will be presented in the next section. As an overall result of the classification, the confusion matrix shows that 139 out of 194 fields were correctly classified which corresponds to a score of 71.7%.

Table 5.1-3 details the results of the confusion matrix for each field separately. The second part of this table lists the 14 fields (indexed 212 to 225) of which the crop type was unknown while the first part gives the 211 fields of known crop. Of these 211 fields those with a remark in the last column correspond with the 17 fields that were excluded from the crop type classification as discussed in Section 5.1.3. The crosses in the last column give the fields that were erroneously classified, i.e. a false crop was assigned with the classification. If no cross is entered, the field was correctly classified.

Table 5.1-2: Confusion matrix of Buitenland crop type classification.

				number of fields					
class	***A***	***B***	***C***	***D***	***E***	***F***	***G***	***H***	**totals**
A	6	0	0	0	0	0	0	0	6
B	0	9	0	3	0	0	0	1	13
C	0	2	9	17	0	0	7	0	35
D	0	0	0	12	1	0	0	0	13
E	1	0	0	0	21	0	1	3	26
F	1	1	0	3	0	19	0	4	28
G	1	1	2	0	1	0	38	1	44
H	0	0	1	0	0	2	1	25	29
									194
				percentage (%)					
class	***A***	***B***	***C***	***D***	***E***	***F***	***G***	***H***	
A	100.00	0.00	0.00	0.00	0.00	0.00	0.00	0.00	
B	0.00	69.23	0.00	23.08	0.00	0.00	0.00	7.69	
C	0.00	5.71	25.71	48.57	0.00	0.00	20.00	0.00	
D	0.00	0.00	0.00	92.31	7.69	0.00	0.00	0.00	
E	3.85	0.00	0.00	0.00	80.77	0.00	3.85	11.54	
F	3.57	3.57	0.00	10.71	0.00	67.86	0.00	14.29	
G	2.27	2.27	4.55	0.00	2.27	0.00	86.36	2.27	
H	0.00	0.00	3.45	0.00	0.00	6.90	3.45	86.21	

Table 5.1-3: Results of crop type classification of the 194 considered fields. Results are specified per field. Fields with a remark in last column were not included in the classification. An "X" marker in the last column indicates that field is incorrectly classified.

no.	field	crop (truth)	crop (assigned)	remark
1	1	4	4	
2	2	8	8	
3	3	4	2	x
4	4	5	5	
5	5	4	5	x
6	8	4	---	pylon in field
7	9	4	5	x
8	10	5	5	
9	11	2	2	
10	12	7	7	
11	13	10	2	x
12	14	1	1	
13	15	2	2	
14	18	10	10	
15	19	2	2	
16	29	10	10	
17	30	2	2	
18	31	12	12	
19	32	7	7	
20	33	10	10	
21	34	12	8	x
22	36	5	5	
23	37	2	2	
24	39	10	10	
25	40	10	10	
26	41	8	8	
27	42	4	5	x
28	44	7	10	x
29	45	1	1	
30	47	10	10	
31	48	3	---	class 3 < 5 fields
32	49	10	10	
33	50	1	1	
34	51	10	10	
35	52	7	7	
36	53	8	8	
37	54	2	2	
38	55	4	5	x
39	56	4	10	x
40	57	8	2	x
41	58	2	2	
42	59	4	5	x
43	60	4	5	x
44	61	4	4	
45	62	4	10	x

no.	field	crop (truth)	crop (assigned)	remark
46	63	12	12	
47	64	10	10	
48	65	4	10	x
49	66	5	7	x
50	67	7	12	x
51	68	4	10	x
52	69	12	12	
53	70	4	2	x
54	71	12	12	
55	72	5	5	
56	73	12	12	
57	74	12	12	
58	75	10	10	
59	76	11	---	class 11 < 5 fields
60	77	7	12	x
61	78	4	10	x
62	79	10	10	
63	80	2	5	x
64	81	10	10	
65	82	8	8	
66	83	10	10	
67	84	8	5	x
68	85	10	10	
69	86	8	5	x
70	87	7	12	x
71	88	5	5	
72	89	8	12	x
73	91	8	5	x
74	92	8	1	x
75	93	8	8	
76	94	11	---	class 11 < 5 fields
77	95	5	5	
78	96	4	5	x
79	97	10	10	
80	98	4	5	x
81	99	4	5	x
82	100	10	10	
83	101	10	10	
84	102	4	5	x
85	103	10	10	
86	104	12	12	
87	105	2	5	x
88	106	10	10	
89	107	8	12	x
90	108	8	8	

no.	field	crop (truth)	crop (assigned)	remark
91	109	8	8	
92	110	10	10	
93	111	5	5	
94	112	10	10	
95	114	7	7	
96	115	4	4	
97	116	7	7	
98	117	7	7	
99	118	10	---	mixture of crop
100	119	7	7	
101	120	7	7	
102	121	13	---	class 13 < 5 fields
103	122	3	---	class 3 < 5 fields
104	123	10	10	
105	124	4	5	x
106	125	8	8	
107	126	12	12	
108	127	7	7	
109	128	4	5	x
110	129	12	8	x
111	130	4	5	x
112	131	10	10	
113	132	5	5	
114	133	7	7	
115	134	10	1	x
116	136	10	10	
117	137	10	10	
118	138	13	---	class 13 < 5 fields
119	139	6	---	class 6 < 5 fields
120	140	10	10	
121	141	2	5	x
122	142	12	12	
123	143	13	---	class 13 < 5 fields
124	144	12	12	
125	145	12	12	
126	146	5	5	
127	147	8	8	
128	148	10	10	
129	149	10	10	
130	150	12	12	
131	151	7	7	
132	152	12	12	
133	153	12	12	
134	154	12	12	
135	155	8	12	x

no.	field	crop (truth)	crop (assigned)	remark
136	156	10	12	x
137	157	5	5	
138	159	12	---	mixture of crop
139	160	13	---	class 13 < 5 fields
140	161	7	1	x
141	162	7	7	
142	163	4	5	x
143	165	1	1	x
144	166	4	5	x
145	167	12	12	
146	168	8	12	x
147	169	10	10	
148	170	10	10	
148	171	7	7	
150	172	8	8	
151	173	8	1	x
152	174	10	4	x
153	175	5	5	
154	176	3	---	class 3 < 5 fields
155	177	12	12	
156	178	4	4	
157	180	7	7	
158	182	12	12	
159	183	1	1	
160	184	8	8	
161	185	7	7	
162	186	12	12	
163	187	8	8	
164	188	4	4	
165	189	12	12	
166	190	12	12	
167	191	10	10	
168	192	10	10	
169	193	10	10	
170	194	4	4	
171	195	10	10	
172	196	8	8	
173	197	2	2	
174	198	8	8	
175	199	12	10	x
176	200	12	12	
177	201	4	10	x
178	202	2	12	x
179	203	4	5	x
180	204	9	---	class 9 < 5 fields

no.	field	crop (truth)	crop (assigned)	remark
181	205	12	12	
182	207	12	12	
183	208	7	7	
184	209	10	10	
185	210	8	8	
186	212	4	4	
187	213	10	10	
188	214	4	5	x
189	215	4	---	pylon in field
190	216	5	5	
191	217	10	10	
192	220	12	12	
193	221	7	7	
194	222	12	4	x
195	223	2	2	
196	224	10	4	x
197	225	4	4	
198	226	8	8	
199	227	4	4	
200	228	10	10	
201	229	1	1	
202	230	7	7	
203	232	10	7	x
204	234	4	10	x
205	235	8	8	
206	236	3	---	class 3 < 5 fields
207	237	8	---	mixture of crop
208	238	7	7	
209	239	7	7	
210	240	7	7	
211	241	8	8	
		fields of unknown crop		
212	6	?	---	unknown crop
213	7	?	---	unknown crop
214	35	?	---	unknown crop
215	43	?	---	unknown crop
216	46	?	---	unknown crop
217	90	?	---	unknown crop
218	113	?	---	unknown crop
219	179	?	---	unknown crop
220	181	?	---	unknown crop
221	206	?	---	unknown crop
222	211	?	---	unknown crop
223	218	?	---	unknown crop
224	231	?	---	unknown crop
225	233	?	---	unknown crop

5.1.6 Analyses

From the large numbers on the main diagonal of the confusion matrix it may be concluded that the class mean μ_i and covariance matrix Σ_i are adequate statistic parameters to classify the feature vectors x. The decision to which class a feature vector x is assigned depends on the class means μ_i (i=A to H) and covariance matrices Σ_i in two ways. First of all it depends on the distance from the feature vector to be classified to each of the class means as

expressed by the quadratic form of $(x-\mu_i)$ in Equation (5.1.1). Second it depends on the distribution of the feature vectors that were used to set up a class covariance matrix Σ_i. For instance, if the feature vector that is to be classified has a very large σ_{hh} component, it likely belongs to a class of which the distribution is stretched in the σ_{hh} direction, i.e. a class with a large variance var(σ_{hh}). It should be noted that such a conclusion is only valid if all classes have the same mean for all elements of the feature vector and, more importantly, if the correlation between the feature vector components is negligible so that the class covariance matrices are diagonal, i.e. the elements off the main diagonal are zero (Duda and Hart, 1973). In case of the 8 crop types, the covariance matrices were found to be full, i.e. have elements off the main diagonal that cannot be neglected, which makes an interpretation of their effect on the classifier very difficult.

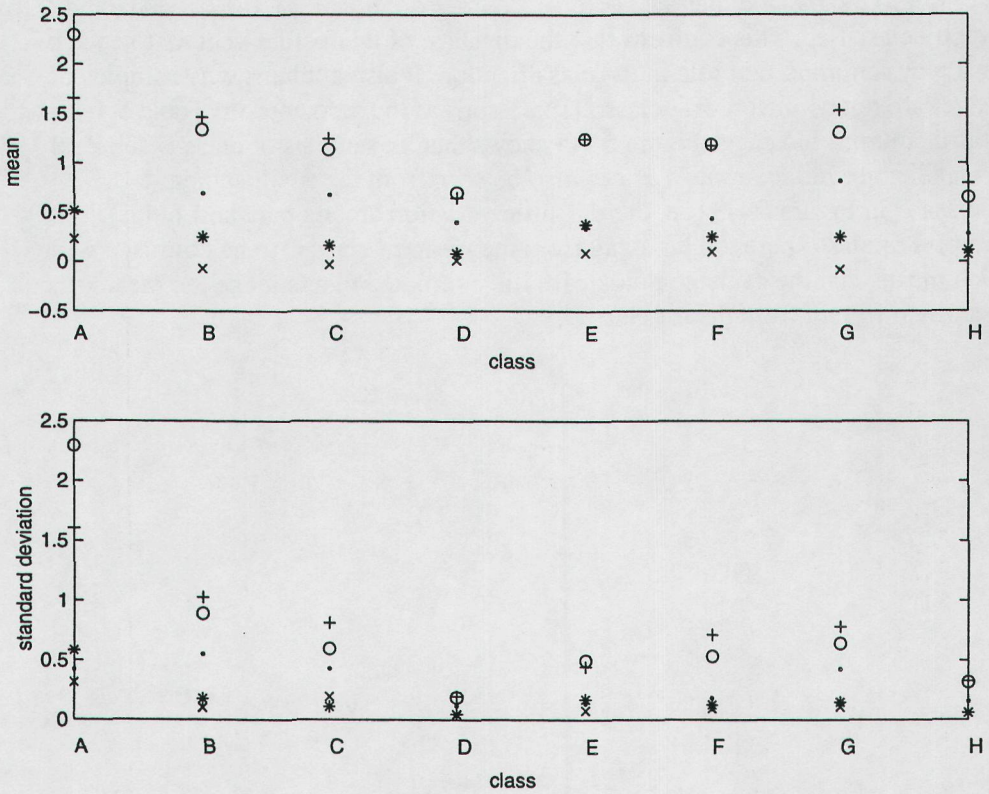

Figure 5.1-3: Mean and standard deviation (both in units of m^2) of feature vector elements of 8 classified crop types. Symbols refer to: +=σ_{hh}, *=σ_{hv}, o=σ_{vv}, •=Re[<$S_{hh}S^*_{vv}$>], x=Im[<$S_{hh}S^*_{vv}$>].

In, the mean and standard deviation (square root of variance) of the feature vectors are presented for the 8 crop types. From the top plot it can be seen that there are considerable differences between the elements of the class means. Hence, it may be expected that the distance from a feature vector to each of the class means plays an important role in explaining the classifier results of Table 5.1-2. Considerable differences are also found between the standard deviations of the feature vectors of the different classes. However, as the class covariance matrices are full, the standard deviations are not used to explain the classification results. The large mean <σ_{vv}> of class *A* is most likely caused by unreliable statistics due to the small number of samples in this class: 6 as can be seen in Table 5.1-1. This is confirmed by the standard deviations of the feature vector elements of class *A* which are significantly larger than those of the other classes (with possible exception of Im[<$S_{hh}S^*_{vv}$>]).

As a first analysis, the confusion of feature vectors of class *C* with class *D* was investigated. In Figure 5.1-4, the distribution of the scatter coefficients in the 5-element feature vectors of class *C* and *D* are shown. The real and imaginary parts of $\langle S_{hh}S^*_{vv}\rangle$ are not displayed. Represented by the circles and crosses are the samples of class *C* while the asterisk markers are the samples of class *D*. In Figure 5.1-4, class *C* provides the samples that are to be classified. If a sample of class *C* is correctly classified, i.e. as class *C*, it is displayed as a circle marker while crosses indicate samples of class *C* that are falsely classified , i.e. as class *D*. Notice, therefore, that in accordance with Table 5.1-2, Figure 5.1-4 contains 13 asterisk, 9 circles, and 17 crosses. Clearly visible is that the samples of class *C* that are close to the mean of class *D*: $(\langle\sigma_{hh}\rangle, \langle\sigma_{hv}\rangle , \langle\sigma_{vv}\rangle)D=(0.65, 0.09, 0.70)$, are confused with class *D*. Obviously these samples correspond with cabbage fields in which the plants had only recently sprouted. Samples of class *C* with a large scatter coefficient (cabbage plants more or less fully sprouted) are closer to the mean of class *C*: $(\langle\sigma_{hh}\rangle, \langle\sigma_{hv}\rangle, \langle\sigma_{vv}\rangle)_C=(1.25, 0.17, 1.14)$, and therefore correctly classified. This confirms that the distance of the feature vectors to each of the class means plays an important role in the classification. It also explains why samples of class *C* (cabbage) are not confused with class *D* (bare soil) as the zero entry in Table 5.1-2 (fourth row, third column) indicates. Figure 5.1-5 shows that all samples of class *D* (circles) are clustered together around their mean as can also be seen from the small standard deviations of class *D* in Figure 5.1-3 (i.e. there is little variation among bare soil fields). Hence, the samples of class *D* are too far away from the mean of class *C* to be confused with that class which means that the cabbage fields with fully sprouted plants make the mean of class *C* sufficiently different from that of class *D*.

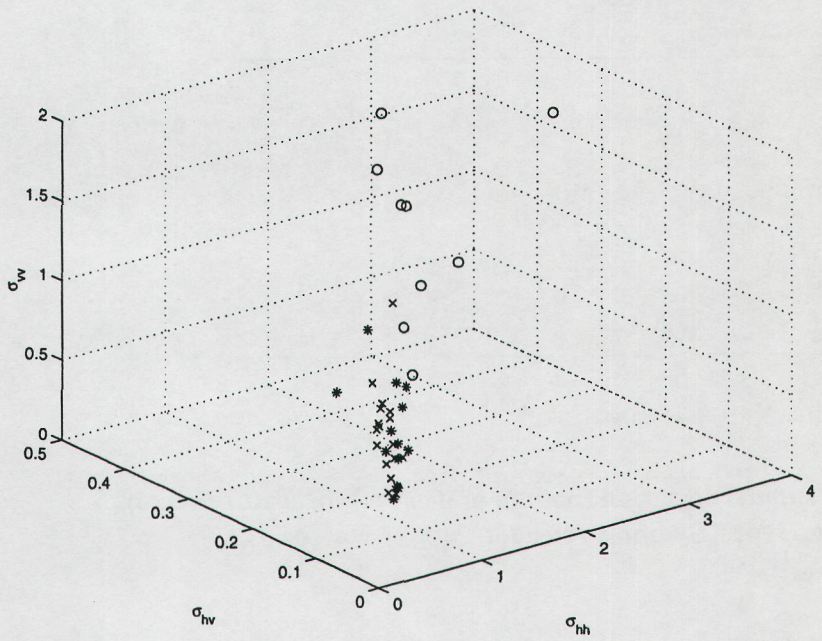

Figure 5.1-4: Distribution of scatter coefficients of class C (*o* and *x* markers) and class D (* markers). Classified are the feature vectors of class C; *o* means correctly classified and *x* means erroneously classified.

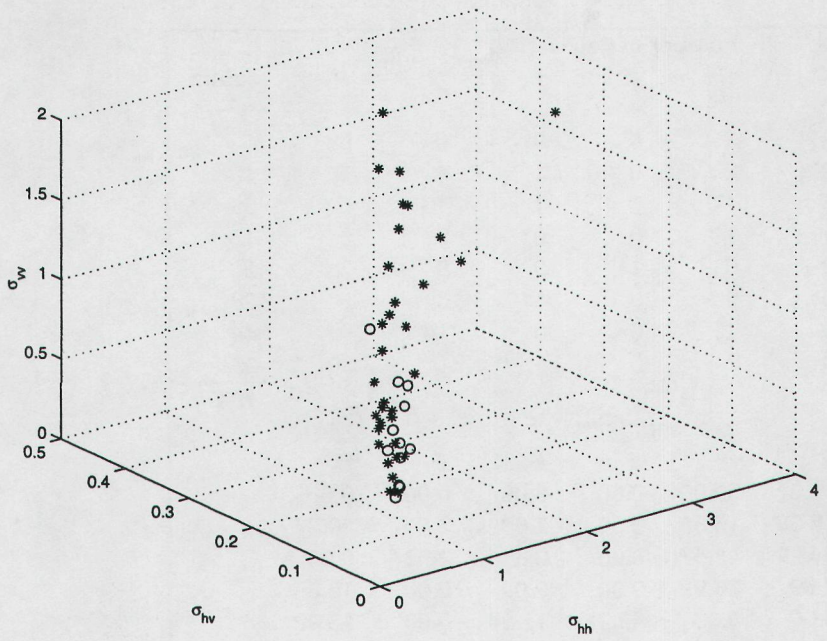

Figure 5.1-5: As in Figure 5.1-4 but now the feature vectors of class D are the ones that are classified.

A second analysis concerns the importance of the covariance Σ_i. To illustrate this importance, a second crop type classification has been performed on the same 194 fields but with the class covariance matrices in the discriminant (5.1.1) equal to the unit matrix **I** so that $g_i(x)=-(x-\mu_i)^t(x-\mu_i)$. This means that the fields are classified on basis of their distance to the class means fully neglecting the covariance matrices. Table 5.1-4 shows the results of this analysis. Comparing Table 5.1-4 with the confusion matrix from Table 5.1-2 we notice that samples from a class are easier confused with other classes if the covariance matrices are neglected. This can easily be seen from the elements on the main diagonal of the confusion matrix which are all smaller in case of Table 5.1-4 than in case of Table 5.1-2. As an overall result, 74 out of 194 fields were correctly classified which corresponds to a score of 38.1%. Hence, although the distance of a feature vector to each of the class means plays an important role in the crop type classification, the class covariance matrices which account for the distribution of the feature vectors are equally important.

Table 5.1-4: Confusion matrix for crop type classification without using class covariance matrices.

	number of fields								
	A	*B*	*C*	*D*	*E*	*F*	*G*	*H*	totals
class									
A	2	0	1	3	0	0	0	0	6
B	2	1	2	2	0	1	1	4	13
C	2	0	5	17	0	1	10	0	35
D	0	0	1	10	0	0	0	2	13
E	3	2	0	0	11	3	0	7	26
F	2	4	0	6	0	11	0	5	28
G	6	1	9	10	0	0	14	4	44
H	0	1	0	2	0	5	1	20	29
									194
	percentage (%)								
class	*A*	*B*	*C*	*D*	*E*	*F*	*G*	*H*	
A	33.33	0.00	16.67	50.00	0.00	0.00	0.00	0.00	
B	15.38	7.69	15.38	15.38	0.00	7.69	7.69	30.77	
C	5.71	0.00	14.29	48.57	0.00	2.86	28.57	0.00	
D	0.00	0.00	7.69	76.92	0.00	0.00	0.00	15.38	
E	11.54	7.69	0.00	0.00	42.31	11.54	0.00	26.92	
F	7.14	14.29	0.00	21.43	0.00	39.29	0.00	17.86	
G	13.64	2.27	20.45	22.73	0.00	0.00	31.82	9.09	
H	0.00	3.45	0.00	6.90	0.00	17.24	3.45	68.97	

5.1.7 Conclusions

From the crop type classification of 194 fields into 8 classes; onion, beet, cabbage, bare soil, grass, barley, potato, and wheat, it may be concluded that approximately 70% or more of the fields in a class can be correctly classified. The overall result is that 139 out of 194 fields were correctly classified (71.7%).

An exception to the above number of 70% must be made for cabbage fields in which the plants have recently sprouted. These fields may be mistaken for bare soil fields as they have a feature vectors that are close to the class mean of bare soil. It was found that about 50% of the cabbage fields were confused with bare soil.

It was found that the distance between a feature vector and the class means plays just as an important role in the classification as the class covariance matrices. Neglecting the class covariance matrices reduces the overall result of correctly classified fields from 71.7% to 38.1%.

5.1.8 References

Duda, R.O., Hart, P.E., pattern classification and scene analysis, John Wiley & Sons, 1973.

5.2 *PHARUS demonstration for forestry application*

5.2.1 Introduction

During several test flights SAR images of the Reichswald were acquired with the experimental PHARUS airborne radar system. The Reichswald is a mixed deciduous and coniferous plantation forest located in Germany along the Dutch border between Kleve (D) and Groesbeek (NL).

The Reichswald area has never been included in any (Dutch) remote sensing campaign previously. Unlike the well studied forest test sites in The Netherlands, namely: the Horsterwold in southern Flevoland and the Speulderbos at the Veluwe, its characteristics were poorly known. It was selected for this study as a target of opportunity. One image was recorded during an early test flight of the PHARUS system in October 1996. During the flights carried out for this project, in the summer of 1997, imaging the Reichswald again, rather then covering one of the regular Dutch test sites as originally proposed, would allow study of multi-temporal effects. A disadvantage of this decision, however, was that a large part of the limited time available for this study was needed to collect and process new ground reference data.

In section 5.2.2 of this chapter a short description of the test site and collected ground reference data and radar data is given. In section 5.2.3 the approach adopted for data analysis is outlined, summarising steps carried out within this (limited) study and steps recommended for a more extended study. In section 5.2.4 the first results are summarised. Section 5.2.5 gives conclusions and recommendations.

5.2.2 Description test site, ground reference data and radar data

The Reichswald is a mixed plantation forest of approximately 1300 ha in size. The main species are beech and pine, followed by spruce, oak, Douglas fir, larch and poplar. Approximately 250 ha consists of old beech forests divided over 12 stands with an average age of 150 years. Stands vary in size from 1 till 30 ha with an average size of ±10 ha. The age of the stands varies from 10 till 170 years with an average of ±50 years.

The radar data were collected at 22 October 1996 at 10:28 local time and at 2 June 1997 at 15:38 local time. The selected mode was the fully polarimetric 'Quad Pol' mode with nominal figures of 4 m for resolution, 4 independent looks per pixel and an image size of 8x8 km. For this study the central part of the Reichswald was selected for which the incidence angle ranged between 50° and 65° for the 1996 image and between 55° and 70° for the 1997 image.

Available ground reference data comprise
(1) Aerial photography map: scale 1:25.000, flown September 1985, Landsvermessungsamt Nordrhein-Westfalen
(2) Topographic map: scale 1:25.000, 4202 Kleve
(3) Forest type map: Forst betriebskarte, scale 1:10.000, October 1995, Forstamt Kleve
(4) Field observations made shortly after both the October 1996 and June 1997 radar flights.

1	yellow	oak
2	red	beech
3	cyan	ALN (other deciduous trees with low rotation time)
4	grey	pine
5	magenta	larch
6	blue	spruce
7	green	Douglas fir

Table 5.2-1 Legend forest classes as shown in

plate 5.2-1 (d) and label numbers as used in Table 5.2-5 and Table 5.2-6.

Sigma HH-HV-VV Pharus; Reichswald October '96

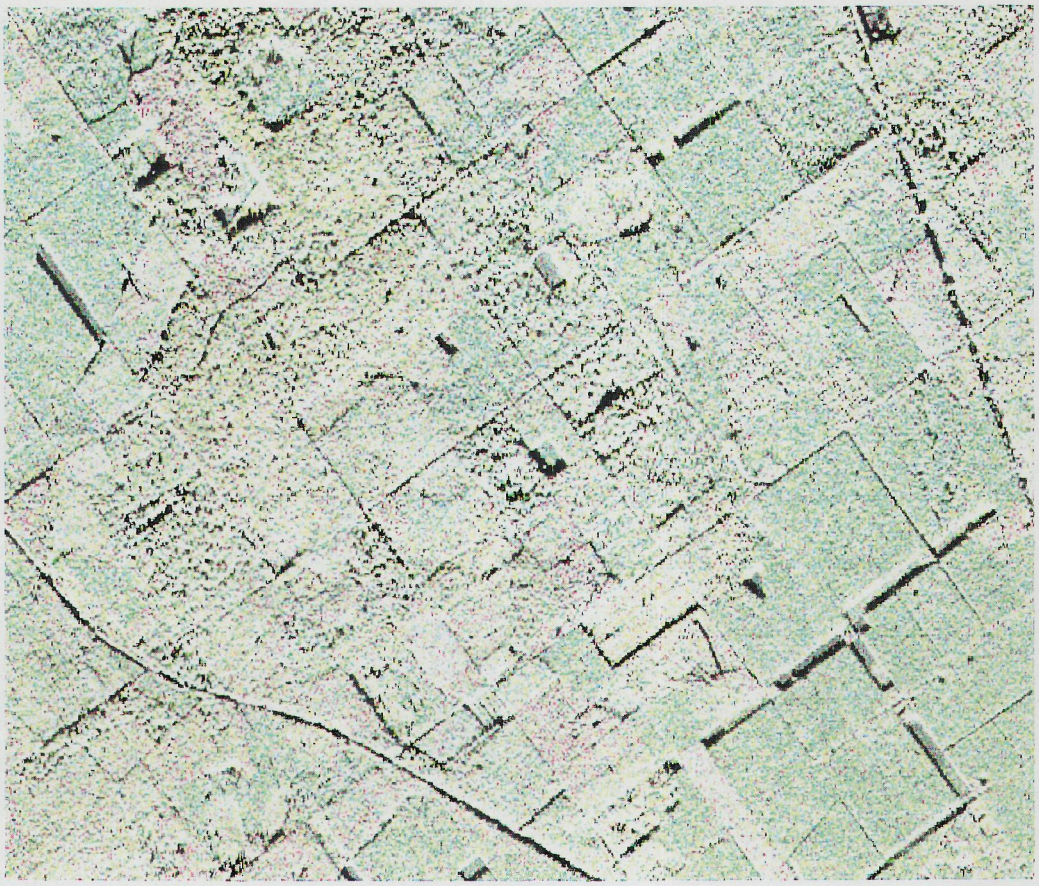

Sigma HH-HV-VV Pharus; Reichswald June '97

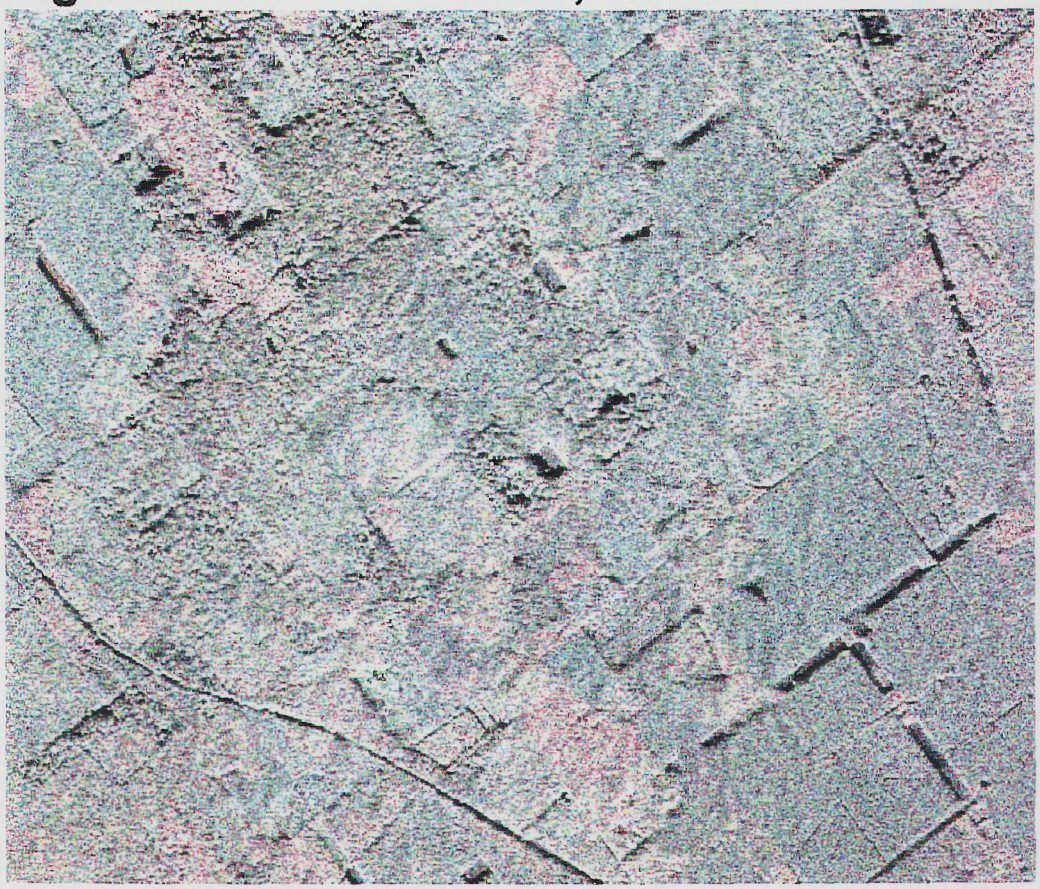

plate 5.2-1 Selected part of the Reichswald PHARUS image of (a) October 1996 and (b) June 1997. The colour coding is: blue for backscatter with HH polarization, green for HV polarization and red for VV polarization.

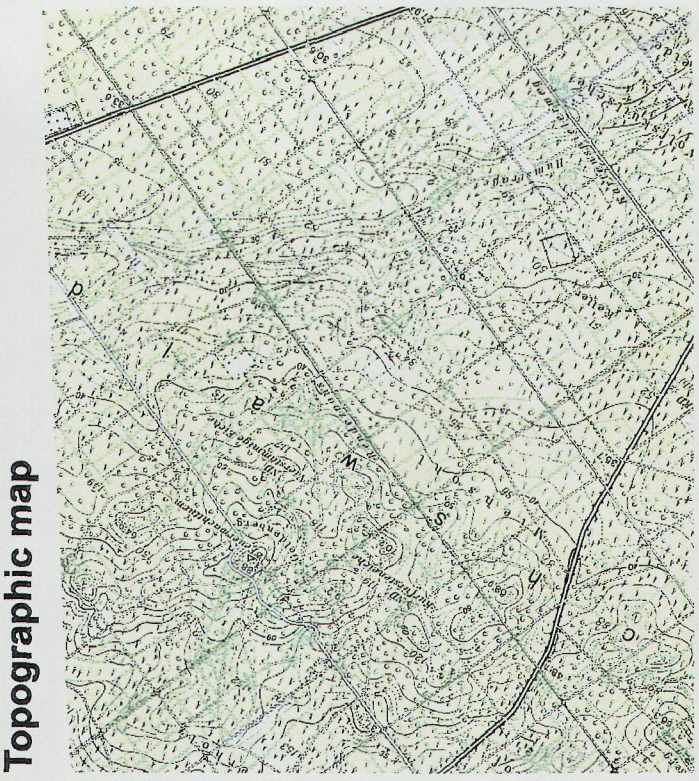

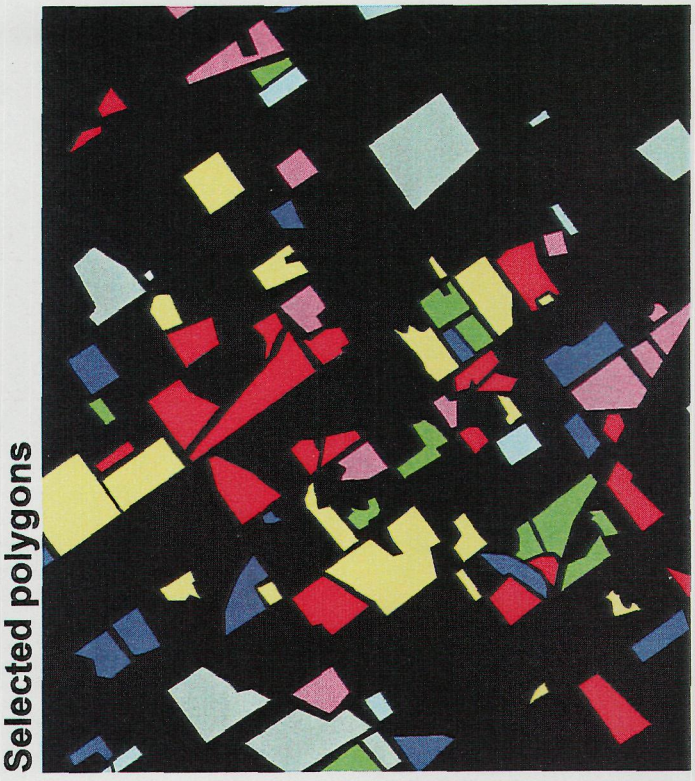

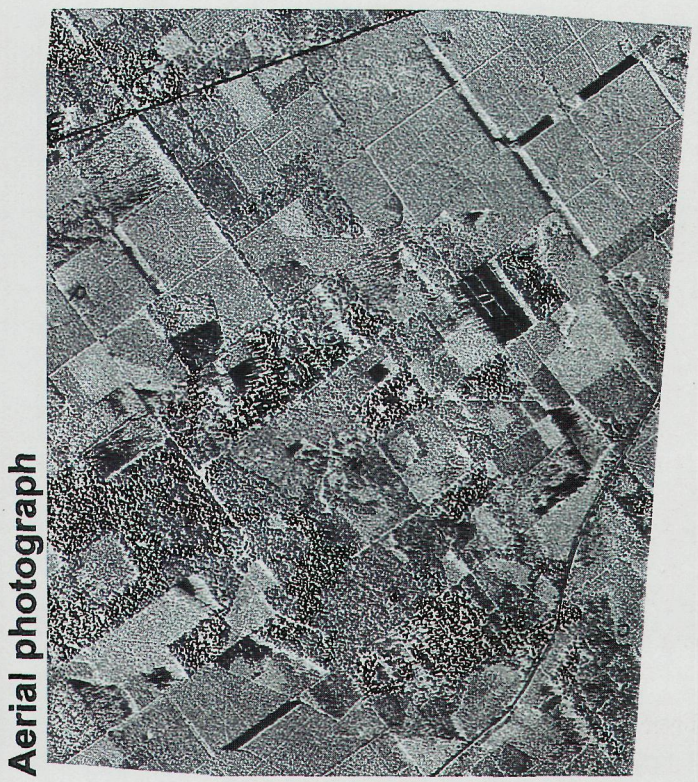

plate 5.2-2 Selected part of Reichswald ground reference data: (a) aerial photograph, (b) topographic map, (c) forest type map and (d) polygon areas of selected test stands. The colour coding of (d) is given in Table 5.2-1.

5.2.3 Analysis approach

5.2.3.1 **Proposed approach**

To make an assessment of the potential of PHARUS for retrieval of forest and stand parameters a sequence of analysis steps is proposed. These steps are summarised next.

Step 1 The first step is the construction of a database which, for example can be used as a training data set for classification studies. Test stands are selected and digitised on the forest map and a radar image. For every test stand such a database contains forest data, such as species, age and other stand characteristics, and radar data, such as incidence angle, number of pixels and averaged Stokes parameters (i.e. 9 numbers).

Step 2 A maximum likelihood classification is executed on 'mono-temporal' or 'single-date' non-polarimetric (i.e. only backscatter with HH-, VV- and HV-polarization) data of the training set (i.e. stand averaged values). The results are evaluated to assess which classes (e.g. species) can be discriminated well.
Step 3 The classification is repeated for multi-date data sets, to assess improvement (if any) on single-date classification results.
Step 4 The effect of speckle is studied by adding speckle artificially. The result will indicate how much averaging should be done to get reliable 'pixel-based' classification results as compared to 'segment-' or 'field-based' approaches.

At this stage the possibilities of 'conventional' C-band radar are more or less determined. Now some of the salient features of PHARUS can be studied to assess additional possibilities. These features are (a) polarimetry and (b) high resolution.

Step 5 These additional features can be used to improve possibilities for classification or bio-physical parameter estimation. To this aim the database should be extended with polarimetric features, such as scatter mechanisms, other polarizations, phase differences, etc., and high resolution features, such as GLCO texture measures.
Step 6 Step 2, 3 and 4 can be repeated with this 'extended' set of classifiers followed by an evaluation. The added value of polarimetry and high-resolution can be assessed.
Step 7 Optimal classifiers, at this stage, have been determined on the basis of stand averages. For automated processing of large data volumes some questions should be addressed such as: Can a simple and robust classifier be designed to make a sufficiently accurate classification on a pixel-basis? Can the non-forest area be masked automatically?
Step 8 Optimisation has been done with species classification at the main level and age classes at the second level. It should be evaluated now how other types of relevant information can be retrieved, such as detection of roads and small-sized clear cuts.

The analysis as discussed above applies to forest plantations in temperate climate zones. For tropical rain forests another, fairly different, series of analysis steps have to be followed. Texture, for example, rather then averaged backscatter, is the main source of information in high-resolution C-band data of tropical forest (van der Sanden, 1997).

5.2.3.2 **Brief description processing steps executed**

A database with 150 samples (stands) was constructed covering the 7 forest classes shown in Table 5.2-1 (step 1). This database can be used to assess classification possibilities using the maximum likelihood procedure (steps 2 and 3) and by studying the effect of speckle (step 4) as described below.

Maximum likelihood (ML) classification
The data samples in the training set are related to a number of classes. In case there are m classes and n channels, then for each class w_i, with i ranging from 1 to m, a n-dimensional mean value vector $\boldsymbol{M}_i$ and a n x n-dimensional covariance matrix $\boldsymbol{C}_i$ is computed. Assuming a n-dimensional normal distribution is applicable, each observation vector $\boldsymbol{X}$ to be classified can be assigned to one of the classes w_i or, in case non of these classes is likely, to a class w_0.

The likelihood that $\boldsymbol{X}$ is a member of class w_i, is

$$P(X \mid \omega_i) = \frac{1}{(2\pi)^{n/2}|C_i|^{1/2}} \exp\left(-1/2(X - M_i)^{\mathrm{T}} C_i^{-1} (X - M_i)\right) \qquad \text{Equation 5.2-1}$$

1)

with $|C_i|$ = the determinant of $\boldsymbol{C}_i$.

For one of these classes the likelihood value is the highest (i.e. the '*maximum likelihood*'). The vector $\boldsymbol{X}$ will be assigned to class w_i according to the classification rule:

$$\ln(P(X \mid \omega_i)) > \ln(P(X \mid \omega_j)) \text{ for all } j \neq i\,. \qquad \text{Equation 5.2-2}$$

and the condition

$$\ln(P(X \mid \omega_i)) > T_i\,. \qquad \text{Equation 5.2-3}$$

where T_i is a suitably chosen threshold value. In case the condition in Equation 5.2-3 is not satisfied the vector X will be assigned to class w_0 (i.e. class 'unknown'). In this study the threshold value for classification was set at the 95% confidence level. Results are presented in a (m +1) x (m)-dimensional 'contingency table' or 'confusion matrix'.

Speckle
In case the sample points relate to pixel values of a 'multi-look' radar backscatter image these samples have an inherent speckle level (Hoekman, 1991). In case the sample points relate to backscatter values averaged over a polygon, then the values are almost free of the influence of speckle when the number of 'independent' looks is large enough. In this study the sample points relate to image areas in the range of 100-19.000 pixels. For example, when the minimum polygon size is 100 pixels, then for 4-look PHARUS images the total number of independent looks is over 400 resulting in an error less than 0.22 dB. For data almost free of speckle, speckle can be added artificially to simulate the effect of speckle level on classification accuracy on multi-look image data. Speckle is added to all sample points and for each channel of the training data set and the data to be classified (in this analysis step these data sets are identical) by randomly selecting realisations from a gamma distribution (in the current approach this was done 10 times per sample point).

5.2.3.3 Brief description of processing steps still to be demonstrated

The special capabilities of PHARUS, i.e. its polarimetric features and high resolution, can be demonstrated in follow-on studies as briefly described below (steps 5 and 6).

Polarimetric classifiers (see also plate 5.2-3)
There are several ways to include polarimetric phase differences in classification procedures or in algorithms for parameter retrieval. It is out of the scope of this project to study these in detail. An example of using the HH-VV phase difference is shown inplate 5.2-3. Here results

of the well-known scattering mechanism classification (van Zijl, 1989) are shown and compared with an improved algorithm developed by the authors. Van Zijl's algorithms shows for each pixel the dominant scatter mechanisms, i.e. 'odd bounce' indicative for surface scattering in blue, 'even bounce' indicative for trunk-ground interactions in red and 'diffuse scattering' indicative for volume scattering in green. The improved algorithm shows for each pixel the fraction of these scatter mechanisms in the same colours. Therefore it retrieves more information and allows a better assessment of physical conditions.

Another way to include phase information is by expanding the ML classification procedure with phase information. The latter has a cyclic Gaussian phase distribution. Multi-look distributions are given, among others, by Joughin *et al.* (1994). Fully polarimetric classification procedures, including all polarimetric phase differences, are currently being developed by the authors.

Texture

The use of texture for high-resolution short wave radar data has been extensively reported by van der Sanden (1997). Selection of optimum textural features for classification and physical parameter extraction is a laborious task, which has to be executed, in principle, for every radar system and every operating mode separately. Visual inspection of the current PHARUS Reichswald images suggests that still a lot of additional information can be retrieved using texture, such as tree dimensions and stand age. Systematic study, however, is out of scope of this project.

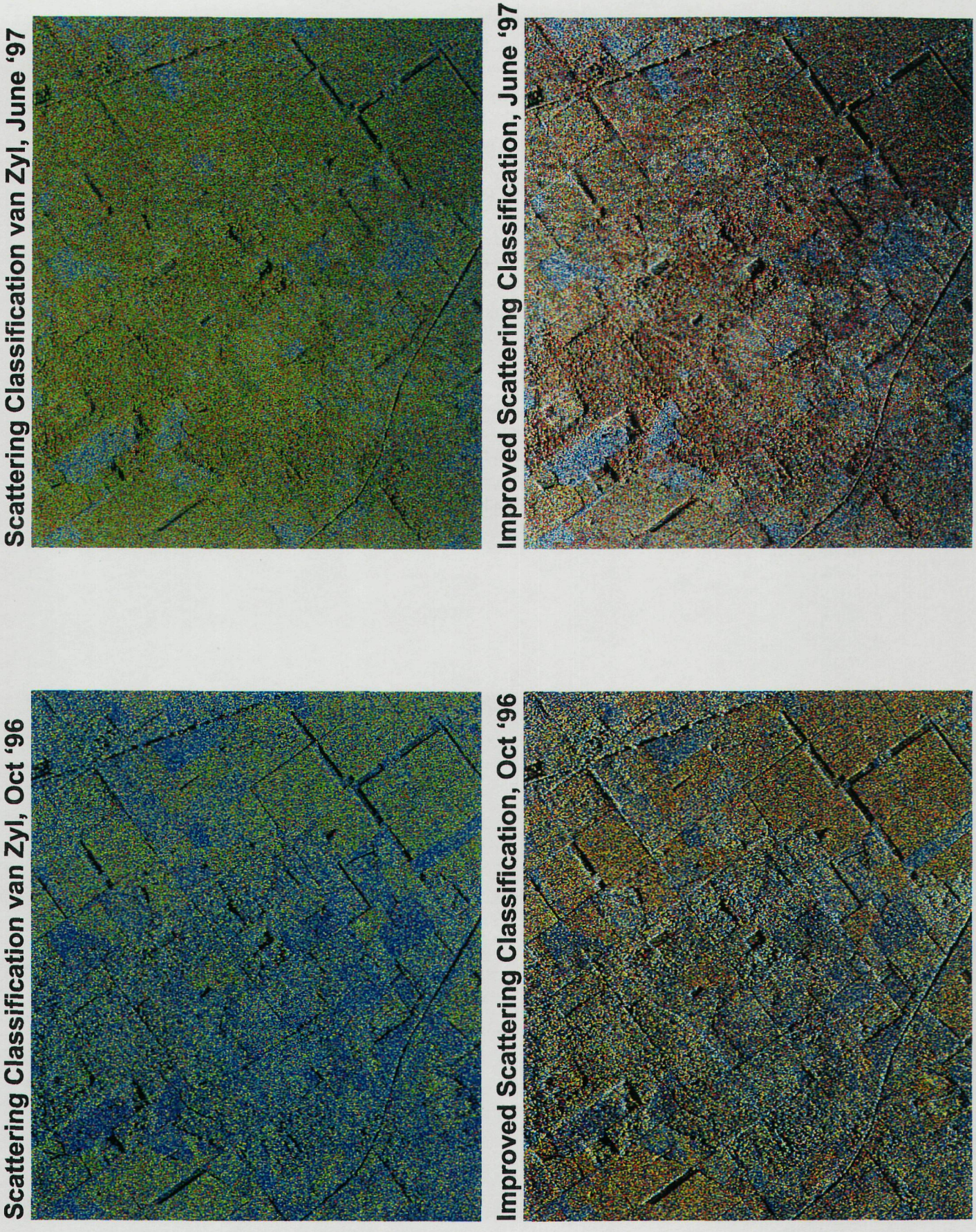

plate 5.2-3 ***Classification of dominating scattering mechanism according the method of van Zijl for the PHARUS image of (a) October 1996 and (b) June 1997. Retrieval of the relative contribution of these scatter mechanisms to the total power per pixel for (c) October 1996 and (d) June 1997. The colour coding is: blue for 'odd bounce', green for 'diffuse scattering' and red for 'even bounce'.***

5.2.4 Results

For the 7 forest types selected for this initial analysis the mean backscatter values for HH-, HV- and VV-polarization for both times of observation are shown in Table 5.2-2. The standard deviations (of the stand averaged values) are shown in Table 5.2-3. Average values do not correspond to values expected for C-band radar. For the first image values are +/- 12 dB too high and for the second image for HH- and HV- polarization +/- 12 dB too low, except for the VV-polarization, which is even +/- 15 dB too low. Assuming relative calibration within one channel is accurate, the ML classification procedure can still be executed. The same applies to an analysis of texture. Care has to be taken, however, when applying polarimetric classifiers or algorithms based on physical or semi-empirical models for physical parameter extraction.

Results for mono-temporal classification of the training set at the 95% confidence level are shown in Table 5.2-4 and Table 5.2-5. For the October 1996 image 55.3% is correctly classified and for the June 1997 image 54.7% is correctly classified. The multi-temporal classification result, also at the 95% confidence level, as shown in Table 5.2-6, is clearly superior with a result of 81.3%. This is mainly a consequence of the different conditions of the forests at the times of observation. In October many deciduous trees have shed their leaves, while remaining leaves are dry. In June almost all species are fully foliated and coniferous trees have formed new shoots. For oak, beech and Douglas fir the multi-temporal approach yields far better results. Pine is an exception showing a single-data result for October which is slightly better than the multi-temporal result. Plate 5.2-4 shows a map of these classification results.

It is remarked that a classification result of 81.3% for a multi-temporal observation is not very high. Multi-temporal observation with X-band SLAR with HH-polarization yielded results in the order of 90% for the Dutch test sites, as mentioned in this chapter's introduction (Hoekman, 1990). With AIRSAR (which is a C-, L- and P-band system) the same result, i.e. in the order of 90%, was achieved with a single observation in July (van Maren and Varekamp, 1994). One of the main reason is the simple fact that in X-band deciduous tree stands show a significantly stronger backscatter than coniferous tree stands while in L-band the reverse is true. In C-band levels of deciduous and coniferous tree stands occupy the same small range. It should be taken in mind, however, that PHARUS results may largely improve when additional information related to its polarimetric and high-resolution features is fully utilised.

Table 5.2-2 Average backscatter per forest class.

	Gamma HH 96	Gamma HV 96	Gamma VV 96	Gamma HH 97	Gamma HV 97	Gamma VV 97
Oak	4.69	-0.85	5.64	-18.29	-23.88	-21.86
Beech	4.54	-0.93	5.47	-19.20	-24.81	-22.51
ALN	5.43	-0.70	6.18	-19.84	-26.40	-23.62
Pine	4.62	-0.64	4.36	-17.26	-22.94	-21.72
Larch	5.21	-0.13	5.77	-17.32	-23.02	-20.89
Spruce	4.99	-1.23	6.17	-16.93	-22.94	-19.20
Douglas	4.95	-0.75	5.46	-17.13	-23.10	-21.12

plate 5.2-4 *(a) Map of selected polygons and forest classes. The legend colour coding is given in Table 5.2-1. Classification results for (b) October 1996, (c) June 1997 and (d) October 1996 and June 1997. the colour coding for the classification maps is: green for correctly classified stands, red for erroneously classified stands and blue for unclassified stands.*

Table 5.2-3 Standard deviation backscatter per forest class.

	Gamma HH 96	Gamma HV 96	Gamma VV 96	Gamma HH 97	Gamma HV 97	Gamma VV 97
Oak	0.84	0.75	0.69	1.88	2.36	1.68
Beech	0.70	0.69	0.52	2.12	2.66	1.79
ALN	1.29	1.24	1.35	2.55	2.95	2.21
Pine	1.63	1.09	1.08	4.05	4.49	3.50
Larch	0.93	0.65	0.57	2.66	2.83	1.93
Spruce	0.92	0.80	0.73	2.96	3.33	2.74
Douglas	0.89	0.76	0.83	2.39	2.82	1.98

In Figure 5.2-1 simulation results for 1-, 2-, 4-, 8- and 16-look data are shown. It can be concluded that pixel-based classification has adverse results. When the number of looks is enlarged further (to 100, 1000 and 10.000), which can be the effect of pixel-averaging or segmentation, the classification accuracy approaches asymptotically the above-mentioned result of 81.3%. The reason much averaging is required may be a property of this particular data set in which differences between classes of the mean values (of stand averaged values) are small. For example, as can be seen in the second column of Table 5.2-2, the total range for the mean values of these seven forest types for HH-polarized backscatter is less than 1 dB(!), while the standard deviation for these means is also in the order of 1 dB.

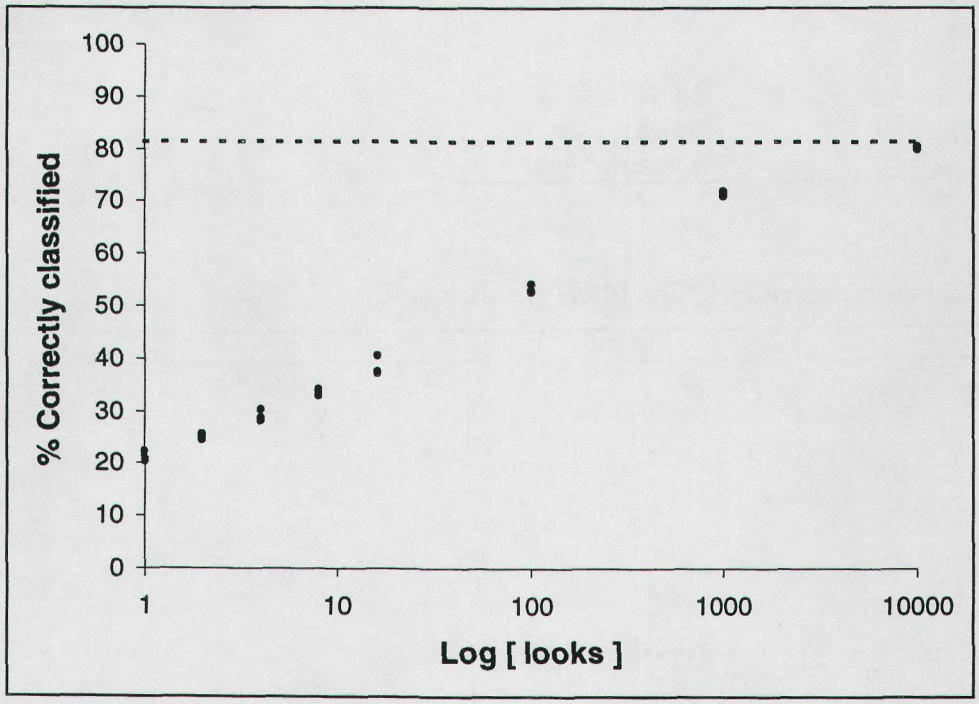

Figure 5.2-1 Simulated results for classification accuracy as a function of speckle-level. Three results are shown for 1-, 2-, 4-, 8-, 16-, 100-, 1000- and 10.000-look data.

Table 5.2-4 Classification results October 1996.

	1	2	3	4	5	6	7
Unknown	1	0	0	0	0	0	0
1 Oak	4	2	1	0	2	0	2
2 Beech	10	15	0	0	1	4	4
3 ALN	1	1	10	0	0	2	2
4 Pine	0	0	0	18	2	0	2
5 Larch	4	6	0	1	15	1	2
6 Spruce	2	3	2	0	0	17	1
7 Douglas	4	2	0	0	0	2	4
Total	150						
Total unknown	1		% UNK	0.7			
Total right	83		% right	55.3			
Total wrong	66		% wrong	44.0			

Table 5.2-5 Classification results June 1997.

	1	2	3	4	5	6	7
Unknown	0	0	1	0	0	1	0
1 Oak	9	5	0	0	3	0	2
2 Beech	5	16	0	1	4	1	1
3 ALN	4	1	7	1	0	0	2
4 Pine	2	1	2	15	1	0	5
5 Larch	5	4	0	2	9	2	2
6 Spruce	0	1	0	0	3	22	1
7 Douglas	1	1	3	0	0	0	4
Total	150						
Total unknown	2		% UNK	1.3			
Total right	82		% right	54.7			
Total wrong	66		% wrong	44.0			

Table 5.2-6 Classification results June 1996 / October 1996.

	1	2	3	4	5	6	7
Unknown	2	0	0	1	1	1	0
1 Oak	18	3	0	0	0	1	1
2 Beech	1	22	0	0	1	0	1
3 ALN	1	1	13	0	0	0	0
4 Pine	0	0	0	17	1	0	2
5 Larch	2	2	0	0	17	0	1
6 Spruce	0	1	0	0	0	23	0
7 Douglas	2	0	0	1	0	1	12
Total	150						
Total unknown	5		% UNK	3.3			
Total right	122		% right	81.3			
Total wrong	23		% wrong	15.3			

5.2.5 Conclusions and recommendations for future analysis

The results show that classification of forest stands in a mixed deciduous-coniferous forest plantation is well possible. A multi-temporal approach is superior to a mono-temporal approach and may be required to meet user requirements for accuracy. The simulated effect of speckle on classification accuracy clearly shows that a 'field-based' approach is necessary

in this particular case where the differences in mean backscatter between the classes studied is very small.

Absolute calibration is still a point of concern. The backscatter values deviate strongly from expected values. Moreover, there seems to be an imbalance between the backscatter values in the different channels for the June 1997 image.

To take full advantage of the special possibilities of PHARUS, which are the high spatial resolution and the polarimetry, more study is needed. These steps have been indicated in section 5.2.3.3. To study polarimetry and the possibilities for geo- and bio-physical parameter retrieval with physical or semi-empirical models a good polarimetric and absolute calibration is essential.

5.2.6 References

Hoekman, D.H., 1990, Radar remote sensing data for applications in forestry, Ph.D. Thesis, Wageningen Agricultural University.

Hoekman, D.H., 1991, Speckle ensemble statistics of logarithmically scaled data, IEEE Transactions on Geoscience and Remote Sensing, Vol.29, pp.180-182.

Joughin, I.R., D.P. Winebrenner and D.B. Percival, 1994, Probability density functions for multilook polarimetric signatures, IEEE Transactions on Geoscience and Remote Sensing, Vol.32, pp.562-574.

van Maren, G. and C. Varekamp, 1994, Modelling and synergetic use of optical and microwave remote sensing. Report 7: Combining optical and microwave remote sensing data of forest vegetation Mac Europe 1991, BCRS-report 93-36, Delft, The Netherlands.

van der Sanden, J.J., 1997, Radar remote sensing to support tropical forest management, Ph.D. Thesis Wageningen Agricultural University, 9 Dec 1997.

van Zijl, J.J., 1989. Unsupervised classification of scattering behaviour using radar polarimetry data, IEEE Transactions on Geoscience and Remote Sensing, vol.GE-27, pp.36-45.

5.3 *Precision Agriculture*

5.3.1 Introduction

Current agronomic practices consider individual farmers fields to be the basic management units. Management activities such as seeding, planting and fertilization are based on the average soil and crop conditions within the field. However, considerable differences in soil and crop conditions can develop in the field over the growing season. Practices that are based on the average conditions are bound to produce sub-optimal results. Sub-optimal in terms of crop yields but also in terms of environmental impacts such as leaching of fertilizers and pesticides. Farmers know about many of these differences, but so far operational methods to vary management procedures on-the-go for different parts within a field were not available. Technical developments in the last decade offer perspectives for the development of site specific soil and crop management within individual agricultural fields, that not only result in more efficient crop production but also in lower losses of agrochemicals to the environment. The latter is increasingly demanded by society, and is being codified in environmental laws and regulations.

These new types of management, to be broadly referred to as Precision Farming, Site Specific Farming or Variable Rate Application, consider differences in soil and crop conditions within the field before and during the growing season and uses these differences to fine- tune and vary management within the field on-the go. For instance: fertilizers are applied in varying quantities depending on the initial contents and crop demand; biocides are applied only at spots where weeds or pests occur and different seed varieties are sown in different areas of the field when drainage conditions vary.

Implementation of these new management techniques have been made possible only recently by the development of global positioning systems, sensor technology, equipment for on-the-go yield monitoring and management; remote sensing techniques, geographical information systems, expert systems and simulation models for crop growth and nutrient fluxes.

5.3.2 Objectives

On the Van Bergeijk farm a study was conducted in 1997 in which the use of optical remote sensing was explored and combined with monitoring, variable rate application of agrochemicals, and simulation modelling. One result of this study was that crop stress could not be differentiated into nitrogen stress and water stress with the 3 band optical sensor used (CAESAR). In this study the additional value of radar was investigated to detect those differences.
In summary the objectives were to explore:

- The use of PHARUS in detecting variability within agricultural fields.
- To investigate the additional value of radar next to optical remote sensing
- To correlate PHARUS images with ground-measured crop and soil characteristics

5.3.3 Van Bergeijk farm

The study was carried out on the Van Bergeijk farm in the Netherlands.
The Van Bergeijk farm is a commercial farm of approximately 100 hectares and is situated on Voorne-Putten, one of a series of (former) islands located to the south-west of the Netherlands. Soils in Voorne-Putten consist of marine deposits and are generally calcareous and textures range from fine loam to heavy clay-loam. With the excellent drainage, induced by a dense system of pipe-drains, these soils are considered to be prime agricultural soils.

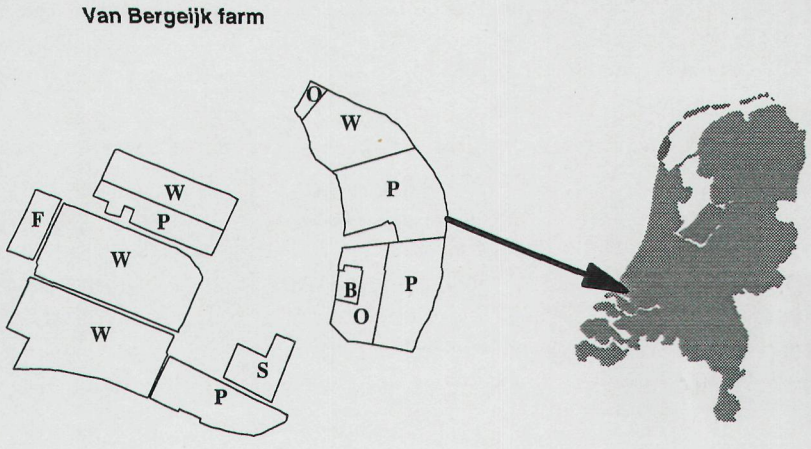

Figure 5.3-1 Farm layout of the Van Bemmelenhoeve in 1994 and Van Bergeijk farm in 1997. Abbreviation p stands for potato, w for wheat, b for barley, s for sugar beets, f for fallow and o for other crops.

A detailed soil survey was carried out at the Van Bergeijk farm in the spring of 1997 (see section 5.3.3). A basic farm layout of the Van Bergeijk farm is presented in. Crop rotation on this farm is mainly winter wheat, consumption potatoes and sugar beets.

5.3.4 Data acquisition

5.3.4.1 **Remote sensing**

Two types of remote sensing data were collected: (i) on may 29 1997 a PHARUS image was taken of the van Bergeijk farm, and (ii) on May 30 1997 a CAESAR optical image was taken. PHARUS measured at three polarizations: HH, HV en VV, with a spatial resolution of 4 m pixels. The CAESAR-scanner measures in three spectral bands: green (535-565 nm), red (655-685 nm) and NIR (845-895) with a spatial resolution of 0.75 m pixels.

5.3.4.2 **Groundtruth**

On 65 plots on the farm groundtruth was collected on crop and soil characteristics. Collected data was:

- Soil water content (top 5 cm)
- Crop density
- Crop height
- Leave angel of the plants
- Crop biomass (specified in leaves, storage organs and stems)
- Crop water content
- Crop nitrogen content
- Crop reflection (using a CROPSCAN)

All this information was stored in a georeferenced relational database.

5.3.5 Variability among fields

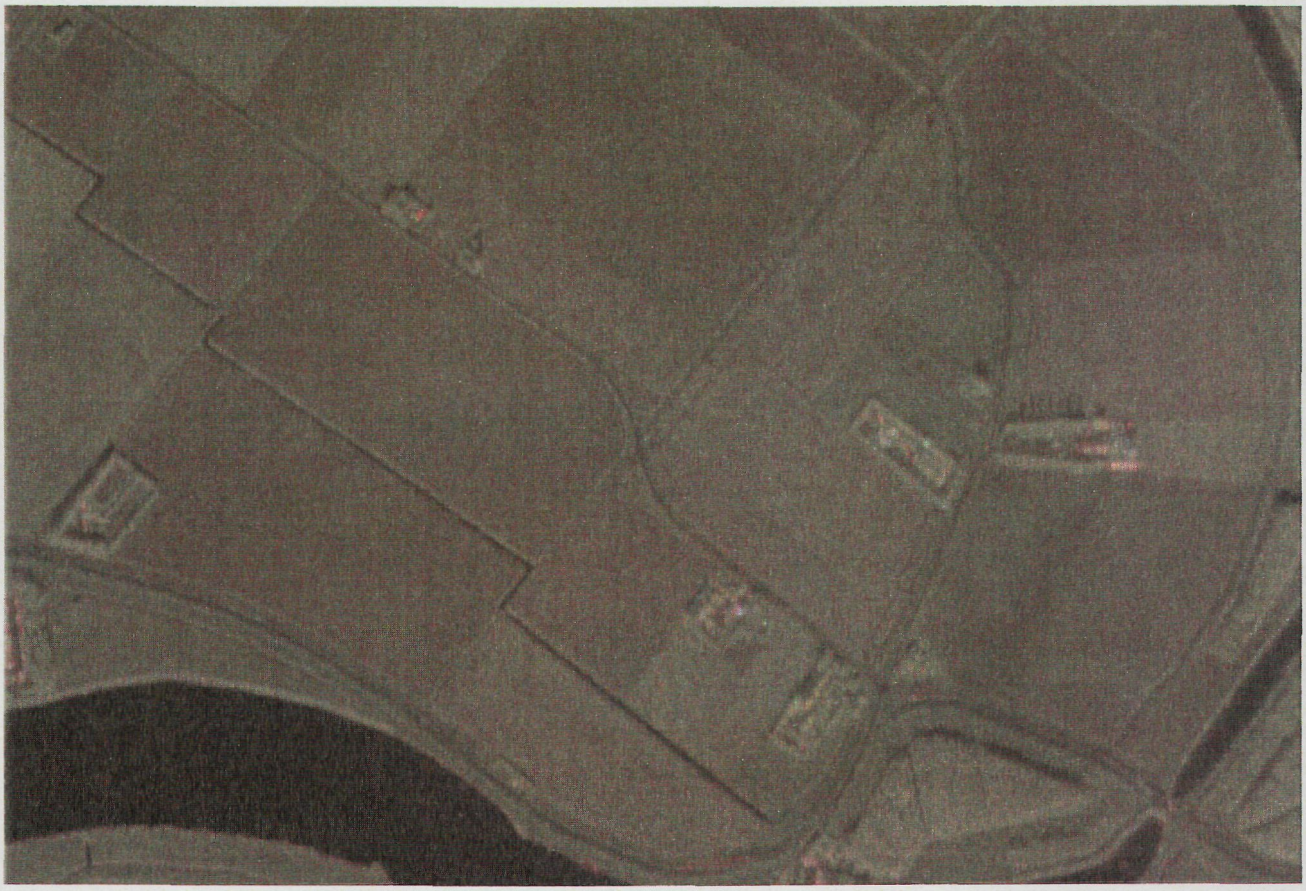

Figure 5.3-2 PHARUS false colour composite (HH, HV, VV) of the Van Bergeijk farm

In Figure 5.3-2 an image of the Van Bergeijk farm in Zuidland is shown. A clear difference could be observed among different crops (see Figure 5.3-1 for the crop rotation). However, even differences could be seen between different varieties of the same crop. On the upper left field (field 1)an early variety of winter wheat was grown. At time of the recording this variety had already ears. The variety on field 6 (lower left of Figure 5.3-2) was a little later which resulted in a clearly different backscatter pattern. In field 2 where two varieties of potatoes were grown this differences could also be observed. Furthermore, the orientation of the potato ridges also resulted in significant different patterns. As can be seen on field 2 and 3 in Figure 5.3-2 (left side)

5.3.6 Variability within fields

Precision farming is mainly dealing with the use of spatial variability within fields, rather than differences among fields. This aspect is, therefore, of much more importance. In Figure 5.3-3 a PHARUS image of one individual field (15 ha) is shown. Spatial variability within this field was considerably, as illustrated with the ground truth measurements and the Leaf Area Index image based on the CAESAR data of that field and the final yield map in September (Figure 5.3-5). This spatial variability was not detected with PHARUS. Partly because the more coarse resolution, however, even the main patterns (upper an lower parts of the field) was not detected even though this had a scale that extended the 4 m pixel size with order of magnitudes. When looking at the ground truth data, aspects that influence radar are crop structure and water content. The first did not differ very much over the field maximum crop

height difference never exceeded 10 cm. Differences in water content did not vary that much either, when expressing it as amount (multiplied with the biomass) the differences were significant. This was not detected by PHARUS.

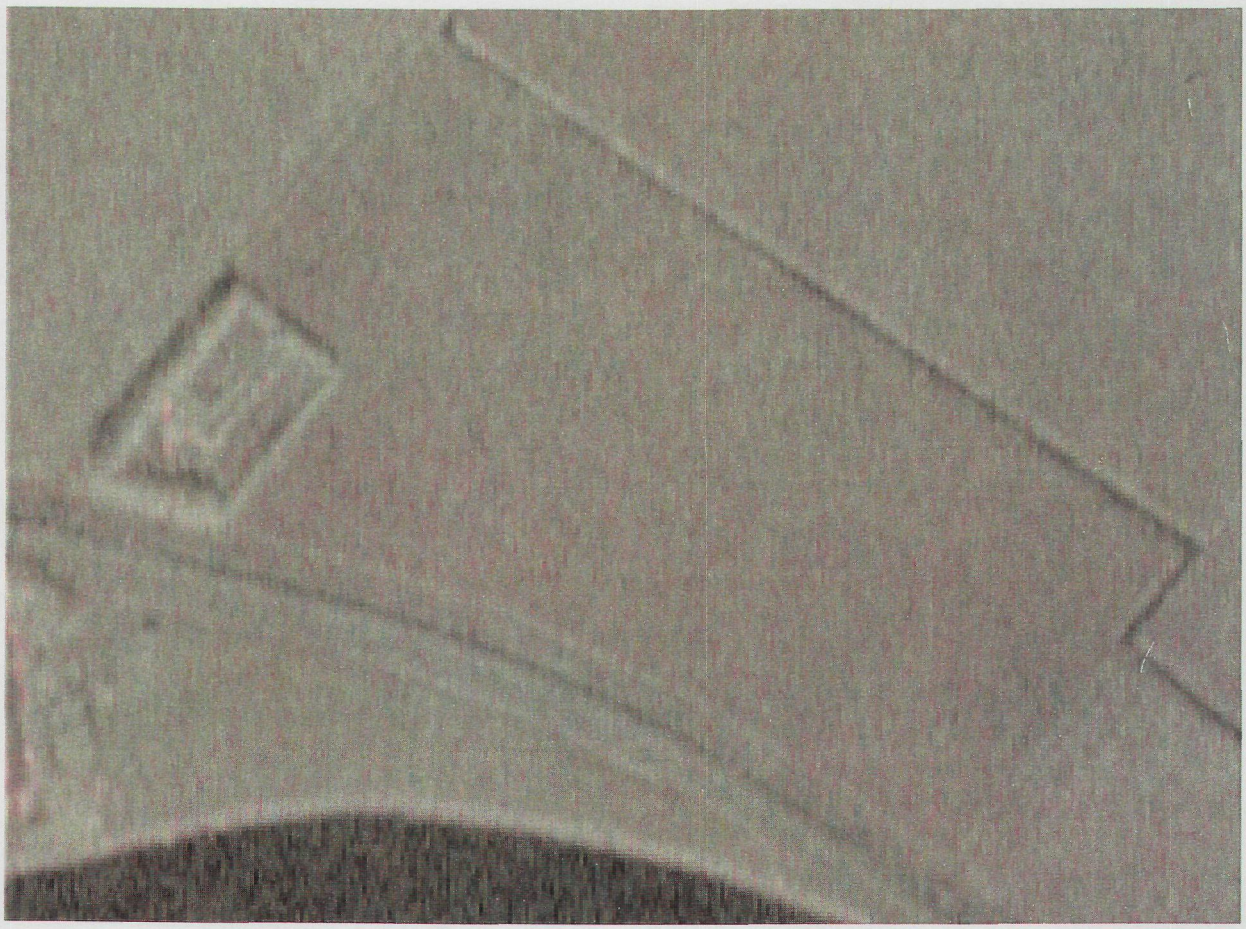

Figure 5.3-3 PHARUS false colour composite (HH, HV, VV) of field 6 (winter wheat) for may 30 1997

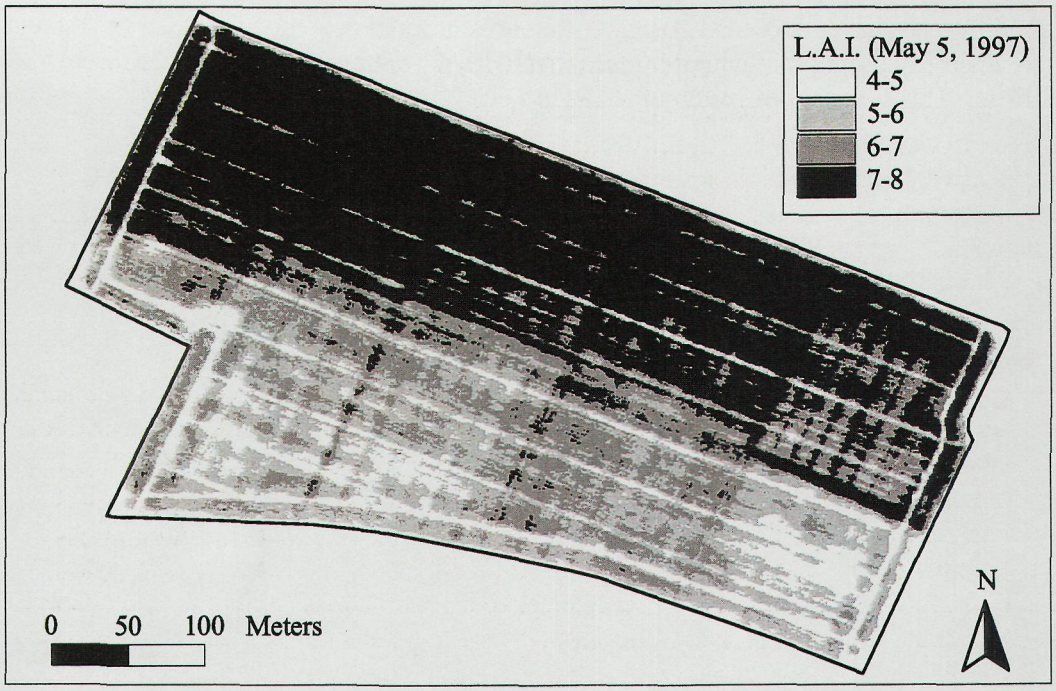

Figure 5.3-4 LAI-map for the Van Bergeijk experimental farm (Winter wheat) for May 30 1997

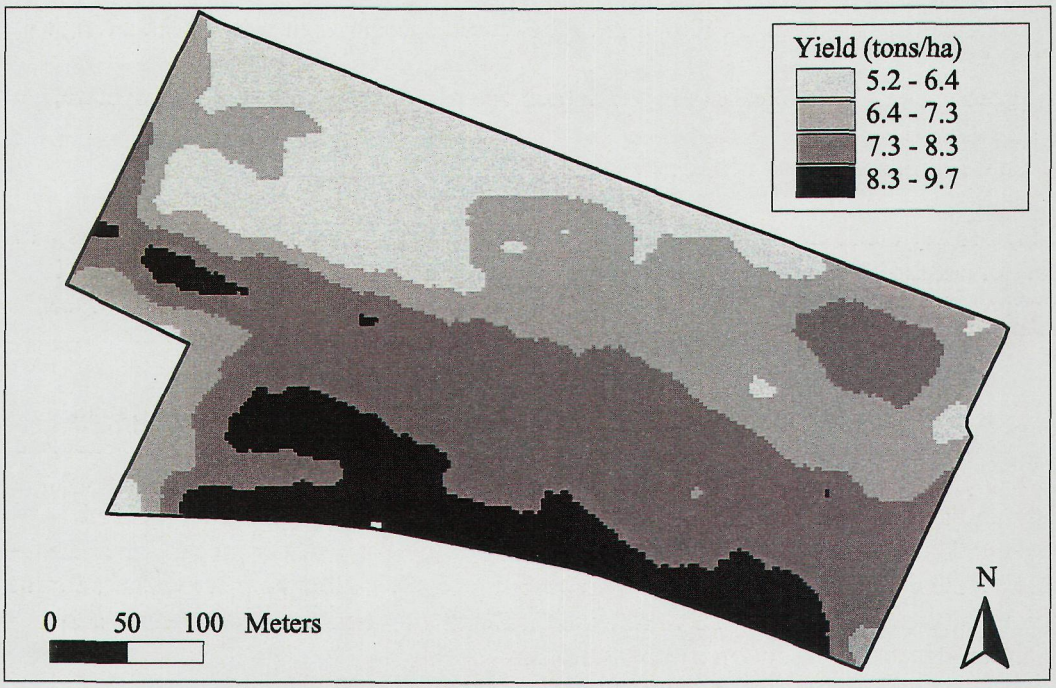

Figure 5.3-5 Wheat grain yield in September 1997 of field 6 on the Van Bergeijk farm.

5.3.7 Conclusions

For the use in precision farming PHARUS (C-band) seems not very promising. Lack of spatial resolution may be one reason. Not detecting the appropriate crop characteristics seems the most important reason. Later in the growing season when drought effects are generally more significant PHARUS images will probably show more detail. However, precision farming is mainly dealing with the detection of differences in an early phase of the growing season to allow management adaptations.

6. Data quality control and evaluation of the use of PHARUS

The technical evaluation of the Familiarization program includes two parts: 1) The data quality control (section 6.1) and 2) the evaluation of the use of PHARUS. The second part can be subdivided into (a) flight operations (section 6.2), since these are essential in the use of PHARUS, and (b) an analysis of the PHARUS system performance. The system performance can be assessed by an absolute calibration of the data. For this purpose a paper has been included in section 6.3.

6.1 *Data quality control*

A separate task has been defined for the data quality control. Since PHARUS is a new sensor, the quality of the data it produces is examined carefully and the data are compared with the system specifications. For each of the applications it was necessary to perform quality control on the data. Most of the checks are performed in the Generic SAR Processor (GSP). But between the conversion of the radar data from DCRSi tape (in-flight storage) to Exabyte (processing medium) a first quality check is performed by checking for a specific (sync) pattern in the radar header data. Then the number of correct and incorrect lines are counted and if the number of incorrect lines is larger than expected the data is classified as erroneous.

The quality control in the GSP involves the following steps:

1. Inspection of radar header data
2. Inspection of flight data
3. Calculation of Doppler bands, to check for excessive frequency excursions, leading to signal loss
4. Inspection of range and azimuth spectra (average amplitude check, shape of spectra, noise floor)
5. Visual inspection of radar image

When necessary the results of the quality evaluation were discussed with the users. A small number of additional image recordings was used to optimize the observability of critical system parameters, which were evaluated to assess the data quality of the image products supplied to the users.

The data quality control also included a technical evaluation to see whether the system performs according to the specifications and meets the user requirements, with the exception of a slightly degraded range resolution. This degradation can most likely be restored by a processing modification. Several technical problems appeared, which could be solved adequately. Unfortunately, these problems could only be observed after processing at TNO-FEL, since the Quick Look Processing (QLP) facility of TNO-FEL was not available for the Familiarization program. The QLP allows the monitoring of the acquired images in a low resolution mode, with no motion compensations.

An absolute calibration of the data was performed for the technical evaluation of the system. For the calibration corner reflectors and transponders were set up and imaged. Internal and external calibration signals were compared to check the system stability (see section 6.3).

A polarimetric or relative calibration has been performed for the applications, which affects the quality of the data. Due to this relative calibration it is possible that differences in absolute intensity occur. These differences are not related to the performance of PHARUS. Tower measurements, performed at TNO-FEL, show that the measured sensitivity of the radar compares well with the original system specification. However, the occurring differences in absolute intensity have led to confusion, in particular for the applications sea-bottom topography, cartography in tidal areas and forest monitoring. For the information

extraction process of the sea-bottom topography application and cartography in tidal areas, the differences had no influence on the results. But for the forestry application, however, the differences disturbed the information extraction process, which was changed because an additional image was made available, allowing for a temporal analysis of the data. It is unfortunate that this procedure has been applied to the relatively calibrated data: in particular for forest backscatter it is possible to perform a type of calibration in which the amplitudes of the backscatter on the different days become meaningful.

6.2 *Flight operations*

A large amount of data has been acquired, not only for the Familiarization program but also for PR activities, for instance on the potential Indonesian market. Furthermore, an additional image could be delivered for the application forest monitoring. No oil spill detection was performed because the quality of the data was too bad due to technical problems.

At the beginning of the project five flights have been planned for the acquisition of the data. Therefore, data acquisitions for several applications had to be combined. Due to the technical problems it appeared that this number was not enough. An improvement of the efficiency of the data acquisition and additional financial contributions of TNO-FEL and NLR, permitted to perform a total of seven flights during which data for all applications were acquired.

From the familiarization flights much experience has been obtained in the planning and logistics for the deployment of the PHARUS system. In particular the planning of the first two familiarization flights (PV07 and PV08, see Table 1.2-1) was very tedious because of the time-critical applications. During these two flights an oil spill was to be detected in co-operation with RWS-DNZ, a marine vessel on the North Sea was to be found through radio communication, and there were several people working in the field collecting ground data or for the operation of calibration devices. It is a pity that these efforts were in vain because of the technical problems that occurred.

Another lesson which has been learned from the Familiarization program concerns the use of the platform from which PHARUS is operated. This platform is a Cessna Citation II, which is owned by both NLR and TUD. The use of this platform has two major limitations:

1. Because of the shared ownership the Citation is not always available. This availability has put constraints on the agricultural applications which are time critical because of the growing season.
2. Another constraint on the use of the PHARUS system is due to weather conditions. It is possible that there is ice accretion during a flight, in that case the aircraft is not certified for the deployment of PHARUS and the flight must be cancelled.

In particular due to the first constraint the application precision farming was restricted to an early period in the growing season. This might be an explanation for the unsatisfactory results of that application.

6.3 *Calibration of polarimetric PHARUS data*

CALIBRATION OF POLARIMETRIC PHARUS DATA

R.J. Dekker and A.C. van den Broek

TNO Physics and Electronics Laboratory
P.O. Box 96864, 2509 JG The Hague, The Netherlands

ABSTRACT

This paper presents a procedure for the calibration of polarimetric PHARUS data, based on the JPL POLCAL procedure, including some first results. Because the phase differences between the various polarization channels of PHARUS turned out to be range dependent, the procedure had to be adapted by calibrating the phase before conversion to Stokes matrix. Through this, the phase relationship between the channels could successfully be recovered. Cross-talk was reduced to less than -30 dB. The gain imbalance, measured by PARC responses, appeared to be high but was reduced to 0.65 dB. This relatively large uncertainty is mainly due to differences in the antenna patterns and insufficient antenna measurements. For the same reason the absolute calibration was not more accurate than a few dBs. Both gain imbalance and absolute calibration will be improved by a series of antenna measurements.

Keywords: Calibration, Polarimetry, SAR, Phased Array.

1. INTRODUCTION

PHARUS is the C-band polarimetric SAR that is developed by the TNO Physics and Electronics Laboratory, the National Aerospace Laboratory and the Delft University of Technology (Ref. 1). One of the most prominent features of PHARUS is the active phased-array antenna, which allows fast beam-steering capabilities for platform drift correction, spotlight SAR, ScanSAR and moving target indication (MTI). The active phased-array antenna is made up of 2×24 transmit/receive modules (Figure 1).

Every module contains a patch antenna, fed by a rat race, rotating the polarization basis of the patch to horizontal/vertical. The transmitted polarization is selected by a switch after the power amplifier (PA). In the polarimetric modes the transmitted polarization is altered every other pulse. Both polarizations can be recorded simultaneously because of two equal receiver circuits, starting with two low-noise amplifiers in the transmit/receive module. The only difference between both receiver circuits is the number of switches (see Figure 1). The direction of the beam is determined by the phase-differences between the individual modules, controlled by the vector modulators. The gain of the IF amplifiers of both receivers can be adjusted separately, every other polarization, for optimal AD conversion.

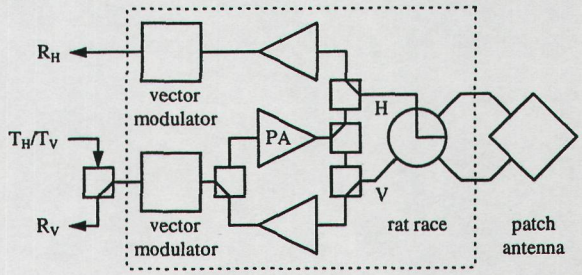

Figure 1. *Simplified diagram of a transmit/receive module, switched in receive mode.*

Before recording, internal calibration is performed to line-up all modules (Ref. 2, 3). In this way, proper boresight antenna patterns are achieved for all polarization channels. The internal calibration considers all active components, including switches, in both transmit and receive paths. The imperfections of the rat races and patches are thus not internally calibrated. After recording follows the external calibration, from now on referred to as simply 'calibration', if not stated otherwise. The nominal resolution of PHARUS is 3 m in range and azimuth. PHARUS is carried by a Cessna Citation II aircraft, which can reach an altitude of 12 km. The maximum swath width is 20 km.

The processing of PHARUS data is done by the Generic SAR Processor (GSP), developed in co-operation with ICT Automatisering (Ref. 4). The operations that are performed by the GSP are: raw data quality analysis and improvement, range compression, azimuth compression, motion compensation, radiometric correction, multi-looking, slant-to-ground-range conversion, calibration, and more. Figure 2 shows the GSP processing set-up for PHARUS data, compared to a more common processing set-up, as based on the POLCAL calibration procedure for data of the JPL DC-8 SAR (Ref. 5).

The GSP uses the same format as the JPL DC-8 SAR software (Ref. 6), referred to as CM format (compressed Stokes matrix format). For the benefit of phase calibration, this software determines the phase difference between HV and VH before the conversion to CM format, and saves it in the header. A necessary condition is that the phase difference is constant: only one value is considered. PHARUS data however, holds a HV-VH phase difference that is range dependent (see

section 3). Therefore, maintaining the CM format, the data must be phase-calibrated before conversion. Conversion of PHARUS data to CM format also requires correction for the adjusted IF gain factors and symmetrization (averaging HV and VH). Further details on the procedure and results are presented in the following sections.

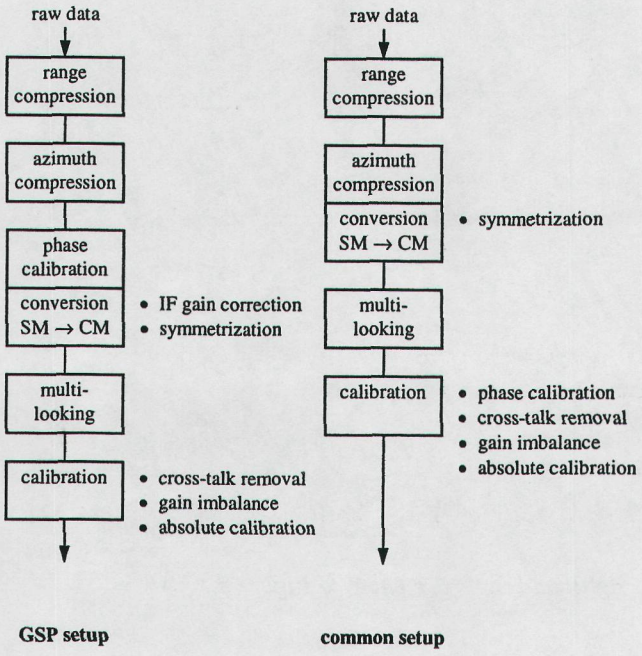

Figure 2. *GSP processing set-up compared to a more common set-up. SM = scattering matrix format, CM = compressed Stokes matrix format.*

2. PHARUS DATA

Two PHARUS images were recorded for testing the calibration procedure (Figure 3 and 4). The first shows an agricultural area, including forest, located in the Noord-Oost Polder near Flevoland, The Netherlands. The second shows an agricultural area, including many urban and greenhouse areas, around the former airfield Ypenburg (visible) near The Hague, The Netherlands. Both scenes contain two square-based trihedral corner reflectors (40.5 dBm^2). The scene of Ypenburg also comprises two C-band PARCs (polarimetric active radar calibrators, 45 dBm^2). Table 1 shows the specifications of the images. The beam azimuth angles were adjusted to the drift angle of the platform, effecting minimum squint. The antenna boresight angle is determined by a fixed incidence angle of 57.5 ° (mount position) and the beam elevation angle. All polarization channels were radiometrically corrected using the same ideal antenna pattern (sinc squared), because insufficient antenna measurements were available. The total incidence-angle range of both images is 28 to 71 °.

identification	Noord-Oost Polder	Ypenburg
mode	1	3
date (d/m/y)	22/10/1996	29/05/1997
time (GMT)	09:11:03	14:03:04
track	-91 °	-154 °
beam angle (az.)	-4.5 °	-6 °
beam angle (el.)	-10 °	+15 °
incidence angle	28 to 53 °	49 to 71 °
altitude	4640 m	4780 m
swath width	3600 m	8100 m
range (slant)	5260 to 7660 m	7310 to 14450 m
corner 1	6370 m	9120 m
corner 2	6550 m	11990 m
PARC 1	-	9400 m
PARC 2	-	11670 m

Table 1. *Specifications of the PHARUS images. The last rows show the ranges (slant) of the corners and PARCs.*

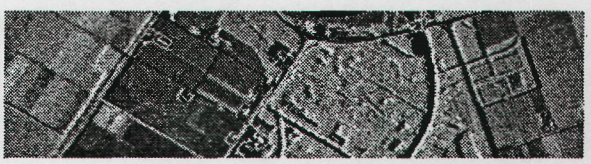

Figure 3. *PHARUS images of the Noord-Oost Polder. Illumination is from left to right, swath width = 3600 m.*

3. PHASE CALIBRATION

Phase calibration is required to recover the phase relationship between the polarization channels, which can be disturbed due to the differences in path lengths inside the radar hardware (Figure 1, Ref. 7, 8). Due to the fact that the scenes contained only a few calibration devices, clutter is used for determination of the phase calibration functions: the phase differences between HV and VH, and the phase difference between HH and VV.

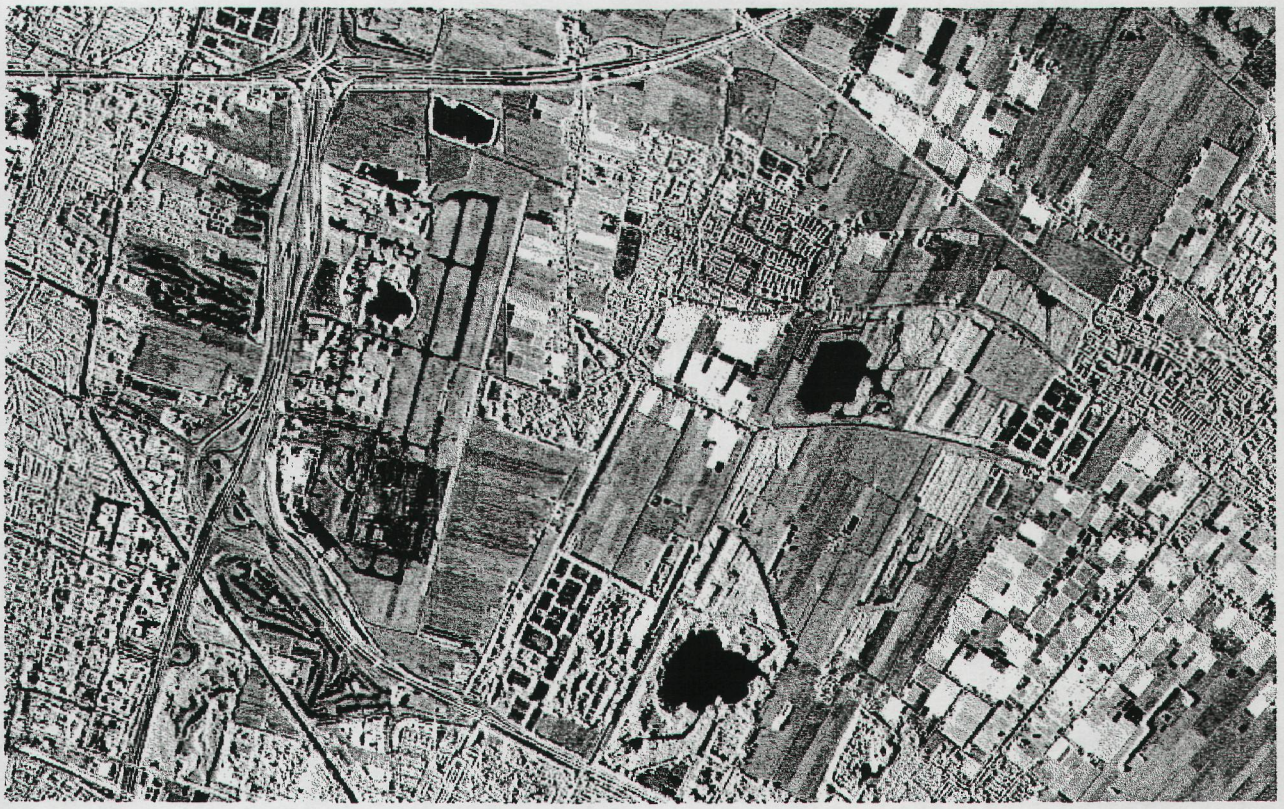

Figure 4. *PHARUS image of Ypenburg. Illumination (left to right) and scale are equal to Figure 3, swath width = 8100 m.*

(Ref. 7) shows from ERIM P-3 SAR data, that the phase differences can be range dependent, if the effective phase-centres of the antennas are displaced. Measuring the phase differences from the images described in section 2, this also turned out to be the case for PHARUS data (Figure 5 and 6). The averaged measurements of both images were combined to one. The individual (not-averaged) phase differences were obtained from the phase difference histograms of each azimuth line. In contrast with the P-3 SAR, the HV-VH phase difference of PHARUS is also range dependent. This is probably caused by a displacement of the effective phase-centres of the horizontal and vertical antennas (P-3 SAR), and of the transmit and receive antennas of both polarizations. As a result of this observation, the common calibration procedure (see Figure 2) is not valid for PHARUS, and had to be altered (see section 1). After phase calibration the spread of the residual phase differences measured 3 °, by the responses of the corners and PARCs. After conversion to CM format, multi-looking was applied by averaging every 10 adjacent azimuth samples, resulting in an azimuth resolution of 3.4 m and an equivalent number of looks of 4.6.

4. CROSS-TALK REMOVAL

Antenna imperfections and squint can change the polarization basis, leading to an undesired component in the horizontal and vertical channels (cross-talk). The amplitudes of the undesired components are reflected by the cross-talk parameters, and can be estimated and reduced (Ref. 5, 9, 10). As the phase calibration functions, the cross-talk parameters are range dependent and can be estimated from clutter. This is usually done by dividing the image in square or rectangular boxes, and subsequently averaging of the parameters of all boxes at equidistant ranges.

Figure 7 and 8 show the worst of both cross-talk functions of the PHARUS images before and after cross-talk removal. The boxes used were 2000 samples large (100 in range by 20 in azimuth), leading to 26 boxes in azimuth for the Noord-Oost Polder image and 185 for the Ypenburg image. The peaks at some range intervals correspond to large urban areas and other strong man-made scatterers. The Figures show a cross-talk level of better than -20 dB before removal, and better than -30 dB after removal. The cross-talk levels were confirmed by the HV responses of the deployed corners.

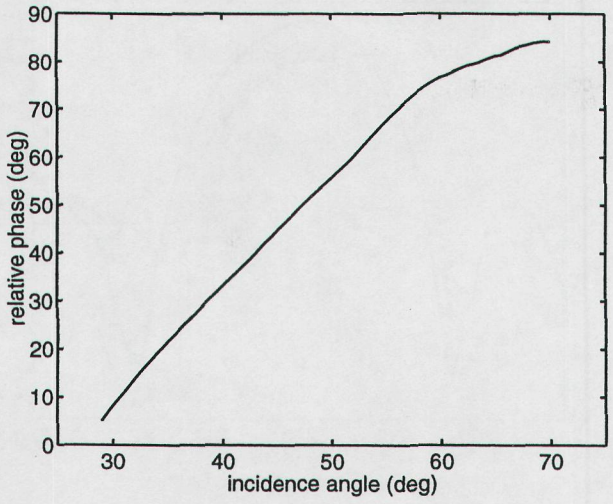

Figure 5. *Averaged phase differences HV-VH as a function of the incidence angle.*

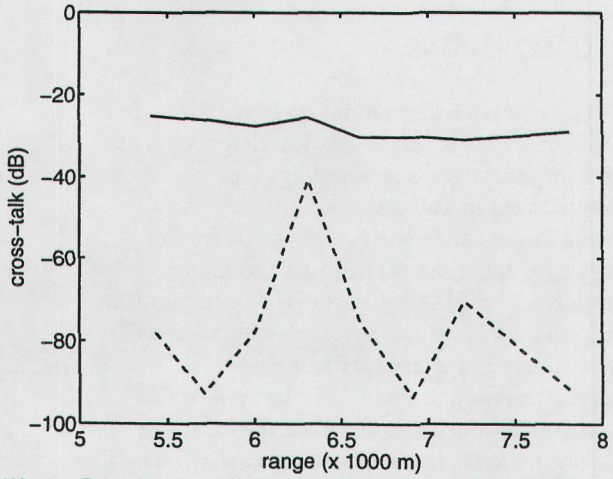

Figure 7. *Cross-talk levels of the Noord-Oost Polder image, before (solid) and after (dashed) cross-talk removal.*

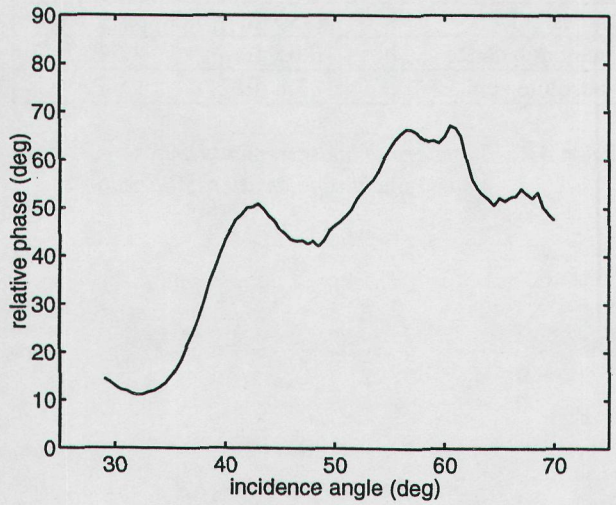

Figure 6. *Averaged phase differences HH-VV as a function of the incidence angle.*

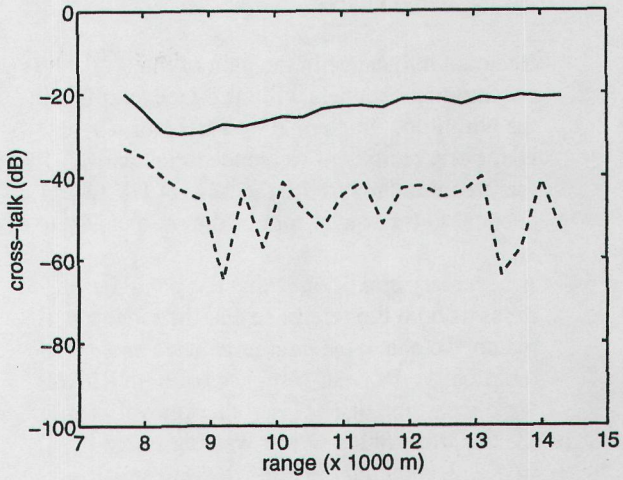

Figure 8. *Cross-talk levels of the Ypenburg image, before (solid) and after (dashed) cross-talk removal.*

5. GAIN IMBALANCE AND ABSOLUTE CALIBRATION

Residual imbalance in the gain of the polarization channels will introduce an offset in the amplitude ratios of HV to HH and VV to HH. For a reciprocal reference target and reciprocal radar system, the ratio of HV to HH is equal to the square root of the ratio of VV to HH.
A necessary condition is that the polarization bases of both the reference and the radar must match. To check the gain imbalance and reciprocity, the peak-responses of both PARCs were measured after cross-talk removal (Table 2). The transmitted power was registered by PARC 2, showing the one-way (transmit) azimuth antenna patterns (Figure 9).

Table 2 shows a nearly reciprocal situation but with a high system gain-imbalance, confirmed by the difference between the one-way (transmit) antenna patterns. The imbalance spread between both PARCs measures 0.65 dB. The main reason for this uncertainty is the difference in the real antenna patterns of the polarization channels. In addition, the patterns were not fitted well because the GSP did not account for the beam elevation angle in determining boresight. The new version is improved at this point, but was not used. For the same reason the absolute calibration is not very accurate yet. To give an indication of the uncertainty at this moment, an attempt was made to estimate the HH elevation antenna pattern from the data. In this way a difference of 1.8 dB was found, between the amplitudes of PARC 1 and 2 in HH.

	PARC 1	PARC 2
HV-HH	-2.66 dB	-3.31 dB
VV-HH	-5.15 dB	-5.66 dB

Table 2. *The gain imbalance after cross-talk removal (peak measurements).*

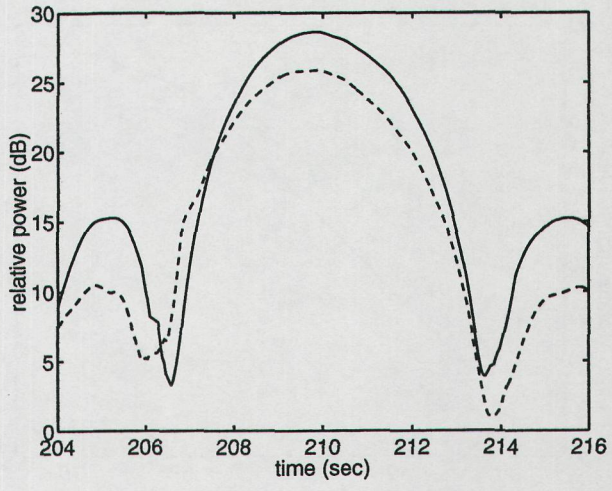

Figure 9. *PHARUS one-way (transmit) azimuth antenna patterns registered by PARC 2. H = solid, V = dashed.*

6. CONCLUSIONS

A procedure for the calibration of polarimetric PHARUS data is presented. The first results of this procedure on two recordings are summarized in Table 3.
From this we conclude that phase calibration and cross-talk removal can successfully be performed on PHARUS data. The uncertainties in gain imbalance and absolute calibration will be improved by a series of antenna measurements and a new GSP version, which accounts for the beam elevation angle. Polarimetric applications using PHARUS data can therefore be guaranteed.

phase difference	3 °	corners, PARCs
cross-talk	< -30 dB	clutter, corners
gain imbalance	0.65 dB	PARCs
absolute gain	1.8 dB	PARCs

Table 3. *Summary of measurements and measurement objects after calibration.*

7. REFERENCES

1. Hoogeboom, P., Greidanus, H., Koomen, P.J., and Pouwels, H., 1994, PHARUS: An Autonomous Airborne SAR Capability, *Symposium on Satellite and Airborne Synthetic Aperture Radar, 28 November 1994, Jakarta, Indonesia.*

2. Vermeulen, B.C.B., Paquay, M.H., Koomen, P.J., Hoogeboom, P., Snoeij, P., and Pouwels, H., 1996, Amplitude and Phase Calibration of an Dual Polarized Active Phased Array Antenna, *Proc. EUSAR '96, Köningswinter, Germany*, 539-542.

3. Vermeulen, B.C.B., Koomen, P.J., Hoogeboom, P., Snoeij, P., and Pouwels, H., 1996, C-band solid state dual polarization T/R modules for airborne SAR systems, *Proc. EUSAR '96, Köningswinter, Germany*, 543-546.

4. Otten, M.P.G., Groot, J.S., and Wouters, H.C., 1994, Development of a Generic SAR Processor in The Netherlands, *Proc. IGARSS '94, Pasadena, California,* 903-905.

5. Zyl, J. van, Burnette, C.F., Zebker, A., Freeman, A., and Holt, J., 1990, *POLCAL User's Manual*, JPL D-7715, Jet Propulsion Laboratory, Pasadena, California, August 1990, 49 p.

6. -, 1990, *AIRSAR Bulletin,* Jet Propulsion Laboratory, Pasadena, California, 22 February 1990.

7. Sheen, D.R., Freeman, A., and Kasischke, E.S., 1989, Phase calibration of polarimetric radar images, *IEEE Trans. on Geoscience and Remote Sensing*, 27, 6, 719-731.

8. Zebker, H.A., and Lou, Y., 1990, Phase Calibration of Imaging Radar Polarimeter Stokes Matrices, *IEEE Trans. on Geoscience and Remote Sensing*, 28, 2, 246-252.

9. Cordey, R.A., 1993, On the Accuracy of Crosstalk Calibration of Polarimetric SAR Using Natural Clutter Statistics, *IEEE Trans. on Geoscience and Remote Sensing*, 31, 2, 447-454.

10. Zink, M., and Freeman, A., 1992, An Examination of the Assumptions in the POLCAL Cross-Talk Removal Algorithm, *Proc. IGARSS '92, Houston, Texas*, 1171-1173.

7. Conclusions and recommendations

7.1 *Conclusions*

From the results of the preceding sections several conclusions on the use of PHARUS can be drawn:

- It has been possible to demonstrate the applications in spite of the technical problems, which occurred during the data acquisition.
- These technical problems have been solved sufficiently, the results of the demonstrated applications show that PHARUS can fulfil the user requirements, which have been determined during the kick-off workshop.
- The performance of the system is good, and according to the specifications only the range resolution needs to be improved.
- The PHARUS team has improved its knowledge considerably on the use of PHARUS, because a satisfactory amount of insight and experience is obtained with the deployment of PHARUS. This has led to an improvement plan (PHARUS beheersplan)
- A large amount of data has been acquired, not only for the Familiarization program but also for PR activities.
- No oil spill detection could be performed because the quality of the data, acquired during a controlled oil spill experiment, was too bad due to technical problems.
- The results from the applications 1) Cartography in tidal areas and 2) precision farming were not completely satisfactory. For the first application one of the two available PHARUS images was probably acquired during high tide. As a result only one image was investigated. For the second application the acquired image did not show variations within fields, which is essential for precision agriculture. It is expected that the results will improve if a temporal analysis is applied.
- A polarimetric or relative calibration has only been performed for the applications. An absolute calibration of the data was performed for the technical evaluation of the system.
- It can be concluded that care must be taken when relatively calibrated data are analysed by users of PHARUS data and that the calibration status must be made more clear.
- The polarimetric calibration showed that a special procedure had to be developed. This procedure differs from the procedure which is commonly used in the AIRSAR software.
- The results of the applications have been obtained with relatively little effort. It is therefore concluded that the PHARUS products are user friendly, which facilitates the use of these data.
- The logistics involved with the PHARUS flights are difficult because the platform is not always available and there are weather conditions which limit the use of the platform further.
- There is a clear need for more images, in particular for the applications cartography in tidal areas. Conclusions drawn for some applications are weakened due to the low number of images used.

7.2 *Recommendations*

With respect to the conclusions and results of the preceding sections several recommendations are given in this section.

- The user requirements and preferences which concern the calibration of data should be made clear because the calibration of PHARUS is an intensive task.
- The planning of the PHARUS flights must be agreed upon between the different users of the aircraft, well in advance of the actual flight itself. A procedure should be developed for this planning.
- Sufficient periods in time should be made available for performing PHARUS flights, in order to enable the use of PHARUS for time critical applications, such as oil spill detection or precision farming.
- It should be possible to have disposal of an extra platform to ensure the availability of the PHARUS system. Such a platform should meet the requirements for the deployment of the radar.
- The current platform for PHARUS should be certified for most weather conditions, in particular ice accretion.
- It is further recommended to perform an additional data acquisition program to complete the introduction of PHARUS products for the (Dutch/international) user market. During the demonstration of results at the final workshop, the need for additional PHARUS images became clear from the discussions.
- For some applications like ship wake and oil spill detection it is recommended to perform controlled experiments with a complete set of in-situ data.
- For full real time benefits, also a data link to the ground should be implemented and the processing should be faster.

The National Remote Sensing Programme 1990-2000, (NRSP-2) is implemented under the responsibility of the Netherlands Remote Sensing Board (BCRS) and coordinated by the Ministry of Transport and Public Works.

The objectives of the NRSP-2 are: to secure the long-term integration of the operational use of remote sensing through temporary stimulation in the user-sectors of government and industry, to strengthen the development of remote sensing applications and the expansion of the national infrastructure.

Publication of:

Netherlands Remote Sensing Board (BCRS)
Programme Bureau
Rijkswaterstaat Survey Department

P.O. Box 5023
2600 GA Delft
The Netherlands
Tel.: +31 15 2691111
Fax: 2618962